UNIVERSITY OF NAPLES FEDERICO II

Department of Structures

for Engineering and Architecture

Ph.D. Programme in Construction Engineering
XXVII Cycle

GIOVANNI MARIA MONTUORI

Ph.D. Thesis

INNOVATIVE STRUCTURAL SOLUTIONS FOR TALL BUILDINGS

TUTOR: PROF. ING. ELENA MELE

2015

Abstract

The main aim of this thesis is to research, study and analyze innovative structural solutions for tall buildings, aiming to optimize the efficiency of the structures and optimize the response under horizontal loads.

Following the recent trends in tall buildings design practice, the first analyzed structural scheme is the Diagrid system, a perimeter structural configurations characterized by a narrow grid of diagonals members which are involved both in gravity and lateral load resistance. Several studies have been carried out with the aim of i) completely understand the structural behavior of the Diagrid, ii) propose design procedure able to maximize the structural efficiency and iii) deepen some specific (local) structural behavior, essential for a precise structural design. The proposed considerations and design procedures have been validated through the results of a great number of finite element analysis, checking the structural performance and the efficiency of the different structural solutions.

Afterwards, a feasibility study is proposed for structural systems characterized by geometries different from the rectangular or triangular shapes. A structural solution obtained by replication of hexagons is analyzed (Hexagrid), focusing on its efficiency and feasibility. The study of the structural behavior of the Hexagrid scheme gave the opportunity to formulate a design procedure based on the homogenization criteria and, in particular, on the definition of a "Representative Volume Element" (RVE). This procedure has the great advantage of be able to be adopted for every geometric patterns, simply varying the mechanical properties of the homogenized material.

Finally, thanks to an effective collaboration with the well-known International firm Skidmore, Owings & Merrill, the structural design of a real tall building with an optimized perimetral frame is described. Firstly the building performances and its structural problems are evaluated,then the optimized structure is compared with more traditional structural solutions for tall buildings. This final part gave the opportunity to highlight the compromise between the practice and the theory, and to understand in particular how the optimum design (i.e. the most efficient solution) should be modified in order to mediate with different issues.

Sommario

Il principale contributo di questa tesi è dato dalla ricerca e dallo studio di soluzioni strutturali innovative per edifici alti, capaci di ottimizzare l'efficienza strutturale e migliorare la risposta sotto carichi orizzontali.
Seguendo i recenti trend nella progettazione di edifici alti, il primo schema analizzato è il sistema Diagrid, una soluzione strutturale caratterizzata da una maglia triangolare con elementi diagonali coinvolti nell'assorbimento delle azioni verticali e orizzontali. Le analisi effettuate hanno consentito di comprendere appieno il comportamento strutturale del sistema Diagrid, di proporre procedure di progettazione capaci di massimizzare l'efficienza strutturale e di approfondire il comportamento locale specifico di tale struttura; tali aspetti si sono dimostrati essenziali per una corretta e consapevole progettazione strutturale.
Le considerazioni e le procedure di progettazione sono state validate attraverso un ampia campagna di analisi numeriche agli elementi finiti, al fine di controllare la risposta strutturale e l'efficienza delle soluzioni strutturali proposte.
Successivamente viene proposto uno studio di fattibilità relativamente a strutture per edifici alti con maglia di forma diversa dalla rettangolare e dalla triangolare. Viene analizzata, in particolare, una soluzione strutturale ottenuta attraverso unità geometriche esagonali (denominata Hexagrid), concentrandosi sull'efficienza e sulla reale fattibilità di tale soluzione. Lo studio del comportamento strutturale del sistema Hexagrid, ha consentito di sviluppare una procedura di progettazione basata sui criteri di omogeneizzazione e, nel dettaglio, sulla definizione di un "Representative Volume Element" (RVE). Tale procedura presenta il grande vantaggio di potere essere adottata per qualunque pattern geometrico strutturale, attraverso la caratterizzazione delle proprietà meccaniche di un materiale omogeneizzato.
Infine grazie alla fattiva collaborazione con la società Skidmore, Owings & Merrill, leader internazionale nel campo della progettazione architettonica e strutturale, si è analizzato il progetto di un edificio alto reale con un telaio perimetrale ottimizzato. Le perfomance strutturali dell'edificio sono state opportunamente valutate e controllate,

confrontando inoltre la soluzione finale ottimizzata con soluzioni strutturali più tradizionali. Tale ultima fase di ricerca ha consentito di evidenziare al meglio il compromesso tra la pratica e la teoria, nonché di valutare come "l'optimum" progettuale (ossia la soluzione più efficiente) debba essere modificata, in fase di progetto, per tenere conto delle diverse necessità ed esigenze.

Acknowledgments

First and foremost, I would like to express my gratitude to my advisor Prof. Elena Mele, for giving me the opportunity of study interesting and challenging topics, for her always competent and acute suggestions and for giving me the opportunity to have a formative experience at the San Francisco office of the international firm Skidmore, Owings & Merrill. I would like to express my gratitude also to Prof. Antonello De Luca, for inspiring me with his passion for the science and research.

I would like to express my gratitude to Mark Sarkisian, partner in SOM's San Francisco office, and to the engineers of the SOM office for their competence and kindness, and for giving me an important and formative work and research experience.

I want to acknowledge my colleague Giuseppe Brandonisio for his suggestions and helpfulness.

Special thanks to Maurizio Toreno e Giuseppe Lucibello, with whom I shared the first part of my Phd course, for their continued support. I want also to acknowledge Alessandra Mazziotti, Gianluca Sarracco, Diana Faiella and Laura Guidi for having spent pleasant time with me during my work days, and Monica Fadda and Vincenzo Della Vista for their contributions to this work.

I also thank my good friends for their support and their encouragements.

Finally, I wish to thank my parents because I owe to them my willingness to do and learn, my curiosity, my strength and my capacities. Words cannot describe my gratitude to Agata, for having been on my side for all these years. This thesis is dedicated to her because without her

unconditional support, strength and happiness I would not been able to get where I am today

The last thought is my uncle, Augusto. I know he would be proud of me.

Napoli, 30 Marzo 2015 Gian Maria Montuori

Ringraziamenti

Desidero ringraziare innanzitutto il mio tutor, Prof. Elena Mele, per avermi dato la possibilità di studiare e fare ricerca su tematiche interessanti e stimolanti, per avermi guidato con professionalità, intelligenza e umanità durante questo percorso e per avermi dato la possibilità di svolgere nell'ambito del dottorato una breve ma intensa esperienza formativa presso la società Skidmore, Owings & Merrill in San Francisco. Unitamente desidero ringraziare il Prof. Antonello De Luca, per avermi trasmesso parte della sua sempre viva passione per la ricerca e lo studio.

Un sentito ringraziamento a Mark Sarkisian, partner della società SOM presso lo studio di San Francisco, e agli ingegneri dello studio SOM per l'accoglienza, la disponibilità e per la significativa e formativa esperienza che mi hanno consentito di realizzare.

Ringrazio Giuseppe Brandonisio per i consigli e la costante disponibilità.

Un grazie ai miei due ex colleghi Giuseppe Lucibello e Maurizio Toreno, con cui ho condiviso la prima parte del mio percorso di dottorato, che non hanno mai fatto mancare il loro supporto, anche da lontano.

Ringrazio i miei attuali colleghi Alessandra Mazziotti, Gianluca Sarracco, Diana Faiella e Laura Guidi per la loro capacità di allietare le mie giornate di lavoro. Grazie inoltre a chi ha contributo all'attività di ricerca che è dietro questa tesi Monica Fadda e Vincenzo della Vista.

Ringrazio i miei amici di sempre, che hanno sempre allietato i miei momenti liberi con la loro allegria e spensierata goliardia.

Ringrazio i miei genitori perché a loro devo la mia voglia di fare, di interrogarmi e di imparare; a loro devo gli strumenti e la forza che mi accompagnano sempre.

Non bastano poche righe per ringraziare Agata, per essere stata sempre al mio fianco in questi anni. A lei dedico questa tesi, perché è grazie al suo appoggio incondizionato, alla sua forza e alla sua allegria che ho raggiunto i miei obiettivi.
L'ultimo pensiero è per mio zio Augusto. So che sarebbe stato fiero di me.

Napoli, 30 Marzo 2015 Gian Maria Montuori

Table of contents

List of figures

List of tables

Nomenclature

$A_{m,d,f}$, area of diagonal on the flange façade;
$A_{m,d,w}$, area of diagonal on the web façade;
A_d and A_h, area of the cross sectional areas of the horizontal and diagonal beams for Hexagrid;
d_{hex}, length of the diagonal beams for Hexagrid;
d, distance of the module from the centroid of the plan shape;
d_h, interstory drift;
e, link length;
E and G, Young and transversal modules of the structural material of diagonal;
E_{grid} and G_{grid}, mechanical proprieties of the homogenized material;
$F_{m,k,M}$, vertical force on the k_{th} triangular scheme of the m_{th} module for overturning moment;
$F_{m,k,Q}$, vertical force on the k_{th} triangular scheme of the m_{th} module for gravity load;
$F_{m,k,V}$, horizontal force on the k_{th} triangular scheme of the m_{th} module for global shear;
H, building height;
h, height of the module;
h_i, interstory height;
h_{hex}, length of the horizontal beams for Hexagrid;
I_{col}, moment of inertia of column;
I and A_s, moment of inertia and shear resistant area of the equivalent cantilever cross section;
I_{zz} and I_{yy}, inertia moments of the diagonals respectively along the zz and the yy directions;

k, number of floors between two consecutive panel points;

K_β, bending stiffness of structure;

K_T, shear stiffness of structure;

L_d, diagonal length;

L_x, L_y, plan dimension along the x and y direction;

M_m, overturning moment at the basis of the m module;

n_{col}, number of columns in the central core;

n_d, number of diagonals on each building façade;

n_f, number of diagonals on the flange façade;

n_k, number of triangular scheme for each floor;

n_m, number of the considered module starting the numbering from the top of the building;

$n_{st\text{-}.}$, number of storey covered by a single triangular module

$N_{m,k,M}$, axial load in the diagonal of the k_{th} triangular scheme of the m_{th} module due to overturning moment;

$N_{m,k,Q}$, axial load in the diagonal of the k_{th} triangular scheme of the m_{th} module due to gravity load;

$N_{m,k,V}$, axial load in the diagonal of the k_{th} triangular scheme of the m_{th} module due to global shear;

n_w, number of diagonals on the web façade;

n_x, n_y , number of diagonals on x and y faces;

$P_{crit,col,S}$, buckling load of the internal column associated at the sway mode;

$P_{cr,col,NS}$ buckling load of the internal column associated at no the sway mode;

$P_{crit,dg}$, buckling load of the diagonals;

q_w, constant distributed horizontal action;

Q_m,gravity load at the base of the m module;

s, ratio between the bending and shear deformation at the top of the building;

u_H, horizontal displacement at the top of the building;

u_γ, displacement due to shear deformation;

u_χ, displacement due bending deformation;

V_m, global shear at the basis of the m module;

w, structural weight;

z_i, vertical distance between the top of the building and the base of the m-th module;

α, angle of the triangular scheme with the direction of wind;

β, spring stiffness simulating the axial stiffness for the SBS;

β_{id}, ideal spring stiffness simulating the axial stiffness for the SBS;

$\beta_{req,b}$, value of the ideal spring stiffness which restrains the column buckling in single-story mode;

γ, shear deformation;

η, factor for the limitation of the interstory drift;

θ, angle of diagonal;

θ_1, top angle of diagonal for the Zhang geometry

θ_2, bottom angle of diagonal for the Zhang geometry;

K, shear modification factor;

χ, bending deformation;

ρ, relative density;

1 Introduction

Recent design trends in tall buildings pose new challenges to structural designers, in addition to the traditional requirements for strength, stiffness, ductility and system efficiency. Ever increasing heights and complexity of form, need for robustness coupled to economy, awareness of limited material resources and sustainability, are all new demanding questions to be tackled with fresh approaches, novel structural systems and open minds.

Structural configurations best addressing the traditional requirements of strength and stiffness for tall buildings are the ones employing the tube concept, whose efficiency is strictly related to the involved shear-resisting mechanism, and in fact the historical evolution of the tube concept has been marked by the attempts of reducing the occurrence of efficiency loss due to shear deformations.
In this thesis the structural behavior of innovative structural solutions for tube structure are discussed, studying the peculiar behavior of each analyzed geometry, proposing new design approaches and evaluating the related structural efficiency. In particular, the first part of this thesis regards the studies and analysis of the Diagrid system, while the second part is mainly focused on proposing alternative structural patterns.

1.1 Diagrid System

Diagrid, or exodiagonal systems, is a perimeter structural configurations characterized by a narrow grid of diagonal members which are involved both in gravity and in lateral load resistance.

It is worldwide recognized that "This is the moment of diagrid". With these words of Ian Volner, on The Magazine of the American Institute of Architects, that states that "the diagonally based structural system of the diagrid is becoming a hallmark of 21st century Modernism" [52].

Diagonalized applications of structural steel members for providing efficient solutions both in terms of strength and stiffness are not new: rather, triangulation can be considered the first, most natural and always fresh (the oldest and the newest solution) design strategy in steelwork applications.

While in the past, the designers considered diagonals highly obstructive and usually embedded them within the building interior cores, with the diagrid system the multiple and variegated use of triangulation brashly characterizes the aesthetics of the buildings.

The conceptual studies of the diagrid system can be found in the seminal work of Myron Goldsmith [20], within the Master Thesis that he developed in 1953 at the Illinois Institute of Technology, Chicago, under the supervision of Mies Van Der Rohe. Goldsmith proposed three diagonalized structures for tall buildings, namely a variable-density diagrid, a regular narrow diagrid, and a mega-diagonal solution (Figure 1-1). The latter was nothing less than the embryonic idea of braced tube, that shortly thereafter Fazlur Khan would have worked out and applied in the smart and impressive John Hancock Center, paradigmatic example of the structural honesty of the second Chicago school. The two Goldsmith diagrid solutions, instead, did not receive comparable attention, probably due to difficulties in detailing and fabrication of curtain walls.

More recent examples of diagrid in medium-rise buildings are dated back to the 1960s, with the sketch proposed by Torroja (Figure 1-2(a)) in his seminal book [49] and, in the practice, with the 13-story IBM Pittsburgh building (Figure 1-2(b)), where the 'exterior load bearing truss frame wall

of welded steel in a diamond pattern grid was a radical break from post-and-beam construction' and 'gives an unusual liveliness to the façade, after so many years of rectangular curtain-walling.' [22]

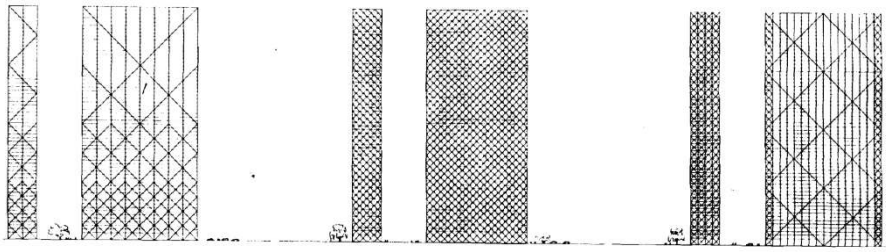

Figure 1-1 Diagonalized structure solutions for tall buildings proposed by Goldsmith (from Goldsmith 1953)

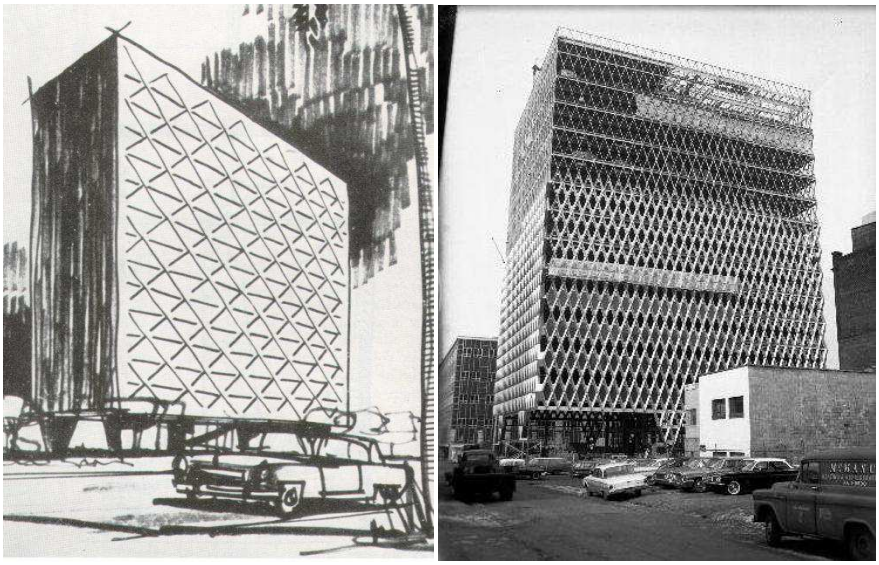

Figure 1-2 On the left sketch of a proposed triangulated wall façade for multistory buildings, on the right the former IBM Pittsburgh building, now United Steel Workers Building

After the conceptual scheme by Goldsmith and the independent pioneering application of diagrid to the IBM Pittsburg building, the structural designer of tall buildings mainly shifted their attention to another variation of diagonalized systems, the braced or trussed tube, employing mega-diagonal instead of the narrow grid of diagonal members characteristic of diagrids.

On the contrary, nowadays a renewed interest in and a widespread application of diagrid is registered. A multiple and variegated use of triangulation which brashly characterizes the aesthetics of important building is the new trend in tall buildings.

The diagrid concept offers the structural possibility of combining high efficiency and aesthetic connotation. Several renowned examples testify this statement: the 30 St. Mary Axe, the Hearst Tower, and more recently the Bow, all designed by Norman Foster but each characterized in an unique manner by triangulation in façade; the CCTV Headquarters (named Best Tall Building Worldwide by the CTBUH on November 2013), designed by Rem Koolhaas with the inspiring structural involvement of Cecil Balmond, where the variable density diagrid wrapping the loop shape contributes to create an affect of complexity and gradation; the Doha Tower, designed by Jean Nouvel, an elegant cylindrical form that stands out for the overlapping and merging of the concrete diagrid structure with the a complex "mashrabiya" pattern, conceived for sun shading purposes; the Capital Gate, "world's furthest leaning manmade tower", characterised by a steel diagrid that finely tessellates the external façade of the tower describing a striking organic form.

A major reason for this "diagrid craze" is undoubtedly the structural efficiency of the triangulated patterns: in fact "… diagrid speaks a reassuring language of stability, a message qualified by its real physical

economy and resilience …. diagrid looks like it should work, and it does" [52].

1.1.1 Diagrid structural behavior

The diagrid structures can be seen as the latest mutation of tube structures, which starting from the frame tube configuration, have increased structural efficiency thanks to the introduction of exterior mega-diagonals in the braced tube solution; in this case the significant improvement in terms of lateral stiffness and shear lag reduction also reflects in the building architecture, strongly connoted by the clear and disciplined structure, "the honesty of the structure", in the words of the architect Bruce Graham. The diagrid system can be considered as a further evolution of the braced tube structures, since the perimeter configuration still holds for preserving the maximum bending resistance and rigidity, while, with respect to the braced tube, the mega-diagonal members are diffusely spread over the façade, giving rise to closely spaced diagonal elements and allowing for the complete elimination of the vertical columns; thus the diagonal members in diagrid structures act both as inclined columns and as bracing elements, and carry gravity loads as well as lateral forces; due to their triangulated configuration, mainly internal forces arise in the members, thus minimizing shear racking effects.

Despite the large number of applications and proposed projects, design criteria for the diagrid system are not yet consolidated as in the case of more traditional structural types, and also building codes do not provide explicit guidelines and provisions for diagrid structures. A major research contribution has been given by Moon, with a series of papers starting from 2007 [30], where a stiffness-based methodology for the preliminary structural design of diagrids is suggested and applied to different building

models; adjustments of the formulation are also given to address both uniform and variable angle diagrids [31], as well as for non-prismatic building forms [34].

In a recent paper finalized to the assessment of the structural behavior of diagrid buildings [25], the authors have pointed out that, thanks to the high rigidity of the diagonalized façade, strength requirements can be of paramount importance, and even be the governing design criterion. In chapter 2 the stiffness-based design criterion proposed by Moon is reviewed and simple formulae for deriving strength demand in the members are defined and applied for alternative "strength-based" design solutions. Considering a building model, different diagrid structural solutions, designed according to stiffness and strength requirements and to strength requirements, are compared in terms of resulting diagonal cross sections and steel weight. Discussion in terms of different response parameters, i.e. top displacement, interstory drift, member strength demand to capacity ratio, is presented also considering the unit steel weight of each single solutions, and design implications are emphasized.

The "ideas" expressed in the Myron Goldsmith thesis (Figure 1-1) as well as some relevant examples in the construction world (the Lotte Super Tower, the CCTV, the 1000 Museum building in Miami, the Sunrise Tower in Kuala Lumpur) suggest an alternative design approach for the diagrid, in addition to the traditional design approach. The variation of stiffness and strength demands along the tall building elevation can be accommodated with a variable-geometry strategies, resulting in diverse geometrical patterns characterized by density, size, scale, angle and/or depth of the base unit varying along the building façades.

In Chapter3, diagrid structures characterized by variable density patterns are considered and compared to regular and variable angle patterns. In particular eight different diagrid patterns (namely three regular, three

variable angle and two variable density patterns) are generated and designed for a 90-story model building: for the regular and variable-angle patterns, the design process is carried out according to the procedures proposed by [30], [32], [53], while for the variable-density patterns, specific design approaches are developed. The resulting diagrid structures are assessed under gravity and wind loads and various performance parameters are evaluated on the basis of the analyses outcomes.

The analysis of the model buildings in Chapter 2 and 3 have shown some peculiar behavior of the diagrid system and in general of the systems with megadiagonals. Though the designed diagrid structure provides the required lateral stiffness to the building under wind loads, large interstory drifts arise at floor levels located within the diagrid module, particularly the ones characterized by the steepest angles (i.e. the tallest diagrid modules) and/or the most flexible diagonal members.

The problem is twofold, and, involving both the perimeter diagrid members and the interior core columns, requires: (i) to reduce or avoid the flexural deformations of the diagonal members along their length, and (ii) to stabilize the core gravity columns at intermediate floor levels. Similar structural issues arise in other lateral load resisting systems for tall buildings, whenever mega-bracing elements spanning over several floors are employed: this is the case of tube configurations characterized by mega-diagonals, namely the braced tube, as well as exoskeleton mega-structures [47]; [1]. However the case of diagrid is unique due to the complete absence of vertical columns in façade.

In Chapter 4 a thorough evaluation of the local behavior of diagonal members and gravity columns within the diagrid module height are provided, and a methodology for establishing the need for a specific secondary bracing system as a function of the diagrid geometry is presented. Further, design criteria for secondary bracings are derived

both for controlling diagonal flexural deformations and gravity column buckling; the application of the above formulations to some 90 story building models, characterized by perimeter diagrid structures with different module height and diagonal cross sections, allows for comprehensive discussion on design implications of secondary bracings.

1.2 Alternative structural patterns

Alternative, non conventional, geometrical patterns are worth of consideration for their structural and aesthetical qualities. Natural patterns, i.e. geometrical patterns observable in nature, can be a fruitful and almost endless source of inspirations for efficient man-made structures, at all scale levels (from the very tiny - material design - to the biggest – tall buildings - embracing all intermediate steps).

In the framework of material science and engineering, micromechanics and physical properties of heterogeneous media have been intensely studied in the last decades [18]; [14]. Nature offers a large number of examples of heterogeneous materials, made of different elements, cells, fibers, differently arranged to form structural networks which guarantee optimal mechanical performances. Examples of efficient structural patterns can be observed in natural cellular solids: balsa (Figure 1-3-a); cork (Figure 1-3b); internal core of the stem of the plants (Figure 1-3-c); trabecular bone (Figure 1-3-d). Here regular and irregular hexagon cells can be recognized.

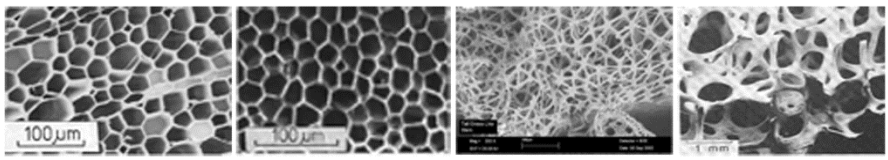

Figure 1-3 Examples of efficient structural patterns in natural cellular solids: a) balsa; b) cork; c) internal core of the stem of the plants; d) trabecular bone (from [Gibson et al., 1988])

Hexagonal structures are often visible in nature also at larger scale level. A classical example are honeycombs, admired since ancient times [43]: in 36 B.C., the Roman scholar Marcus Terentius Varro discussed the hexagonal form of the bee's honeycomb as the shape that holds the largest amount of honey; Kepler states that hexagonal patterns require the least amount of wax; Charles Darwin described the honeycomb as a masterpiece of engineering "absolutely perfect in economizing labor and wax". As reported by [40] "mathematician Thomas C. Hales has recently formulated a proof of the so-called honeycomb conjecture, which holds that a hexagonal grid represents the best way to divide a surface into regions of equal area with the least total perimeter", finally stating that "the honeybee's honeycomb fits neatly into the atlas of mathematically optimal forms found in nature"[40], and can be considered as the two dimensional version of the three dimensional Kelvin problem [21] (i.e. the search for surface minimizing partition of space into cells of equal volume).

Material design engineering has already retrieved this idea, and has exploited the benefits of beehive configurations for creating honeycomb structure which provides a man-made, composite, material with minimal density and relative high out-of-plane compression and shear properties, thereby obtaining high efficiency (strength- or stiffness-to-weight ratio).

In chapter 5 and 6 the results of a wide research activity is reported, starting from the idea that natural structures, as well as cross-fertilization between science and engineering, can provide a radically new repertoire of architectural forms and structural systems for tall buildings. In particular in chapter 5 hexagon-based patterns are examined as tube structural grids for tall building.

2 Design criteria for diagrid tall buildings: stiffness vs. strength

The procedures and formulations suggested in literature for the design of diagrid structures start from the assumption that diagonal sizing process is governed by the stiffness requirements, as usually occurs for other, less efficient, structural types, and that member strength demand is automatically satisfied by the cross section resulting from the stiffness requirements. However, thanks to the high rigidity of the diagonalized façade, strength requirements can be of paramount importance, and even be the governing design criterion. In this chapter, stiffness and strength design criteria for diagrid structures are examined and translated in simplified formulae for quick member sizing. The application of the two approaches for the design of a 100 story building model, carried out for different diagrid geometrical patterns, gives the opportunity of discussing the relative influence of stiffness and strength on the design outcomes, in terms of resulting diagonal cross sections and steel weight, as well as on the structural performance.

2.1 Introduction

The procedures and formulations in literature suggested by Moon in [30], [31] start from the assumption that diagonal sizing process is governed by the stiffness requirements, as usually occurs for other, less efficient, structural types, and that member strength demand is automatically satisfied by the cross section resulting from the stiffness

requirements. However, in a recent paper finalized to the assessment of the structural behavior of diagrid buildings [25], the authors have pointed out that, thanks to the high rigidity of the diagonalized façade, strength requirements can be of paramount importance, and even be the governing design criterion. As also reported in [37] with reference to the Swiss Re building, "the sizing of the steel elements is governed by strength criteria – the total sway stiffness of the diagrid is sufficient to limit the wind sway to 50 mm over the full 180 m height and provides a very good level of overall dynamic performance".

Therefore the major question addressed in this chapter could be formulated as: to what extent stiffness and strength criteria affect the design of diagrid structures?

Providing a comprehensive answer to such question is a non trivial issue. For this purpose, the stiffness-based design criterion proposed by Moon is firstly reviewed and applied for the design of a 100 story building model, by adopting different diagrid geometrical pattern, i.e. different values of the diagonal angle. Simple formulae for deriving strength demand in the members are defined and applied for alternative "strength-based" design solutions.

The two sets of diagrid structural solutions, the ones designed according to stiffness requirements and the ones designed according to strength requirements, are then compared in terms of resulting diagonal cross sections and steel weight. Further, structural analyses of the two sets of diagrid structures under gravity plus wind load are carried out, allowing for a complete assessment of the structural response. Discussion in terms of different response parameters, i.e. top displacement, interstory drift, member strength demand to capacity ratio, is presented also considering the unit steel weight of each single solutions, and design implications are emphasized.

2.2 Definitions – geometry and loads

In order to apply the design methodologies provided in this paper, the diagrid pattern must be preliminarily defined from the geometric point of view. The unit cell of the pattern is the diagrid module, usually extending over multiple floors, which repeats horizontally along the building perimeter and stacks vertically along elevation. The main geometrical parameters of the module and of the global pattern are (Figure 2-1): the diagonal angle (θ), the diagonal length (L_d), the module height (h), the number of modules along elevation n_m, the number of modules along the perimeter n_k, the number of diagonals on each façade (n_x and n_y).

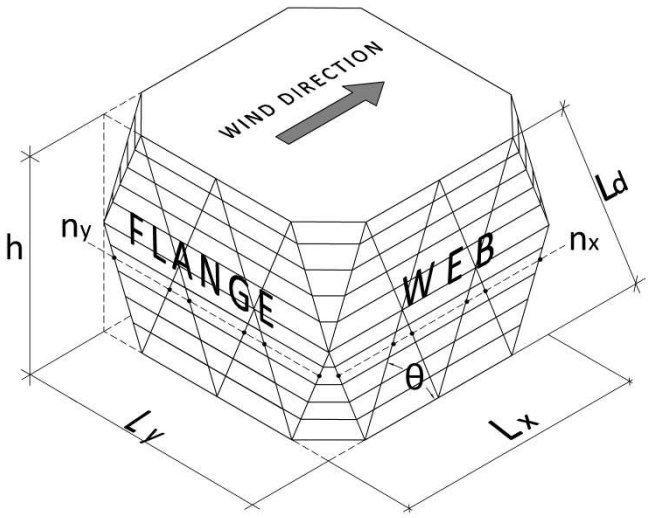

Figure 2-1 Geometrical parameters of the diagrid module

The geometrical attributes of the module and of the global pattern are interrelated parameters, function of the diagrid module as it applies to global building dimensions, i.e. the plan dimension along X and Y,

respectively L_x and L_y, and the building height, H. Quite trivially, the following geometrical relationships can be established:

$$n_k = 2\left(n_w + n_f\right);\ h = \frac{H}{n_m};\ L_d = \frac{h}{sen\theta} \tag{2.1}$$

$$L_{x,y} = \frac{n_{x,y}\ \ L_d \cos\theta_{x,y}}{2};\ \theta_{x,y} = arctg\left(\frac{H\ n_{x,y}}{2\ L_{x,y} n_m}\right) \tag{2.2}$$

The unit cell of the pattern is the diagrid module, usually extending over multiple floors, which repeats horizontally along the building perimeter and stacks vertically along elevation. The main geometrical parameters of the module and of the global pattern are: the diagonal angle (θ), the diagonal member length (L_d), the module height (h), the number storey covered by a single module (n_{st}), the number of modules along elevation (n_m), the number of modules along the perimeter (n_k) and the number of diagonals on each façade (n_{dg}).

The geometrical attributes of the module and of the global pattern are interrelated parameters, function of the diagrid module as it applies to global building dimensions, i.e. the plan dimension, L, the total and the interstory heights, H and h_i, respectively.

The division of the building shaft into diagrid modules is also usefully employed for the structural design and assessment. Since the module usually extends over multiple floors, load are transferred to the module at every floor level, and load effects varies along the diagonal length. However, considering that a single cross section is adopted for the diagonal along the global module height, i.e. diagonal section only varies from one module to another, the loads utilized for the design of a specific diagonal are the ones obtained at the base of the relevant module.

The gravity load (Q_m), the shear force (V_m) and the overturning moment (M_m) for the m_{th} module can be derived as:

$$Q_m = \sum_{i=1}^{m_0} Q_i \; ; \; V_m = \sum_{i=1}^{m_0} V_i \; ; \; M_m = \sum_{i=1}^{m_0} V_i z_i \tag{2.3}$$

where i=1 and i=m_0 correspond respectively to the top level of the building and the base level of the m_{th} module, Q_i is the i-th floor gravity load (unit gravity load multiplied by the total floor area), V_i is the shear force due to wind loads at the i-th floor and z_i is the vertical distance between the top of the building and the m_o level.

2.3 Stiffness-based design

The first design procedure examined in this chapter is based on stiffness requirements and has been originally proposed by [30], [31]. The procedure is based on the results of wide parametric analyses that emphasized the major role of the geometrical attributes of the diagrid pattern, primarily of the diagonal angle θ, on the structural efficiency. In the following, it is briefly reviewed and the formulae for deriving the diagonal cross sections are established.

By making the classical assumption that the building structure under lateral loads behaves as an ideal cantilevered tube, i.e. neglecting the shear lag effects, uniform tensile and compressive force distributions arise in the leeward and windward faces, respectively, as a consequence of the global overturning moment, while the faces parallel to the wind direction are subject to shear forces. The lateral stiffness of the structure which counteracts these global actions is given by the sum of two components, i.e. flexural and shear. Moon suggests simplified criteria for

specifying the optimal ratio between flexural and shear stiffness components as a function of the building slenderness H/B; once a target value of the building top displacement is set, preliminary design formulae for deriving the diagonal member size, on web and flange sides, are provided.

The limit value of the horizontal displacement at the top of the building (u_H) is a design parameter, usually expressed as a percentage of the building height (a typical value is H/500). As mentioned before, it is possible to consider u_H as the sum of contributions due to bending and shear deformations:

$$u_H = \gamma \cdot H + \frac{\chi \cdot H^2}{2} \tag{2.4}$$

where γ and χ are respectively the shear and the bending deformations. Once the limit value of u_H is fixed, eg. u_H=H/500, the design values of the deformation components in equation (2.4) (appointed as γ^* and χ^*), are not univocally determined, since the same target displacement can be obtained by different shares of the bending and shear deformations. However, depending on the building slenderness, optimal values of the relative bending to shear deformation ratio can be established, according to Moon [30], [31].

In particular, defining the "s" factor as the ratio of the bending to shear deformation at the top of the building, i.e.:

$$s = \frac{\left(\frac{\chi^* \cdot H^2}{2}\right)}{(\gamma^* \cdot H)} = \frac{H \cdot \chi^*}{2 \cdot \gamma^*} \tag{2.5}$$

The following empirical formulations for the optimal value of s, using the diagrid weight as term of comparison, are suggested:

$$s1 = \left(\frac{H}{B} - 2\right) \qquad for\ \frac{H}{B} \geq 6\ and\ 60° < \theta < 70° \tag{2.6}$$

$$s2 = \left(\frac{H}{B} - 3\right) \qquad for\ \frac{H}{B} \geq 5\ and\ 60° < \theta < 70° \tag{2.7}$$

From which the design values as γ^* and χ^* for the shear and bending deformations can be derived:

$$\gamma^* = \frac{1}{(1+s)\cdot 500} \tag{2.8}$$

$$\chi^* = \frac{2s}{H\cdot(1+s)\cdot 500} \tag{2.9}$$

Considering that the required shear and bending stiffness of the module (K_T^* and K_β^*) are given by:

$$K_T^* = \frac{V_m}{\gamma^*\cdot h} \tag{2.10}$$

$$K_\beta^* = \frac{M_m}{\chi^*\cdot h} \tag{2.11}$$

On the basis of purely geometrical considerations, the cross section areas of the diagonal member on the web and flange plane, in the m-th module, $A_{d,m,w}$ and $A_{d,m,f}$, respectively, are obtained:

$$A_{m,d,w} = \frac{V_m\cdot L_d\ (1+s)\cdot 500}{2n_w E h\ cos^2\theta} \tag{2.12}$$

$$A_{m,d,f} = \frac{2M_m L_d H(1+s)\cdot 500}{n_f L^2 E h \sin^2\theta \ 2s} \tag{2.13}$$

Where, in addition to the parameters already defined, E is the Young modulus of the diagonal structural material; L is the plan dimension of the building parallel to the considered wind direction (Figure 2-1), which, in the case of rectangular floor shape, should be set both $L=L_X$ and $L=L_Y$, depending on the wind direction.

2.3.1 Alternative definition of the parameter s

Making reference to a prismatic cantilever beam under uniform distributed load, q_w, according to the Eulero-Bernoulli and Timoshenko beam theories, the transversal displacement due to shear (u_χ) and bending (u_γ) flexibilities are respectively given by:

$$u_\chi = \frac{q_w H^4}{8\,EI} \tag{2.14}$$

$$u_\gamma = \frac{q_w H^2}{2\,GA_s} \tag{2.15}$$

where G is the transversal elasticity moduli of the structural material, I and A_s are respectively the moment of inertia and the shear area of the beam cross section.

The factor s can be defined as the ratio of the above expressions for u_χ and u_γ, i.e. :

$$s = \frac{u_\chi}{u_\gamma} = \frac{1}{4}\frac{GA_s H^2}{E\,I} \tag{2.16}$$

Shifting the discussion to the building behavior, and assuming that shear force is only carried by the diagonals on the web sides and overturning moment by the diagonals on the flange sides, it is possible to write:

$$A_s = 2\, n_w A_{d,w} \cos_\theta \tag{2.17}$$

$$I = n_f A_{d,f} \operatorname{sen}_\theta \mathrm{L}^2 \tag{2.18}$$

Substituting in (2.16):

$$s = \frac{1}{2}\frac{G}{E}\,\frac{n_w A_{d,w} cos_\theta\, H^2}{n_f A_{d,f} \operatorname{sen}_\theta \mathrm{L}^2} \tag{2.19}$$

Considering that $n_w A_{d,w}$ should be equal to $n_f A_{d,f}$, it is possible to write:

$$s = \frac{1}{2}\frac{G}{E}\,\frac{cos_\theta}{\operatorname{sen}_\theta}\,\frac{H^2}{\mathrm{L}^2} \tag{2.20}$$

For the steel material, ν=0,3 and the ratio between G and E is equal to 0,38; therefore the s value is finally given by:

$$s = \frac{0.19}{\tan_\theta}\left(\frac{H}{\mathrm{L}}\right)^2 \tag{2.21}$$

It is worth observing that the equation (2.21) provides s values as function of both building slenderness and diagonal angle, while the equations (2.6) and (2.7) establish a dependence of s on building slenderness only. In the following, the values of s calculated according to equation (2.21) are appointed as s3. Figure 2-2a and b show the

comparison among the values s1, s2 and s3, obtained by means the relationships (2.6) (2.7) and (2.21), respectively.

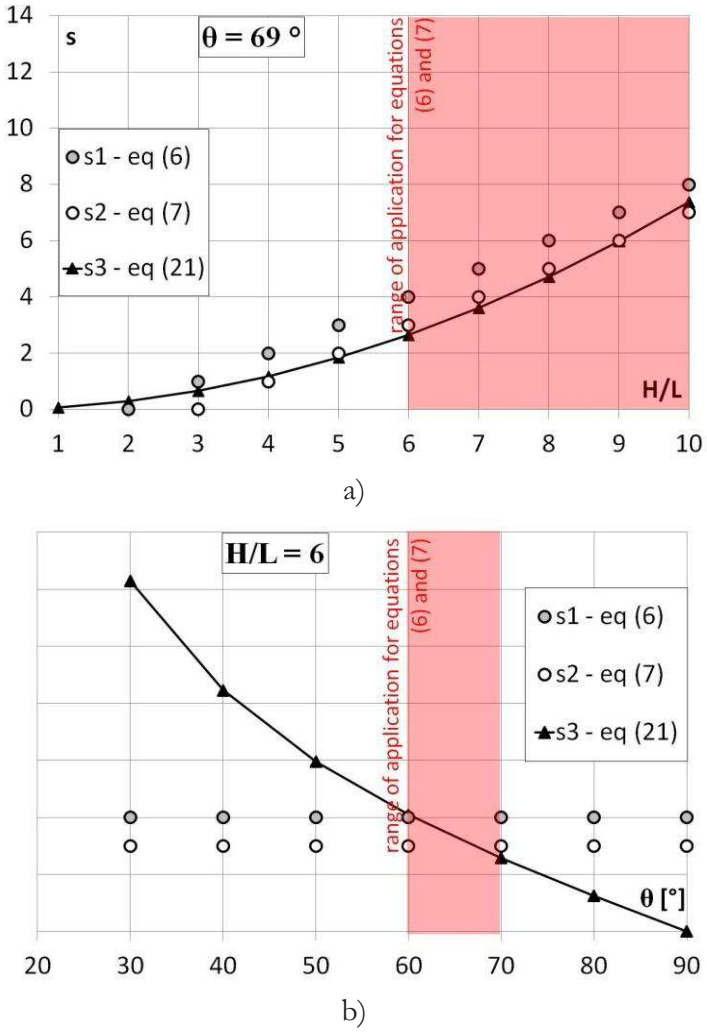

Figure 2-2 a) Parameter s vs. building aspect ratio, fixing θ=69°; b) Parameter s vs diagonal angle, fixing H/B=6

2.4 Strength based design

The second approach considered is based on strength requirements. For this purpose, the same geometrical definitions and load assumptions discussed in section 2.2 are adopted. Following the gravity and wind load paths and considering the predominant resisting mechanism in the diagrid pattern, the procedure suggests simplified formulations for deriving compression and tension axial forces in the diagonals, thus cross sections areas result from member strength and stability checks.

The gravity loads give rise to a global downward force on the generic diagrid module (Figure 2-3), identified by the subscripts m and k along the building elevation and perimeter, respectively. Assuming that the central core occupies the 25% of the floor area, the perimeter diagrid shares the 37,5% of the floor gravity load. The gravity downward load on each module ($F_{m,k,G}$) is given by:

$$F_{m,k,Q} = \frac{0{,}375\ Q_m}{n_k} \tag{2.22}$$

The diagonals under this gravity downward load are both in compression (Figure 2-3), with axial force given by:

$$N_{m,k,Q} = \frac{F_{m,k,G}}{2\ sen_\theta} \tag{2.23}$$

Substituting:

$$N_{m,k,Q} = \frac{0{,}375\ Q_m}{n_k}\ \frac{1}{2\ sen_\theta} \tag{2.24}$$

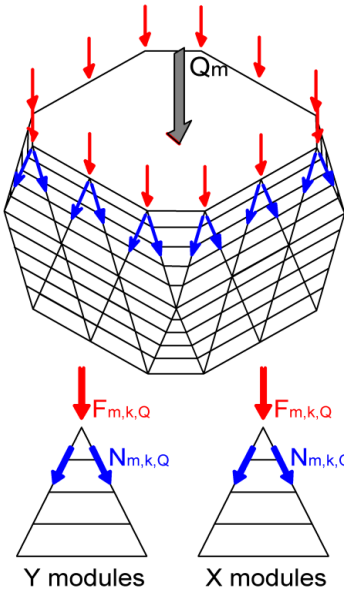

Figure 2-3 Axial forces in diagonals of the k_{th} triangular scheme of the m_{th} module for gravity loads

Horizontal wind load globally causes overturning moment and shear force. The overturning moment (M_m) acting at the m-th level gives rise to a vertical force in each k-th module ($F_{m,k,M}$), whose direction (downward or upward) and intensity depend on the plan position of the module itself (Figure 2-4a), as expressed in following equation:

$$F_{m,k,M} = \frac{M_m \cdot d_k}{\sum_{i=1}^{n_k} d_i^2} \tag{2.25}$$

where d is the distance of the module from the centroid of the plan shape (Figure 2-4a). The diagonals of the module on the windward building face are both in compression, while the ones on the leeward face are both in tension. The axial forces in the diagonals of the generic module are given by:

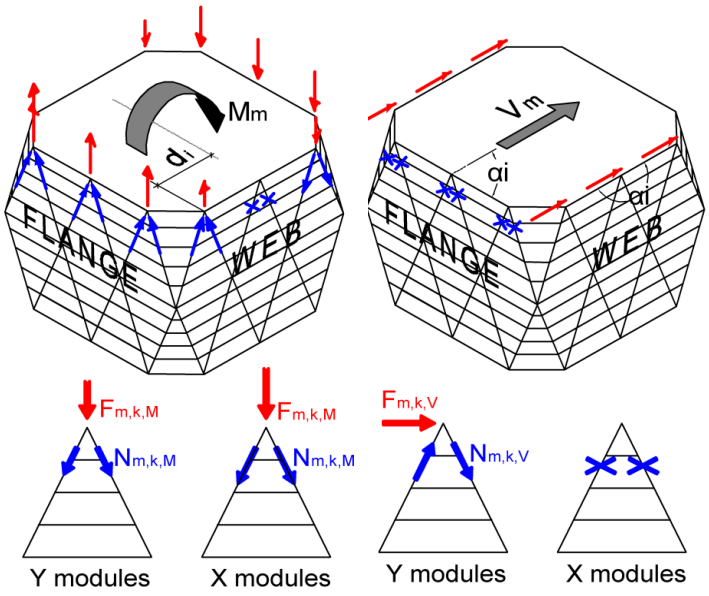

a) b)

Figure 2-4 Axial forces in diagonals of the k_{th} triangular scheme of the m_{th} module for a) overturning moment, M_m; b) global shear, V_m

$$N_{m,k,M} = \pm \frac{F_{m,k,M}\ sen_\theta}{2} = \pm \frac{M_m \cdot d_k}{\sum_{i=1}^{n_k} d_i^2}\ \frac{sen_\theta}{2} \tag{2.26}$$

The global shear force acting at the m-th level (V_m) gives rise to a horizontal force in each k-th module ($F_{m,k,V}$), which intensity depends on the angle of the module with the direction of wind (α) (Figure 2-4b):

$$F_{m,k,V} = \frac{V_m \cdot cos_{\alpha,k}}{\sum_{i=1}^{n_k} cos_{\alpha,i}} \tag{2.27}$$

Under this horizontal force, one diagonal of the module is in compression while the other is in tension. The diagonal axial force is given by:

$$N_{m,k,V} = \pm \frac{F_{m,k,V}\ cos_\theta}{2} = \pm \frac{V_m \cdot cos_{\alpha,k}}{\sum_{i=1}^{n_k} cos_{\alpha,i}}\ \frac{cos_\theta}{2} \qquad (2.28)$$

Under both gravity and wind loads, the axial force in the diagonals of generic the diagrid module, can be calculated as the sum of the three contributions above, i.e.:

$$N_{dg,i,k} = N_{dg,k,G} + N_{dg,i,k,M} + N_{dg,i,k,V} =$$
$$= \frac{0{,}375\ Q_m}{n_k}\ \frac{sen_\theta}{2} \pm \frac{M_m \cdot d_k}{\sum_{i=1}^{n_k} d_i^2}\ \frac{sen_\theta}{2} \pm \frac{V_m \cdot cos_{\alpha,k}}{\sum_{i=1}^{n_k} cos_{\alpha,i}}\ \frac{cos_\theta}{2} \qquad (2.29)$$

Once the axial force in the diagonals has been computed, the cross section area can be sized according to strength and stability requirements.

2.5 Design applications

With the aim of comparing the results of the two proposed design approaches, an application to a building model has been defined. Three different diagrid patterns have been considered (Figure 2-5b, c and d) for a building model with rectangular plan 65 x 40 m, and 100 stories, with a total height of 332,3 m (Figure 2-5a). To define completely the diagrid geometries, the diagonal angle (θ=64°, θ=69° and θ=79°) and the total number of modules (i.e. $n_{m\text{-}64}$= 12,5 , $n_{m\text{-}69}$=10 and n_m= 8) have been set, while the others geometrical parameters have been calculated using equations (2.2) (tab. 2.1).

In each geometrical configuration the height of the diagrid modules on the two façades are the same; the module width is slightly different, i.e.

13 m on the broad side and 13,3 m on the short side. Of course, in the three geometrical patterns the height of the module is different (tab. 2.1, Figure 2-6 and Figure 2-7), comprising 8, 10 and 20 stories, respectively for θ=64°, θ=69° and θ=79°.

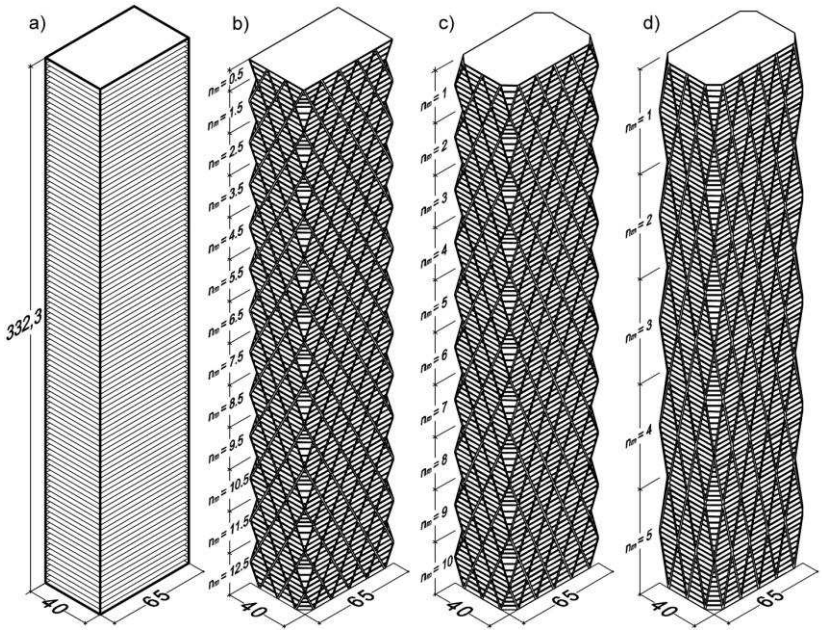

Figure 2-5 a) Building model; b) Diagrid pattern with θ=64°; c) Diagrid pattern with θ=69°; d) Diagrid pattern with θ=79°

θ [°]	64°	69°	79°
n_m [-]	12,5	10	5
h [m]	26,6	33,23	66,5
L_d [m]	29,6	35,7	67,7
n_x [-]	10	10	10
n_y [-]	6	6	6
n_k [-]	16	16	16

Table 2-1 Geometrical parameters for the three diagrid patterns

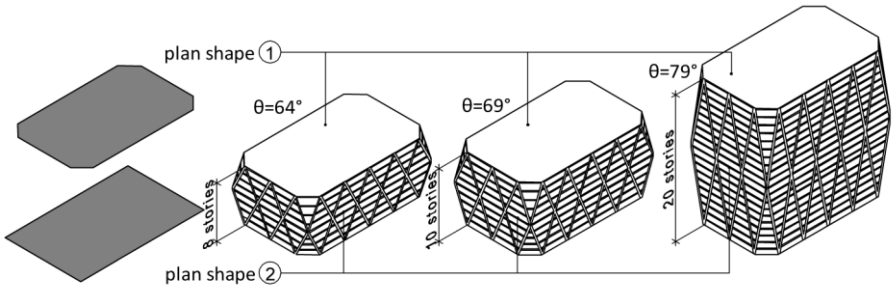

Figure 2-6 Plan variations in the diagrid module for the three diagrid patterns

The framing floor structure is depicted in Figure 2-8; the dead load is 7 kN/m^2 including the contributions of the floor steel structure, internal partitions and external claddings. The live load contribution has been assumed equal to 4 kN/m^2. The horizontal load due to wind pressure has been calculated (Figure 2-9) according to ASCE-7 provisions, on the basis of wind speed equal to 40 m/s (90 mph) (see tab 2).

The three diagrid solutions for the building model have been designed both with stiffness and strength approaches, as reported in following subsections. Built-up box sections, with welded plates made of steel S275 (f_{yk}= 275 MPa, f_{tk}=430 MPa), are adopted for the diagonals.

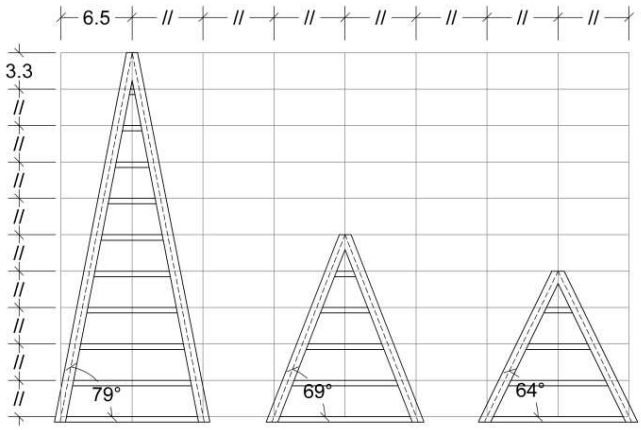

Figure 2-7 Geometry of triangular schemes for the three diagrid patterns

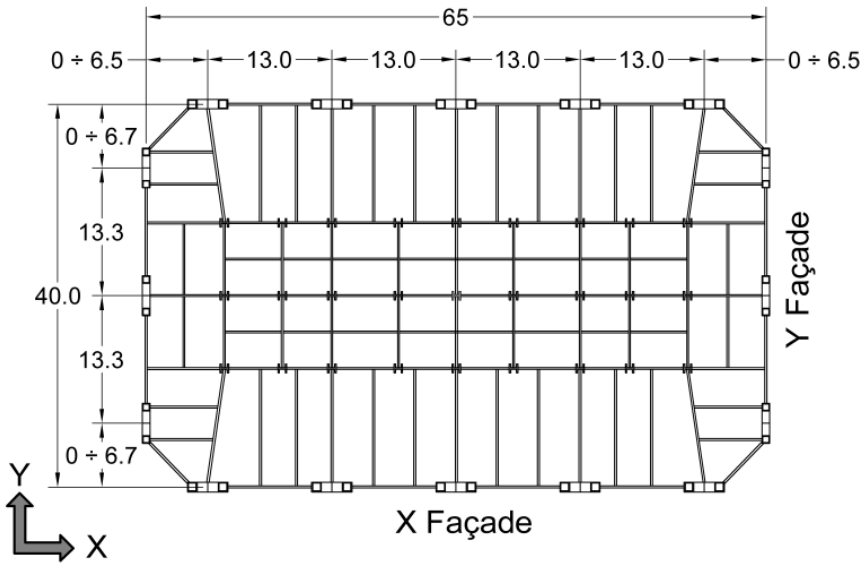

Figure 2-8 Typical framing floor structure

GRAVITY LOAD [kN/m^2]	
Dead	7
Live	4
HORIZONTAL LOAD – WIND	
Wind base shear [MN]	
x direction	19,0
y direction	34,9
Wind overturning moment [MN m]	
x direction	3346,2
y direction	5978,1

Table 2-2 Loads assumed in the analysis

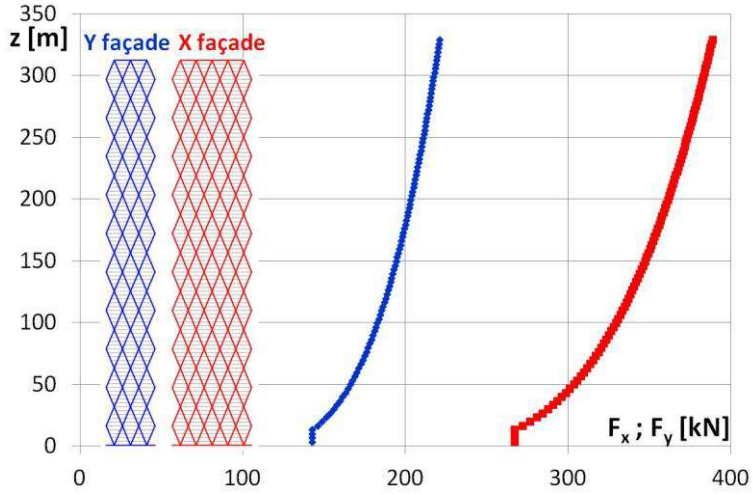

Figure 2-9 Horizontal loads due to wind action

2.5.1 Stiffness approach

The aspect ratio for a building with a rectangular plan is function of the considered plan direction. Assuming the coordinate system reported in Figure 2-8, for the building model the aspect ratios are: H/B_X = 5.11 and H/B_Y = 8.31. According to equations (6), (7) and (21), two values of the s factor have been calculated (see tab. 3); as already observed, only the equation (21) proposed in section 3.1 gives s values depending on the diagonal angle.

The three diagrid structures are divided into stacking modules along the building elevation (12.5 modules for θ=64°, 10 modules for θ=69° and 5 modules for θ=79°, see Figure 2-5) and the diagonals of each module have been sized according to the stiffness criterion using equations (2.12) and (2.13). The resulting box sections vary from 1000x1000 mm to 300x300 mm, with thickness varying between 100 mm and 20 mm.

In order to find the most efficient solution in terms of diagrid structural weight, the design process has been iterated varying the parameter s between 1 and 10; the results, diagrid structures all satisfying the top drift limit of H/500 with different steel material consumption, are shown in Figure 2-10 for the three different angles in terms of unit steel weight (i.e. total diagonal weight divided by the gross floor area). It is worth noticing that the optimal value of s is strongly affected by the diagonal angle, resulting s_{64}=3.3, s_{69}=2.53 and s_{79}=1.27; however the curves depicted for θ=64° and θ=69° show a wide range of s values corresponding to solutions characterized by similar structural weights, namely s between 2 and 6 for θ=64°, and s between 2 and 4 for θ=69°. The curve for θ=79° shows a steeper trend, suggesting similar structural weight, i.e. equally efficient solutions, only for s between 1 and 2.

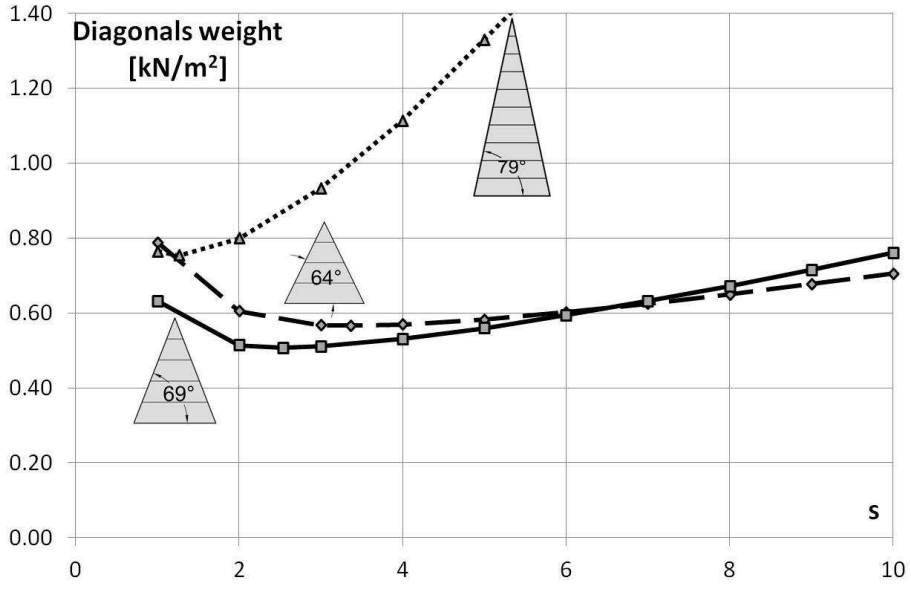

Figure 2-10 Unit steel weight (diagrid only) as function of s

ù

Comparing these values to the ones provided in tab.2-3, it can be observed that they are closer to the s_x values (broad side) than to the s_y values (short side). Figure 2-11 shows the comparison among the optimal values derived from equations (6), (7), (21), and the optimal values obtained by means of the design iterations; the range of s values for which the structural solutions show almost no scatters is also depicted in the chart.

Equation	s_X	s_Y
s1 – (eq. 6)	2.11	5.31
s2 – (eq.7)	3.11	6.31
s3 – (eq. 21)		
for $\theta = 64°$	2.45	6.47
for $\theta = 69°$	1.93	5.10
for $\theta = 79°$	0.98	2.58

Table 2-3 Values of the s factor

The unit steel weight of the final design solutions obtained for the three diagrid patterns are compared in Figure 2-13; the solution $\theta=69°$ is the most advantageous, having a structural weight of the steel diagrid equal to 0.51 kN/m^2. The solution with $\theta=79°$, instead, is the heaviest one with a structural weight of 0.75 kN/m^2. These results are consistent with the ones obtained in [30] by means of parametric analyses.

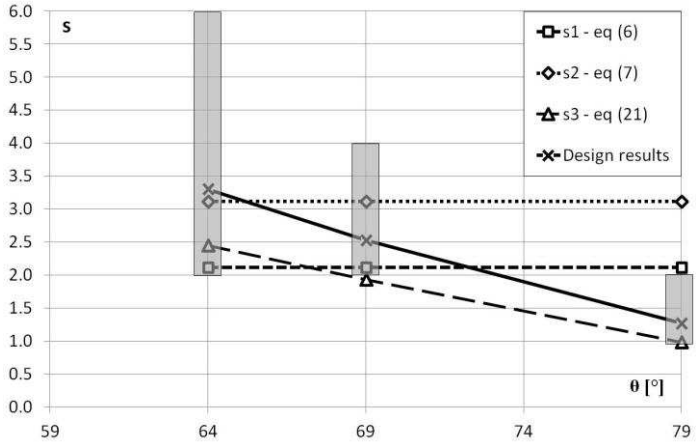

Figure 2-11 Comparison among the values of s obtained as design results and according to simplified formulations

2.5.2 Strength approach

The three diagrid patterns have also been designed on the basis of strength requirements, by using equation (2.29) and assuming S275 steel grade for the diagonal members.

The comparison between the diagonal cross sections obtained according to stiffness (black bars) and strength (grey bars) approaches is shown in e) f)

Figure 2-12; in particular the charts a) and b) refer to diagrid with θ=64°, for x and y façade respectively; the charts c) and d) refer to diagrid with θ=69°, for x and y façade respectively; the charts e) and f) refer to diagrid with θ=79° for x and y façade respectively. The cross sectional areas for the diagonal members are equal to the maximum values obtained considering both x and y wind direction, therefore considering each diagrid façade acting both as web and flange.

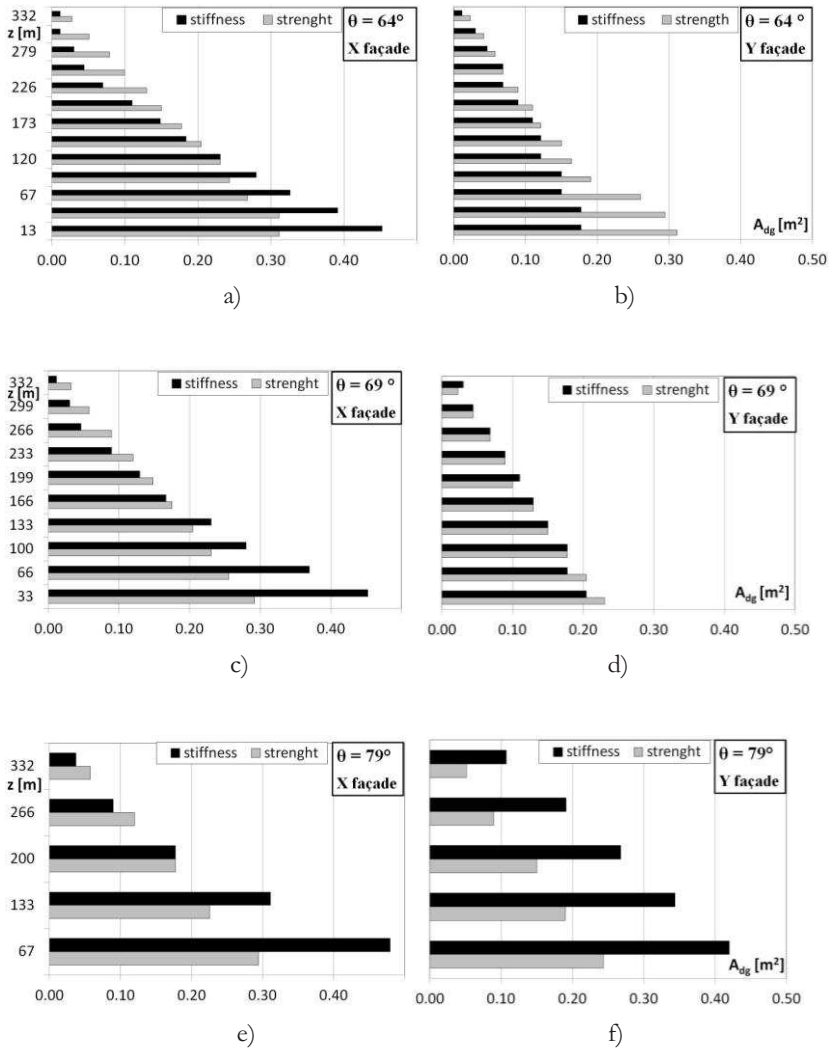

Figure 2-12 Diagonal cross sections: comparison between stiffness (black bars) and strength approach (grey bars). a) and b) θ=64°; c) and d) θ=69°; e) and f) θ=79°

First of all it can be stated, simply observing the chart scales, that larger section areas are required for the diagonals on the broad side than on the short side. Further, stiffness requirements generally govern the design in the lowest modules, while strength requires larger sections in the upper modules. However, a different trend of the governing criterion along elevation can be observed considering the broad and the short side of the building, as well as considering the three different diagrid patterns.

More in detail, for the building broad side, strength always prevails over stiffness at the upper modules; the point where the governing demand switches from stiffness to strength is approximately 120 m, 150 m and 200 m (36%, 45% and 60% of H) respectively for θ=64°, 69° and 79°.

On the building short side, strength prevails over stiffness throughout the elevation for the solutions θ=64°; on the contrary, for θ=79°, stiffness demand always governs the diagonal sizing along the height. In the solution with θ=69° the cross sections required for stiffness and strength are almost the same along elevation, suggesting that the two design criteria tend to converge as the diagonal angle approaches the optimal value, that is also the most efficient (i.e. the lightest) solution.

The comparison of the structural weight reported in Figure 2-13 suggests that the strength-design solution for the diagrid with θ=64° is heavier than the stiffness counterpart, while, conversely, the stiffness-design solution for θ=79° is heavier than the strength counterpart; for the structure with θ=69° the weight of the two solution is only slightly different (0.50 vs. 0.54 kN/m^2), as expected on the basis of the previous observation.

Generally speaking, on the basis of the above results it can be stated that the geometrical configuration, i.e. the diagonal angle, has a strong effect in determining the prevalent design criterion and the resulting structural weight. Further stiffness and strength approaches are both necessary and

unavoidable; they are not separately sufficient for an exhaustive sizing process of the diagonal members.

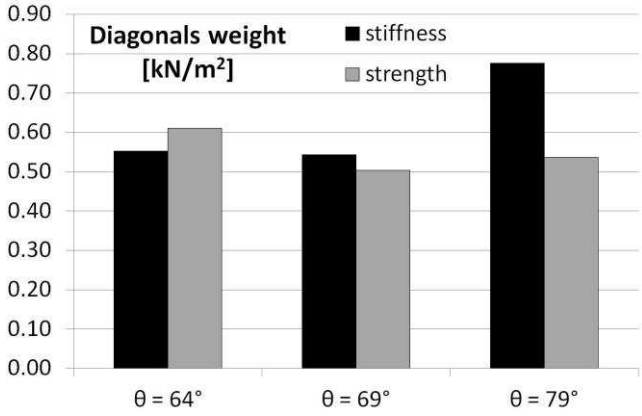

Figure 2-13 Unit steel weight (diagrid only) for the three diagonal angles – stiffness (black bars) vs. strength (grey bars) approach

2.6 Structural analyses and performance assessment

The structural diagrid solutions considered for the building model, by varying the diagonal angle and the cross sections, as obtained with the stiffness and strength approaches, are analyzed using FEM numerical models (see Figure 2-14). Factored gravity and wind loads previously specified (tab 2.2) have been applied to the models; the wind load has been applied both along X and Y directions of the building plan.

The results of the numerical analyses are expressed in terms of some major response parameters, which jointly allow for a complete assessment of the structural performance, i.e. horizontal displacements, u, interstory drifts, d_h, demand to capacity ratio in the diagonal members, DCR; the latter is defined as the tension/compression axial force normalized to the yield/buckling capacity of the relevant member.

The results are shown in Figure 2-15 (for θ=64°), Figure 2-16 (for θ=69°) and Figure 2-17 (for θ=79°); in each figure, the charts appointed by the letters a and b refer to the results in terms of horizontal displacements for the stiffness and strength design solutions, respectively; the charts appointed by the letters c and d refer to the results in terms of interstory drifts, for the stiffness and strength design solutions, respectively; the charts appointed by the letters e and f refer to the results in terms of diagonal DCR for the stiffness and strength design solutions, respectively. In each chart, both the results for wind applied along X and Y directions of the building plan, are provided.

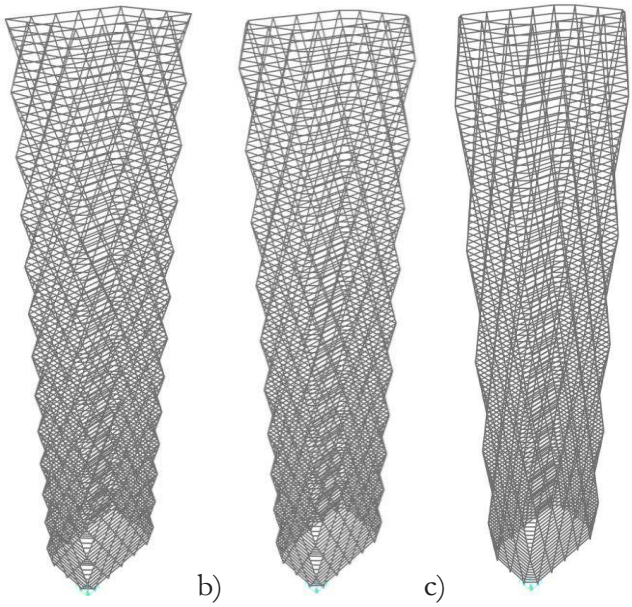

Figure 2-14 FEM models. a) θ = 64°; b) θ =69°; c) θ=79°

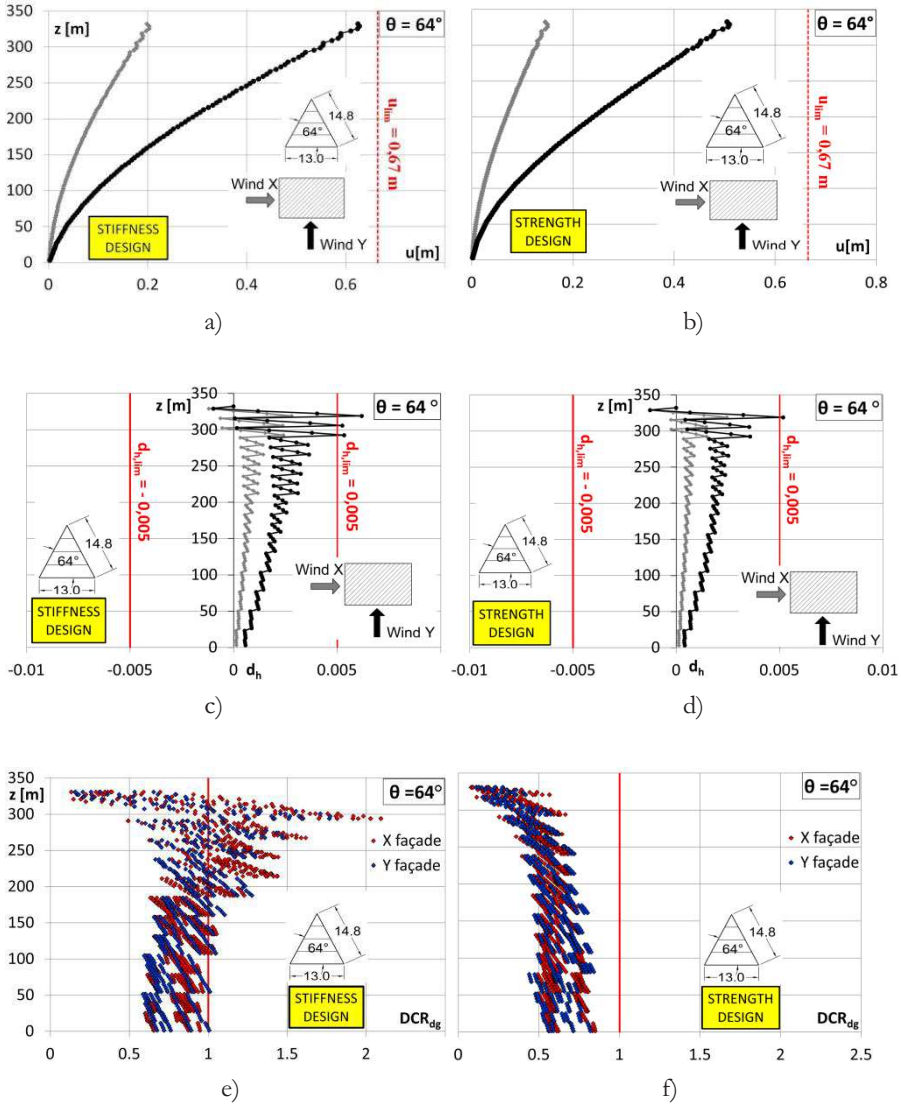

Figure 2-15 θ = 64°: a) and b) lateral displacement; c) and d) interstory drift; e) and f) DCR in diagonals

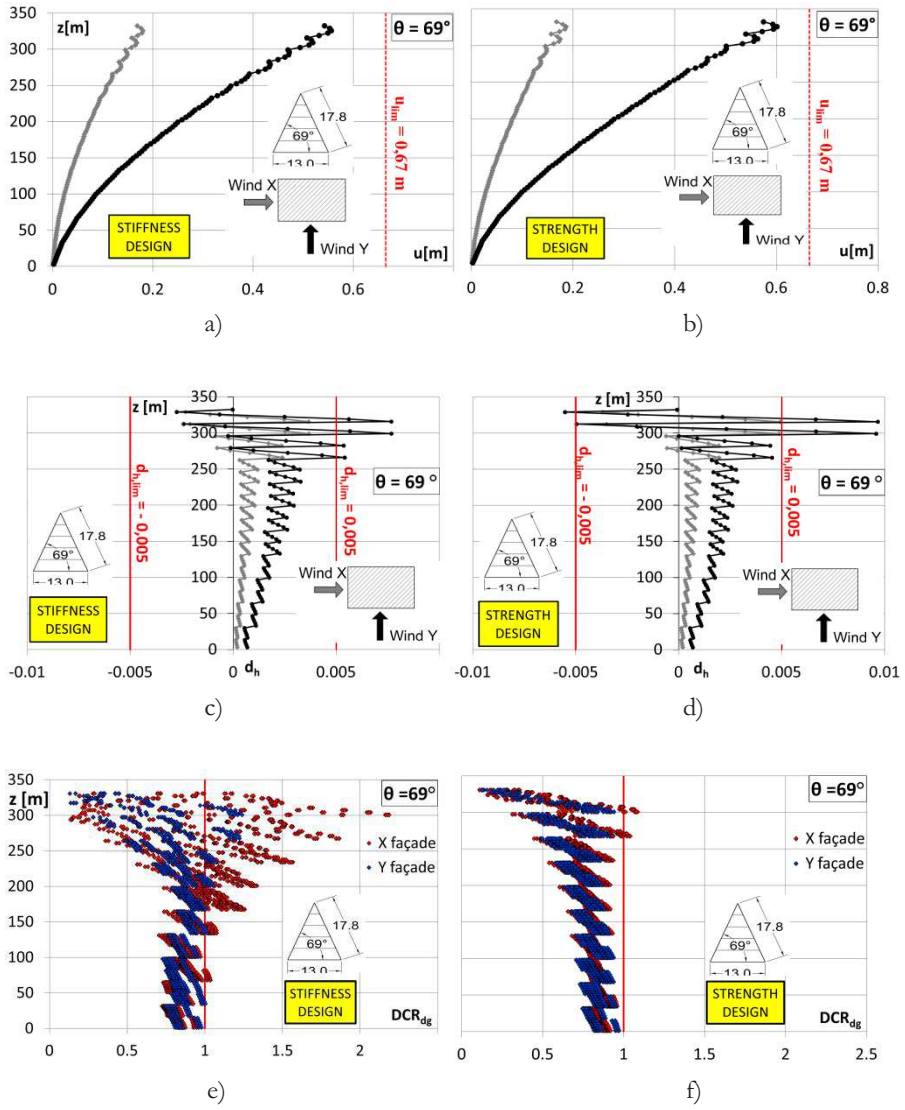

Figure 2-16 θ = 69°: a) and b) lateral displacement; c) and d) interstory drift; e) and f) DCR in diagonals

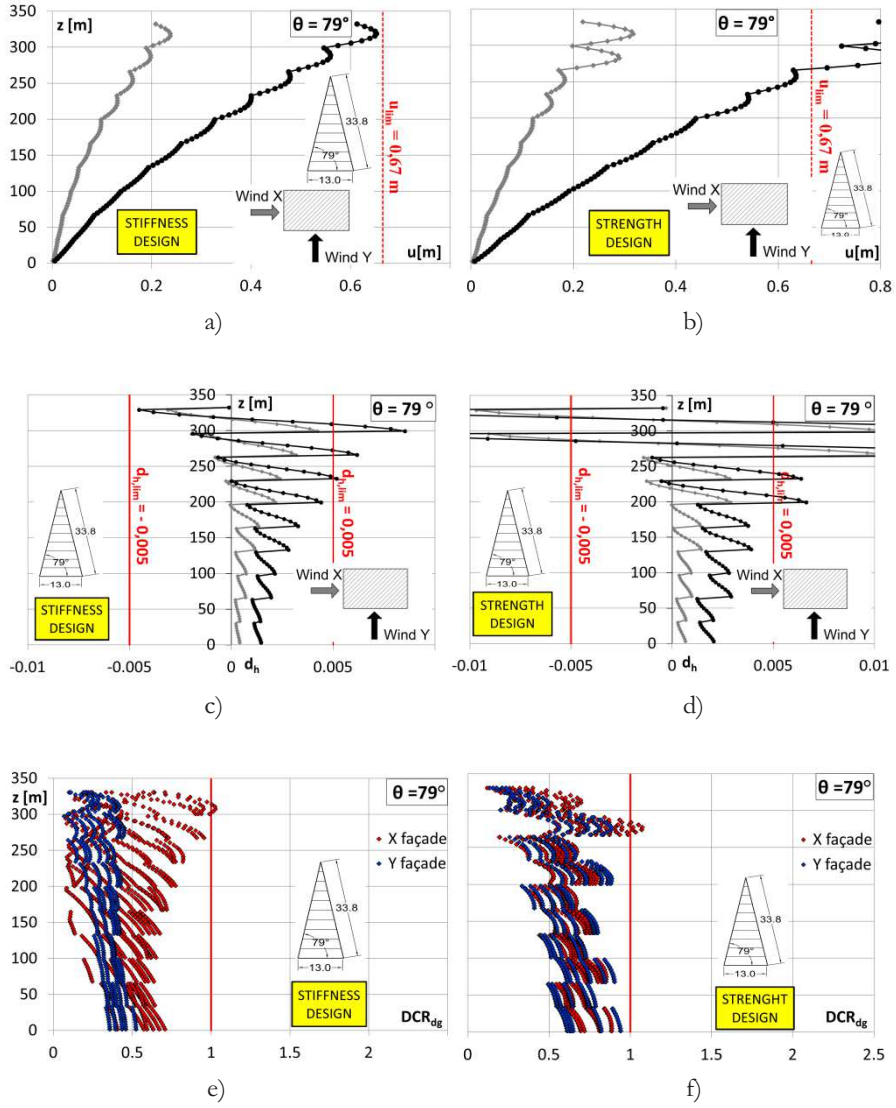

Figure 2-17 θ = 79°: a) and b) lateral displacement; c) and d) interstory drift; e) and f) DCR in diagonals

2.6.1 Diagrid structural solutions - stiffness design

A first consideration to be made by observing all charts of the horizontal displacements concerns the shape of the deformed configuration, clearly resembling an almost purely flexural behavior, thus confirming the great efficacy of diagrid structures in reducing the contribution of racking deformation.

The top horizontal displacement (Figure 2-15a, Figure 2-16a, Figure 2-17a) is always larger for wind load in Y direction (normal to the broad face) than in X direction. For all three geometrical configurations, the building top displacement is very close to the target value H/500 (i.e. 0,67 m), being equal to 0,63 m for θ= 64°, 0,62 m for θ=69°, 0,62 m for θ=79°.

An unsatisfactory performance can be observed in terms of interstory drift (Figure 2-15c, Figure 2-16c, Figure 2-17c) and DCR of diagonals (Figure 2-15e, Figure 2-16e, Figure 2-17e).

Concerning interstory drifts, none of the structural solutions meets the assumed limit $d_{h,lim}$ =0,5%; in particular, the maximum values of d_h increase with the diagonal angle, being equal to 0,62% for θ=64°, 0,77% for θ=69°, 0,85% for θ=79°. This issues will be deeply analyzed in Chapter 4; at this point of the thesis, it is just useful to underline that this effect mainly occurs at upper levels, where diagonals members are more flexible and slender than in lower modules; further it is the more evident the steeper is the diagonal angle, i.e. the longer is the diagonal member (L_d=29,6 m for θ=64°, L_d=35,7 m for θ=69°, L_d=67,7 for θ=79°) and the larger is the number of floors in a module.

The strength check for diagonals sized according to the stiffness procedure has been carried out considering the effects of both gravity and wind loads; the results are provided in terms of demand to capacity ratio (DCR) in Figure 2-15e for θ=64°, Figure 2-16e for θ=69°, Figure

2-17e for θ=79° and in Figure 2-18a for a global comparison. It can be observed that in the diagrid solution with θ=64° several members, almost one fourth of the total number (i.e. 824, 26% of elements), have DCR larger than 1; most of them are concentrated at the upper modules and equally distributed between X and Y sides. Also for θ=69°, several members have DCR larger than 1 (23% of elements), but they are mainly located on the broad side, in the upper half. On the contrary, only few diagonals (i.e. 8, 0,3 % of elements) are overstressed for θ=79°. For θ=64° and 69° the largest percentage of diagonals (around 75%) has DCR between 0,75 and 1, with a good exploitation of the cross section strength capacity.
Recognizing that the performance assessment in terms of DCR is strictly related to the steel material used in the stiffness-based design, the member strength/stability checks have been also carried out by adopting a higher steel strength, namely f_y = 355 MPa, which corresponds to the European steel S355 and approximately to the US steel Gr. 50. However, a large number of diagonals still have DCR larger than 1 also in these alternative solutions.

2.6.2 Diagrid structural solutions – strength design

The horizontal displacements of the diagrid structures designed according to the strength criterion (Figure 2-15b, Figure 2-16b, Figure 2-17b) are smaller than the stiffness-design counterparts for the solutions θ=64° and θ=69°; in particular the top displacement is respectively 0,51 m and 0,57 m, vs. 0,63 m and 0,62 m in the analogous stiffness-design solutions.
On the contrary, the strength-based design for the diagrid pattern characterized by θ=79° gives rise to a more flexible structure than the

stiffness-based design, and exhibits a top displacement ($\delta_{H,79°}$=0,80 m) that exceeds the design limit H/500 (equal to 0,67 m).

As already observed for the stiffness-based solutions, also the structures designed according to the strength approach do not respect the interstory drift limitation (Figure 2-15d, Figure 2-16d and Figure 2-17d), with maximum interstory drift values increasing with the diagonal angle ($d_{H,64°}$=0,52%; $d_{H,69°}$=0,97%; $d_{H,79°}$=1,99%).

The outcomes of the strength checks (Figure 2-15f, Figure 2-16f, Figure 2-17f and Figure 2-18b) show no diagonals, or almost no diagonals, with DCR larger than 1, namely 0 elements for θ = 64°, 17 elements (i.e. 0,53%) for θ = 69°, 8 elements (i.e. 0,3%) for θ = 79°.

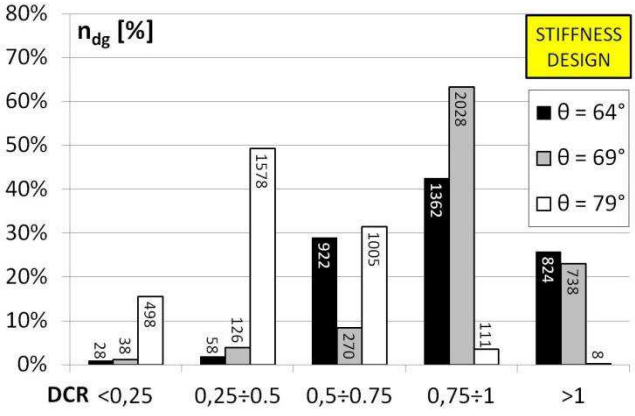

a)

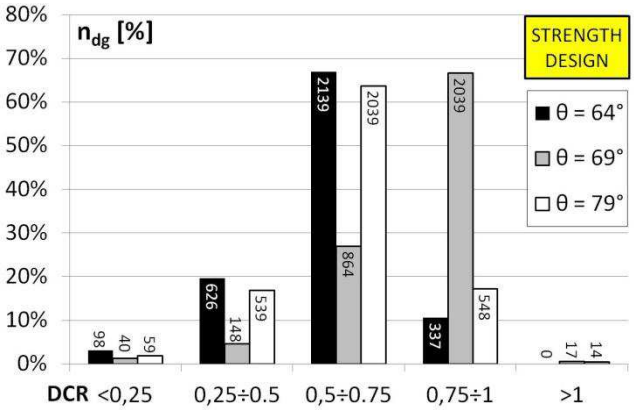

b)

Figure 2-18 Results of FEM analyzes. DCR in diagonals, comparison between stiffness (a) and strength (b) design.

2.7 Discussion of the results and design implications

The results of the structural analyses show that the two proposed procedure are both reliable, but none of them can be used without the other one. In fact, with reference to the specific case study, a 100-story building with rectangular plan and maximum slenderness H/B=8,31, it is

not possible to predict in a preliminary phase which will be the "predominant" approach, namely if either global stiffness demand or member strength demand will govern the design.

In particular the results show that in structures with low values of the diagonal angle (i.e. $\theta=64°$) the strength design is more stringent and drives to larger diagonal sections than stiffness design, throughout the short side of the building and along two third of the broad side elevation; while the opposite occurs in the case of steeper diagonal angles, where the stiffness thoroughly governs the design of diagonals on the short side. In the solution with $\theta=69°$ the cross sections required for stiffness and strength are almost the same along elevation, suggesting that the two design criteria tend to converge as the diagonal angle approaches the optimal value, that is also the most efficient (i.e. the lightest) solution.

It should be underlined that these results have been obtained for a single case study, therefore a wider range of building characteristics, wind loads, steel properties are currently being investigated in order to have a complete and definitive assessment of the problem.

It is worth to noticing that an overview of the structural behavior of some real diagrid structures, namely the Swiss Re Tower, the Hearst Tower and the Guangzhou West Tower [25], has given results that are well aligned with the ones obtained in this paper: in particular the analyses of the first two diagrid structures (Swiss Re and Hearst Towers) under horizontal plus vertical loads have shown high values of diagonal DCRs and building top displacement close to the design value (H/500). These results testify that thanks to the inherent high rigidity of the diagonalized façade, the sizing of the steel member is mainly governed by strength criteria.

Therefore, on the basis of the above considerations, it could be guessed that the design of diagrid buildings in the range of 40 stories (like Swiss Re and Hearst Towers) is mainly governed by strength, while for taller

buildings, like the one examined in this paper, both strength and stiffness criteria should be considered, and the predominance of one over the other is strictly related to the choice of the diagonal angle. Quite trivially, the outcomes of the two design criteria tend to converge in the optimal geometrical pattern that allows for the full exploitation of employed structural material and gives rise to the most efficient (i.e. the lightest) solution.

It should be also underlined that all diagrid structures considered in this paper show unsatisfactory performance in terms of interstory drift. However, this is a problem arising in all structure types characterized by a primary bracing system employing mega-diagonals which span over multiple floors, as in braced tubes and exoskeleton systems [1]. As deepen in the following Chapter 4, in the diagrid module as well as in the mega-diagonal, concentrated lateral loads are applied along the diagonal length, at the locations where intermediate floors intersect the diagonal member. Therefore, while the overall lateral stiffness of the building structure, thanks to the triangle configuration, strictly depends on the axial stiffness of the diagonal members, on the contrary, the lateral stiffness within the module length only relies on the flexural stiffness of the diagonals, that could not be adequate [38]. Of course the magnitude of this problem increase with the diagonal angle, or better, with the number of floor comprised in a single module.

2.8 Conclusive remarks

In this chapter stiffness and strength design criteria for diagrid structures are examined and translated in simplified formulae for quick member sizing.

The application of the two approaches for the design of a 100 story building model, carried out for different diagrid geometrical patterns, gives the opportunity of discussing the relative influence of stiffness and strength in the design process and on the design outcomes, expressed in terms of resulting diagonal cross sections and steel weight. Having recognized the major role of geometrical pattern attributes, criteria for selecting optimal solutions in terms of diagonal angle and share of bending to shear flexibility are identified.

The analytical assessment of the structural solutions under design loads allows for stating the following observations and remarks.

In general, stiffness and strength approaches are both necessary and unavoidable; they are not separately sufficient for an exhaustive sizing process of the diagonal members. Taking into account the design variables, i.e. the diagonal angle and the bending to shear flexibility ratio, even for a single, specific case study like the one here examined (100-story building, rectangular plan, maximum slenderness H/B=8,31), it is not possible to predict in advance which will be the "predominant" approach, namely if either global stiffness demand or member strength demand will govern the design.

As a guideline, it has been observed that in structures with lower values of the diagonal angle the strength design is more stringent and resulting diagonal members are larger than according to stiffness design, while the opposite occurs in the case of steeper diagonal angles, where the stiffness mainly governs the design.

It should be underlined that these results have been obtained for a single case study, therefore a wider range of building characteristics, wind loads, steel properties are currently being investigated in order to have a complete and definitive assessment of the problem.

Unacceptable performance in terms of interstory drift has been observed for all structural solutions designed in this study; in the case of lower

values of the diagonal angle, i.e. in the case of small number of multiple floors spanned by diagonals, an iterative design process can quickly converge to a satisfactory solution, while in the case of steeper angles, i.e. numerous floors comprised in a diagrid module, the need for a specific secondary bracing system arises (please see Chapter 4).

3 Geometrical patterns for diagrid buildings: exploring alternative design strategies from the structural point of view

In this chapter, a first step toward a systematic and comprehensive study of geometrical patterns for diagrids is provided. For this purpose, diagrid structures characterized by regular patterns (similar to the ones analyzed in chapter 1) are compared to alternative geometrical configurations, obtained by changing the angle of diagonals (variable-angle, VA) as well as by changing the number of diagonal (variable-density, VD) along the building height. Eight different diagrid patterns are generated and designed for a 90-story model building, according to procedures either provided in the literature or suggested by the authors. The resulting diagrid structures are assessed under gravity and wind loads and various performance parameters are evaluated on the basis of the analyses results. The comparison in terms of structural weights and performances finally allows for discussing efficiency potentials of the different patterns.

3.1 Introduction

The studies on the structural behavior, design criteria and performance assessment reported in the previous Chapter 1 regards geometrically regular diagrids, namely diagrid patterns obtained by the uniform

tessellation of a triangle base unit, characterized by constant geometrical attributes (width and height, angle, scale).

In this traditional approach the variation of stiffness and strength demands along the tall building elevation is accommodated adjusting the cross sections and/or the steel strength of the structural members, while preserving the structure geometry, namely preserving column spacing in frame tubes, mega-diagonals length in braced tubes, module scale/size and density in diagrids, etc. However, in the case of diagrids, variable-geometry strategies can also be adopted according to specific structural rationales, resulting in diverse geometrical patterns characterized by density, size, scale, angle and/or depth of the base unit varying along the building façades.

Relevant examples of variable-geometry diagrids come from the construction world: the Lotte Super Tower structure, proposed by SOM [9], has a diagrid with variable angle in order to optimize the involvement of the diagonal members along elevation in counteracting lateral loads; the CCTV Headquarters has a diagrid with the base unit differently scaled throughout the building façades for responding to changes in local stresses; the projects of the 1000 Museum building, in Miami, and of the Sunrise Tower, in Kuala Lumpur, both by Zaha Hadid, as well as the Hypergreen tower designed by Jacques Ferrier, are only some additional examples among several proposals of variable geometry diagrids.

In the scientific literature, variable-angle diagrid structures have been studied in [32], [33], [53] as more efficient design solutions than uniform-angle configurations for very slender buildings, and design/optimization procedures have been proposed. In particular Moon [31] and [32] subdivides the building elevation into stacking macro-modules, each characterized by a constant diagonal angle, with increasing angle going from the uppermost to the lowest macro-modules; a specific formula for deriving the angle values to be adopted in each macro-module is not

provided in the paper. Zhang [53], instead, proposes a geometrical construction for the generation of the variable-angle pattern made of continuous and straight diagonal members, and provides ad-hoc stiffness-based formulae for sizing the structural members.
However, no contributions in the literature can be found on variable density patterns for diagrid structures. Therefore in this chapter diagrid structures characterized by variable density patterns are considered and compared to regular and variable angle patterns. In particular eight different diagrid patterns (namely three regular, three variable angle and two variable density patterns) are generated and designed for a 90-story model building: for the regular and variable-angle patterns, the design process is carried out according to the procedures proposed in [32], [33], [53], while for the variable-density patterns, specific design approaches are developed by the authors. The resulting diagrid structures are assessed under gravity and wind loads and various performance parameters are evaluated on the basis of the analyses outcomes.

3.2 Building model and diagrid patterns

The building model used for generating different patterns of the diagrid façade, assessing the resulting geometrical properties and weight, and analyzing the structural performance is different from the one considered in Chapter 1, mainly to avoid the problems related to the rectangular plan of the first model.
The new reference building has 90 storey, a square plan 53x53 m, with a central core 25,4x25,4 m; the total height is 351 m, with interstory height equal to 3.9 m (Figure 3-1a). The floor framing plan is depicted in Figure 3-1b; the dead load is 7 kN/m^2, including the weight of the floor steel structure, of the internal partitions and the external claddings. The live

load has been assumed equal to 4 kN/m^2. The horizontal load due to wind pressure has been calculated according to ASCE-7 05 provisions [6], considering wind speed equal to 50 m/s (110 mph) (see Table 3-1). A global building drift of H/500 is adopted as the maximum drift allowable under design loads.

The steel material used both for the horizontal floor structures and for the vertical structures (exterior diagrid and interior core columns) is S275 with f_{yk} = 275 N/mm^2; for the framing floor structure, beams IPE 600 (depth =600mm , width = 220mm) have been selected, spaced at 2,5 m to support a composite steel deck (total thickness = 110 mm); for all diagrid patterns, members with built-up box sections have been thoroughly adopted.

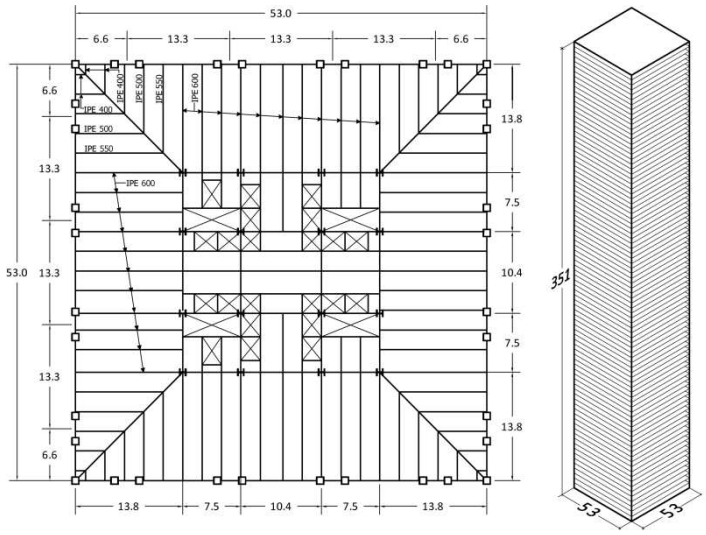

Figure 3-1 Building model : a) overall dimensions b) floor framing plan

GRAVITY LOAD [kN/m^2]	
Dead	7
Live	4
HORIZONTAL LOAD – WIND	
Base shear [MN]	69,4
Overturning moment [MNm]	13043,2

Table 3-1 Design loads

Three different strategies have been adopted for generating eight diagrid patterns (Figure 3-2), i.e.:

Strategy 1: Regular diagrid – 3 patterns (Figure 3-2a, b, c) - module with constant angle along the height (θ = 60°, 70°, 80°); resulting pattern characterized by constant module size and uniform diagonal density.
Strategy 2: Variable angle – 3 patterns (Figure 3-2d, e,f) - module with variable angle along the height; resulting pattern characterized by (either slightly, Figure 3-2d, or strongly, Figure 3-2e and f) variable module size and uniform diagonal density.
Strategy 3: Variable density – 2 patterns (Figure 3-2g, h) - module with constant angle but variable size along the height; resulting pattern characterized by variable module size and non-uniform diagonal density.

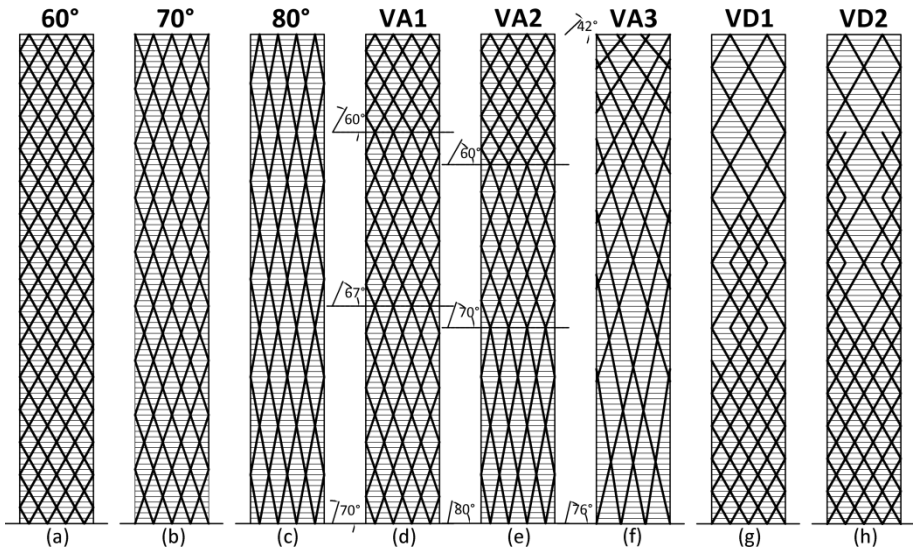

Figure 3-2 Regular patterns: a) θ=60°; b)θ=70°; c)θ=80°. Variable angle patterns: d) VA1 ; e) VA2 ; f)VA3. Variable density patterns: g) VD1 ; h)VD2

It should be observed that by varying the diagrid angle along the height (Figure 3-2d, e,f), according to the procedures that will be illustrated in the next paragraphs, modules characterized by a decreasing size, from the base to the top, are obtained; therefore a variable scale of the trussed façade (more evident for patterns in Figure 3-2e and f than for the one in Figure 3-2d) results as an indirect consequence of the diagrid generation strategy: in particular modules of larger size, i.e. a wider structural mesh, are obtained in the lower part of the buildings, due to the required steeper angle, while smaller size modules, i.e. a narrower structural mesh, is obtained towards the building top. However in this case, an uniform diagonal density, i.e. constant number of diagonals along elevation, is obtained.

From the aesthetic point of view the vertical tessellation of the base units which progressively contain fewer storey as they repeat vertically (Figure 3-2d, e and f), appears oddly truncated and transmits an affect of

finiteness, particularly in building of prismatic shape, as the one considered in this chapter. Furthermore, these variable angle patterns seem to contradict the expectancy of larger strength and stiffness demand toward the base than at the building top, which instead is reflected in the variable density patterns (Figure 3-2g and h), able to transmit an affect of verticality and gradation even in extruded form buildings [36].

3.3 Regular diagrid - geometry definition and design criteria

As shown in the previous Chapter 1, assuming a diagrid module with constant angle along the height, the resulting pattern is characterized by constant module size and uniform density.
Recalling the observations of paragraph 2.2, the following geometrical relationships can be established for the regular triangle pattern:

$$h = n_{st}h_i; n_m = H/(n_{st}h_i); L_d = n_{st}h_i/sen\theta;$$
$$\theta = arctg[n_{dg}/(2Ln_{st}h_i)] \quad (3.1)$$

In this Chapter, the number storey covered by a single module (n_{st}) and the number of diagonals on each building façade (n_d), have been fixed in the generation of three regular patterns. Assuming n_{st} respectively equal to equal to 6, 10, 18, and n_d equal to 8 for all three cases, the first three patterns depicted in Figure 3-2a, b and c have been obtained, with the corresponding geometrical parameters given in Table 3-2.
The resulting module angle is respectively equal to 60°, 70° and 80° (Figure 3-2a, b, c), therefore in the following the three diagrid structures will be identified according to the angle value.

H [m]	L_x [m]	h_i [m]	n_x […]	n_{st} […]	h [m]	n_m […]	θ [°]	L_{dg} [m]
351	53	3.9	8	6	23.4	15	60.5	26.9
				10	39.0	9	71.2	41.2
				15	70.2	5	79.3	71.4

Table 3-2 Regular diagrid – geometrical parameters

The preliminary design procedure based on stiffness requirements (i.e.: $D_{top} < H/500$), originally proposed by [30],[33] and described in Chapter 2 (see also [27]), is applied; in particular the simplified equations (2.12) and (2.13) are utilized for deriving the cross section areas of the diagonal members in the generic m-th module located on the web and flange planes (i.e. on the façade parallel and orthogonal to the wind direction), $A_{d,m,w}$ and $A_{d,m,f}$

As already reported in Chapter 2 (see also, [30] and [27]), the member sizes and the resulting structural weight are remarkably affected by the value of the parameter s; therefore the formulae (2.12) and (2.13) have been applied for s going from 1 to 10 and the minimum weight solution has been adopted as optimum solution for each geometrical pattern. The cross sectional areas obtained for the diagonal members in the three regular patterns are reported in Table 3-3.

For the building slenderness H/L = 6,62 and the module angles considered in this chapter, the formula (2.21), defined for the evaluation of the optimal value of s, provides s_{opt} equal to 4,7 for θ=60°, s_{opt}= 2.8 for θ=71° and s_{opt}=1,6 for θ=80°. In the chart of Figure 3-3 the above values of s_{opt} are graphically shown as red bullet points and compared to the results of the parametric design (grey bullet points). It can be observed that the formula (2.21) actually allows for establishing the value of s corresponding to the minimum weight solutions.

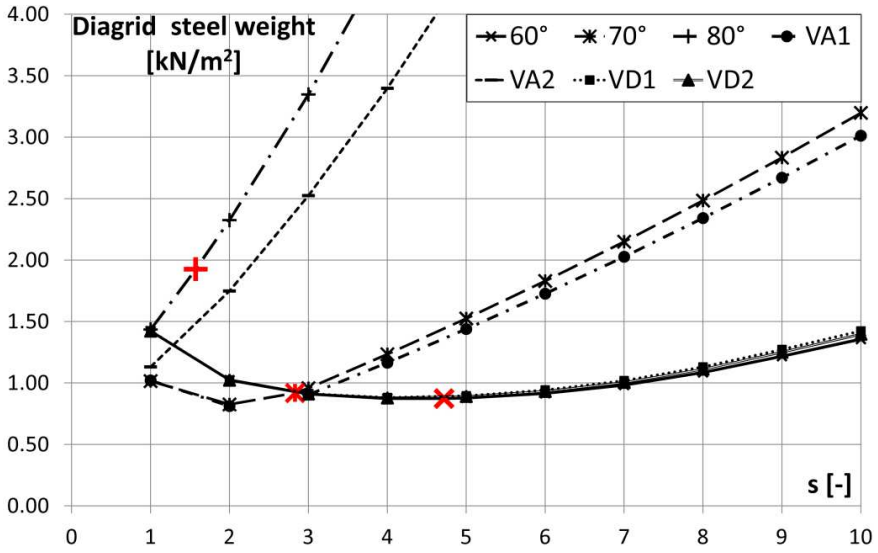

Figure 3-3 Unit steel weight (diagrid only) as a function of s

Mod.	60°	70°	80°	AV1	AV2	AV3	DV1	DV2
1	1200 x115	1200x 105	1300x 125	1200x 105	1200x 125	1100x 120	1200x 115	1200x 110
2	1100 x110	1000x 100	1100x 120	1100x 90	1100x 110	1100x 140	1200x 115	1100x 105
3	1100 x95	800x 100	1000x 95	1100x 65	800x 80	1100x 160	1200x 115	1100x 90
4	1000 x90	800x 75	800x 65	1000x 60	800x 50	1000x 190	1200x 115	1000x 85
5	1000 x75	600x 90	600x 35	800x 65	600x 40	1000x 180	1200x 115	1000x 100
6	800x 80	600x 65		800x 45	400x 40	1000x 140	1200x 115	1000x 90
7	800x 65	600x 50		600x 45	400x 20	1000x 90	1200x 115	1000x 80
8	800x 50	400x 45		600x 35	300x 15	800x 70	1200x 115	1000x 110
9	600x 55	300x 20		400x 35	200x 10		1200x 115	1000x 95
10	600x 50			400x 25			1200x 115	1000x 80
11	600x 40			300x 25			1200x 115	800x 85
12	600x 30						1200x 115	800x 90
13	600x 25						1200x 115	800x 100
14	400x 20						1200x 115	600x 80
15	300x 10						1200x 115	400x 45

Table 3-3 Built up box cross sections for diagonals

3.4 Variable angle (VA) diagrid – geometry definition and design criteria

The rationale behind the design strategy adopting variable angle (VA) patterns [32], [53] is that the share of bending and shear stiffness demands in a diagrid building is a function of the building slenderness, and, for a given building, it varies along elevation. Since the module angle strongly affects both the bending and the shear stiffness of the diagrid structure, it is likely that the most efficient diagrid structures (i.e. the solutions exhibiting maximum stiffness to weight ratio) should be characterized by variable angle configurations. In particular, it is expected that the diagonal angle should be steeper at the lower levels, where bending stiffness demand is higher, than at upper levels, where shear stiffness demand generally prevails.

In the following the preliminary design procedures suggested by Moon and Zhang ([32], [53]) are both employed for deriving three variable-angle patterns of the building diagrid structure (VA1, VA2 and VA3) and the relevant diagonal member cross sections.

3.4.1 Moon procedure – VA1 and VA2 patterns

According to [32] the building elevation is subdivided into stacking macro-modules, with diagrid angle kept constant within each macro-module and increased going from the highest to the lowest macro-modules. In the paper no specific formula is provided for defining the angle values in the macro-modules; Moon designs diagonal structures using the optimal angle obtained in the uniform pattern as the median angle of the variable-angle pattern.

This approach is applied to the building model by dividing the structure into three macro-modules. Two patterns are generated: the former, appointed as VA1, is obtained by considering a moderate angle variation,

with diagonal angles equal to 70°, 67° and 60°, in the lower, intermediate and upper macro-modules, respectively (VA1 model, Figure 3-2d); the latter, appointed as VA2, is obtained by considering a more radical angle variation, with diagonal angles equal to 80°, 70° and 60°, in the lower, intermediate and upper macro-modules, respectively (VA2, Figure 3-2e).
In the VA1 model, the first macro-module (θ=70°) extends from 0 to 156 m, with four sub-modules, each encompassing 10 storey; the second macro-module, (θ=67°) extends from 156 m to 280.8 m, with four sub-modules, each encompassing 8 storey; finally, the third macro-module (θ=60°) extends from 280.8 m to 351 m, with three sub-modules, each encompassing 6 storey.
In the VA2 model, the first macro-module (θ=80°) extends from 0 to 140.4 m, with two sub-modules, each encompassing 18 storey; the second macro-module, (θ=70°) extends from 140.4 m to 257.4 m, with three sub-modules, each encompassing 10 storey; the third macro-module (θ=60°) extends from 257.4 m to 351 m, with four sub-modules, each encompassing 6 storey.
The sizing process of the diagonal members is based on stiffness criteria and consists in deriving the member cross sectional area through the application of the formulae (2.12) and (2.13) within each macro-module.
In order to obtain the optimal value for s, corresponding to the minimum weight solution, the sizing procedure has been iteratively applied varying s from 1 to 10. The results, providing the structural weight as a function of s, are depicted in Figure 3-3, and suggest that s=2 can be considered the optimal value for VA1, while the optimal value for VA2 is s=1. These results are in line with the observations suggested by [32], and confirm that for patterns characterized by a strong variation of the diagonal angle (pattern VA2), the optimal value of s is much less than the uniform pattern counterpart (for 70°, s=2); on the contrary, for

patterns with a moderate variation of angle (VA1), the optimal value of s is much closer to the uniform pattern counterpart.

3.4.2 Zhang procedure – VA3 pattern

According to the previous approach, the diagonals abruptly change direction at the interface between two subsequent mega-modules, thus straightness and continuity of the diagonals are compromised, with a consequent loss of efficiency in the load transfer path. Therefore Zhang [53] suggests the use of variable angle diagrids with continuous and straight diagonal members, and proposes a geometrical construction for the pattern generation, starting form a couple of diagrid angles, the top angle θ_1 and the bottom angle θ_2.

The key point of the design procedure is the definition of the values for θ_1 and θ_2 that lead to the most efficient solution (i.e. minimum structural weight); the following empirical formulations, defined on the basis of a parametric analyses, are provided for this purpose:

$$\theta_{2opt} = \arctan \frac{H/L}{1+0{,}475\sqrt{\frac{H/L}{4{,}75}}} \tag{3.5}$$

$$\theta_{1opt} = \theta_{2opt} \qquad \text{if} \qquad H/L \le 3{,}5 \tag{3.6}$$

$$\theta_{1opt} = \frac{1}{\left(1+\ln\frac{H/L}{3{,}5}\right)^{\frac{H/L}{2}}}\left(\theta_{2opt} - \arcsin\frac{1}{\sqrt{3}}\right) + \arcsin\frac{1}{\sqrt{3}} \tag{3.7}$$

if $H/L \ge 3{,}5$

It is worth noticing that the above formulae only depend on the building aspect ratio H/L. For the building model examined in this paper,

characterized by H/L = 6.62, the optimal couple of angles is: $\theta_{2,opt}$=76.7° and $\theta_{1,opt}$=43.4, that lead to the diagrid configuration shown in Figure 3-2f (appointed as VA3).

Once the angle couple is defined, Zhang proposes a design procedure based on stiffness requirements, particularly on the limitation of interstory drift, which finally allows to derive the area of cross sections for diagonals along elevation according to the following two formulae:

$$A_{d,i,w} = \frac{V_i}{2E\gamma_i \sum_{k=1}^{n_{wi}} (\sin\theta_k \cos^2\theta_k)} \tag{3.8}$$

or

$$A_{d,i,f} = \frac{M_i}{EL^2 \chi_i \sum_{k=1}^{n_{fi}} (\sin^3\theta_k + \delta)}$$

where the subscript i refers to the i-th storey, and, in addition to the symbols already defined, γ_i is the i-th storey shear strain, χ_i is the i-th storey curvature due to overturning moment, and δ, as in the formula (3.4), takes into account the contribution of the web diagonals to the flexural stiffness (Zhang suggests δ=2).

The ratio between χ_i and γ_i is:

$$\frac{\chi_i}{\gamma_i} = \frac{4M_i \sum_{k=1}^{n_{wi}} (\sin\theta_k \cos^2\theta_k)}{VL^2 \left(\sum_{k=1}^{n_{fi}} (\sin^3\theta_k + \delta) \right)} \tag{3.9}$$

while the limitation of the lateral displacement can be expressed as:

$$\gamma_i + \chi_i h_i + \sum_{j=1}^{i-1} \chi_j h_j = 1/500 \tag{3.10}$$

which, at the first level (i=1), reduces to:

$$\gamma_1 + \chi_1 h_1 = 1/500 \tag{3.11}$$

Starting from the first level, the values of γ_1 and χ_1 can be calculated substituting equation (3.9) in (3.11); substituting γ_1 and χ_1 in equation (3.10) and iterating the procedure, the values of γ_i and χ_i can be obtained for i=2, 3, ...n, and the diagonals are consequently sized.

Applying the above sizing process to the pattern VA3, the diagonal cross sectional areas provided in Table 3-3 have been obtained for each module.

Applying the above sizing process to the pattern VA3, the diagonal cross sectional areas provided in Table 3-3 have been obtained for each module. It can be observed that, according to the design procedure previously described, the diagonal cross sections are evaluated on a story-by-story interval; however a variation of cross section at every story seems quite onerous from the constructional point of view, and in fact the diagrid buildings that have been so far realized preserve the same diagonal cross section at least for one module. Furthermore, for the sake of consistency with the other patterns designed according to global stiffness demand (top drift ratio), this procedure has been applied making the following assumptions: (i) the choice of adopting one single cross section for diagonals within each module has been preserved, as in the other patterns; for this aim (ii) both the largest and the smallest cross sections out coming from the interstory stiffness demand have been evaluated within each module; (iii) an average value of the diagonal cross section, among the ones obtained from the story-by-story sizing process, has been adopted throughout each module.

It is worth noticing that the original formulation proposed by Zhang is based on the limitation of interstory drift within $h_i/500$; the procedure, as applied in this paper, actually controls the inter-module drift to 1/500 of height; on the contrary, the procedures proposed by Moon, both for regular and variable-angle patterns, are based on the limitation of global top drift within H/500. Therefore, though similar characteristic of global stiffness are expected for the previous and the VA3 patterns, a more regular distribution of local (module) stiffness can be anticipated for the VA3 model.

3.5 Variable density (VD) diagrid – geometry definition and design criteria

The decrease of stiffness and strength demands along the tall building elevation is traditionally accommodated through varying the structural member cross sections and/or steel strength, while preserving the structure geometry, namely preserving column spacing in frame tubes, mega-diagonals length in braced tubes, module scale/size and density in diagrids, etc... An alternative design strategy is here proposed, consisting in a variable density (VD) geometry of the structural configuration: the decrease of stiffness and strength demands along the elevation is addressed by reducing the number of diagonals going from the building base to the top.

3.5.1 Constant diagonal section – VD1 pattern

In the design approach here considered, the reduction of lateral strength and stiffness demands toward the top is accommodated both by rarefying the diagrid pattern and by varying the cross sections of

diagonals. For this aim the structure is divided into stacking modules; within each of them, the required number of diagonal members and the relevant cross sections are derived by inverting the formulae (3.2) and (3.3), having fixed the values θ, and obtaining of $A_{dg}\, n_w$ and $A_{dg}\, n_f$.

Of course the final number of diagonals within each macro-module should satisfy some appropriate feasibility constraints: n_{dg} should be an even integer, equal to or larger than the maximum value between n_w and n_f; furthermore, a minimum value for n_{dg} should be established, as a function of the façade width, in order to avoid the occurrence of excessive span (say, less than 27 m) for the perimeter beams.

This procedure has been applied to the building model, dividing the elevation into 15 stacking modules and starting from the assumption of a diagrid angle equal to 60°; given the building geometry, the minimum number of diagonals on each façade is four ($n_{dg,min}$=4). Grouping the modules into three clusters characterised by different diagrid density, a number of diagonals equal to the minimum value (four) has been adopted for the upper cluster; for the middle and lower clusters, two and four more diagonals are respectively added up. In this way a rule for the minimum diagrid density is somehow fixed a priori; however a broad variety of solutions can be obtained, for instance by varying the height of the module clusters along the building elevation.

According to this approach, two building models have been generated. In the first model, appointed as VD1 (Figure 3-2g), the height of the three module clusters is the same (117 m, 30 floors), while in the second model, VD2, (Figure 3-3h) the cluster heights are different, namely equal to 40% of H (140,4 m, 36 floors) for the lower and middle cluster, and to 20% of H (70,2 m, 18 floors) for the upper part.

Once the variation of diagonals has been established, the diagonal section areas are obtained within each cluster, characterized by a

different value of n_{dg}, on a module scale, as derived from the equations (3.2) and (3.3), with $n_w = n_f = n_{dg}$.
For both the variable density patterns, the design equations have been iteratively applied by varying the value of the coefficient s between 1 and 10, in order to find the best, minimum weight, solution, which ultimately corresponds to s=4 (Figure 3-3), close to the value obtained for regular diagrid with $\theta=60°$.

3.6 Structural analyses and performance assessment

The diagrid patterns generated for the building model are analyzed using FEM numerical models (Figure 3-4), by means of SAP2000 computer code. Frame elements are adopted for the structural members of the diagrid characterized by the cross sections specified on the basis of procedures outlined in the previous paragraphs; the Frame element uses a general, three-dimensional, beam-column formulation which includes the effects of biaxial bending, torsion, axial deformation, and biaxial shear deformations (CSI, 2009). Diagonal elements have been considered continuous on the module height, reflecting the actual construction modes. Hinged connections have been introduced at diagonal-to-diagonal intersections, at the beam ends and at beam-to-column joints of the internal gravity frames. Static analyses in the elastic field have been carried out with and without P-Δ effects, under factored gravity and wind loads, as specified in Table 3-2.

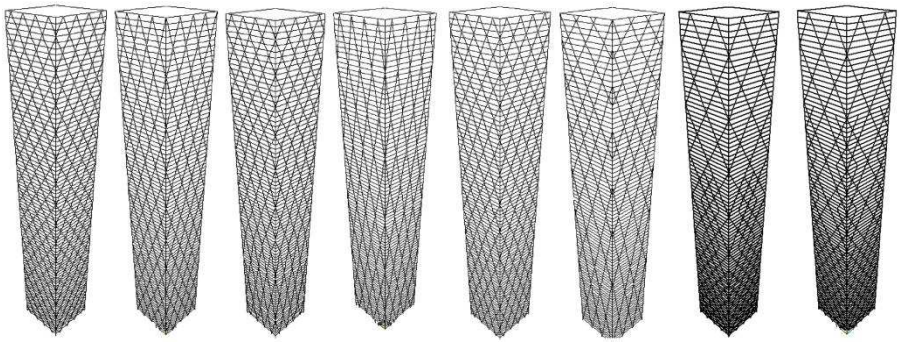

Figure 3-4 FEM models

In order to present a complete assessment of the structural performance exhibited by the different diagrids, the major response parameters, which have been obtained by processing the analysis results, are thoroughly examined and compared; in particular the following parameters are considered: horizontal displacement, u; interstory drift ratio, d_h; strength demand to capacity ratio in the diagonal members (DCR_{dg}), defined as the tension/compression axial force under design loads normalized to the yield/buckling capacity of the relevant member.

The charts in Figure 3-5 (black dashed lines) show the lateral displacement under wind load as a function of the building height, while in Figure 3-6 (black points) the maximum horizontal displacements registered in the eight design solutions are provided as a function of the unit weight of the diagrid structures; in the same graph, the red horizontal line identifies the design limit (H/500 = 0,70 m). In Figure 3-5 and Figure 3-6 the results referring to building structural solutions equipped by internal secondary bracing systems (SBS) are also provided and depicted by means of grey dashed lines and grey points, respectively; these SBS solutions will be discussed in the next paragraph and more in detail in the next Chapter.

It is worth observing that, despite the stiffness based design procedures described in the previous paragraphs, five patterns out of eight do not satisfy the design limit (Figure 3-5 and Figure 3-6): in particular the models 70°, 80°, VA2, VD1 and VD2 exhibit a maximum displacement respectively equal to 0,82 m, 0,75 m, 0,78 m, 1,47 m and 1,46 m. Considering these results, the described design procedures might seem ineffective and inconsistent; however a more accurate evaluation of the models' responses reveals that the top displacement is always within the design limit of H/500, and local deformations only compromise the correct behavior of the structure. The source of such concentrated flexibility is related to the fact that the primary bracing system, i.e. the diagrid structure, employs diagonals that span over multiple floors, thus can be considered as a vertical truss with panel points located several floors apart [1]; [27]; in particular the structural behavior of the diagonal between the panel points (diagrid nodes) can be idealized as a simply supported beam, with end restraints corresponding to the panel points, with concentrated loads corresponding to the horizontal forces acting at intermediate floors, and with beam stiffness related to the flexural stiffness of the diagonal member. Figure 3-7a shows the diagrams of bending moment and axial force in the upper diagonals of the 70° diagrid pattern. The flexural engagement within the module height can be clearly observed looking at the moment diagram, with maximum value equal to 290 kNm; the axial force is equal to 568 kN, leading to a maximum eccentricity of 0,51 m.

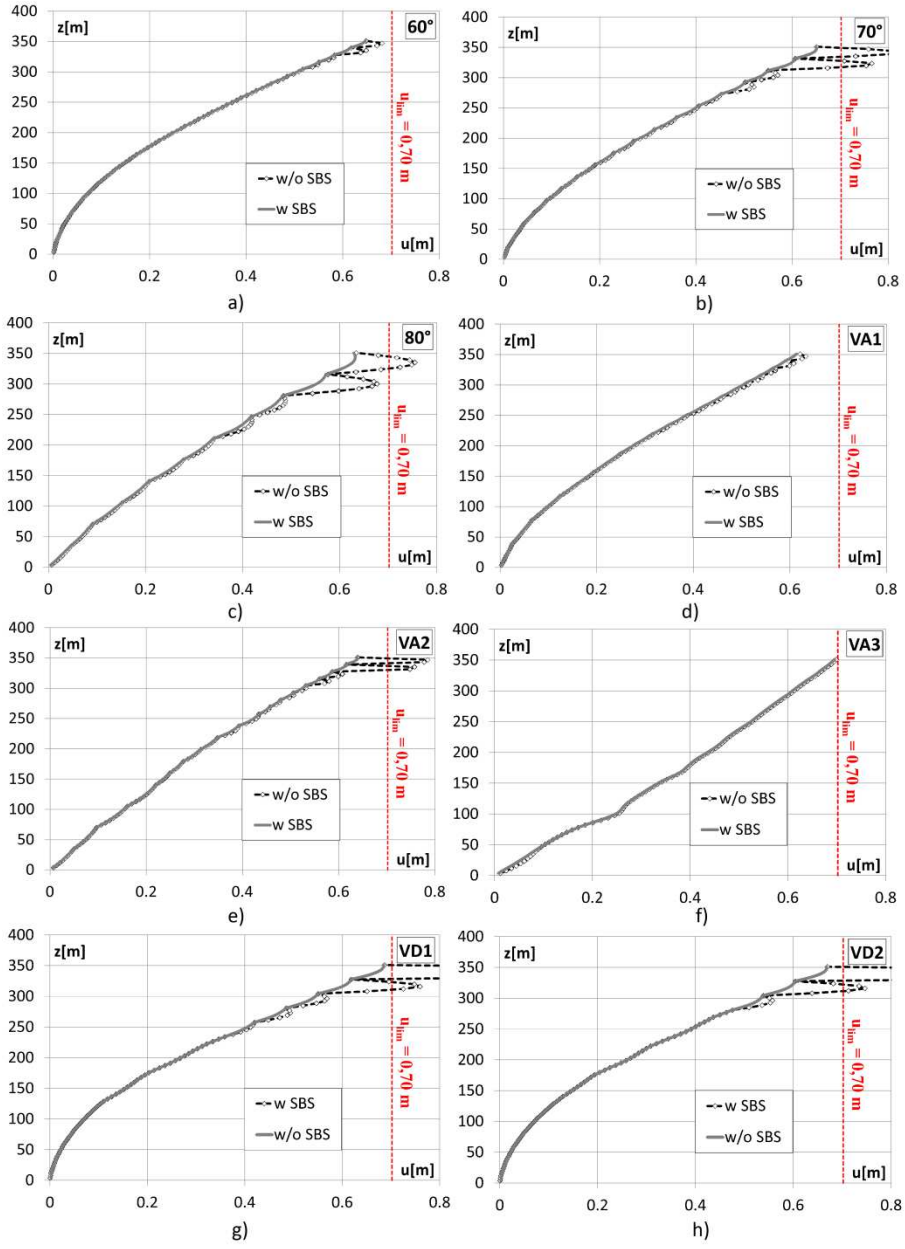

Figure 3-5 Lateral displacement under wind forces. a) 60°; b) 70°; c) 80° ; d) VA1; e) VA2; f) VA3; g) VD1; h) VD2

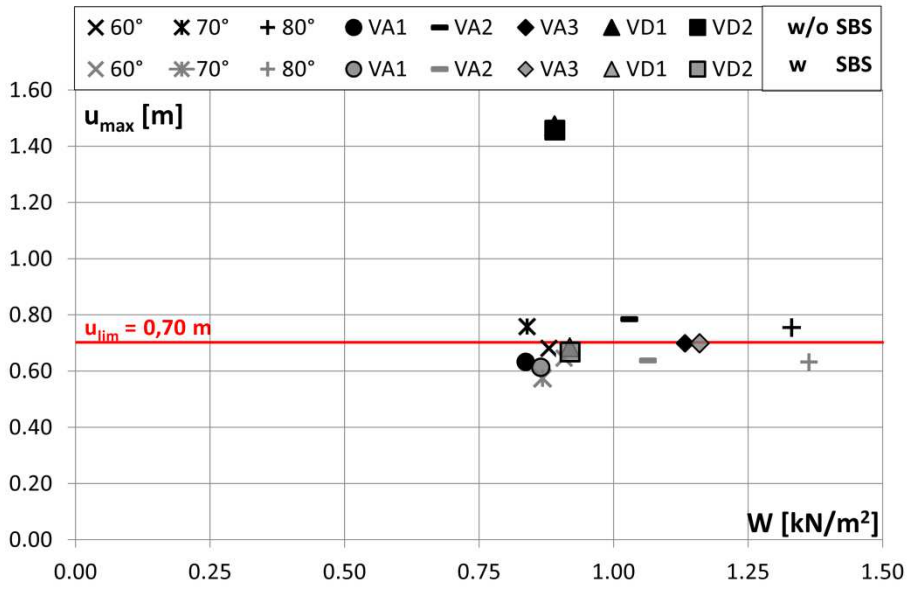

Figure 3-6 Maximum lateral displacement under wind loads as a function of the unit structural weight

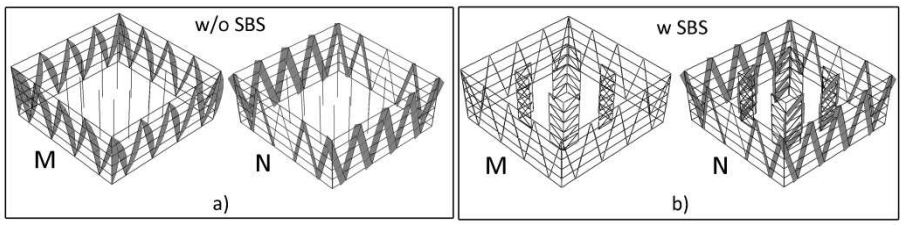

Figure 3-7 Bending moment diagram and axial force diagram in the top module of 70° diagrid: a) without SBS; b) with SBS

Therefore, even though the diagonals are continuous along the elevation, the floors between the panel points are laterally braced only by the flexural stiffness of the diagonal members, which is largely lower than the axial counterpart. The smaller the diagonals cross sectional areas (namely at the upper levels) and the more the number of storey between the panel points (namely, the higher the module), the larger the

magnitude of the local displacements. Taking the top modules of the 70° diagrid pattern as an example, the ratio of the axial to flexural stiffness ($A L^2/I$) of the diagonal members ranges approximately between 1000 and 4000 along elevation, while reaches values beyond 10000 at the very top modules.

This effect can be better appreciated by analyzing the results in terms of interstory drift. Figure 3-8 (black dashed lines and black points) shows the interstory drift ratio ($d_h=u_i/h_i$) along the building height, while Figure 3-9 (black points) shows the maximum value of the interstory drift ratio as a function of the diagrid unit weight for the different design solutions. It is worth noticing that all but the VA3 pattern do not respect a reasonable design limit, here assumed equal to 1/200, particularly at the upper levels, where the diagonal cross sectional areas (and inertia moments) are smaller. As illustrated in the paragraph 3.5.2, the structural solution for the pattern VA3 has been obtained according to a severe limitation on interstory drift, i.e. $h_i/500$, which is much smaller than the one here adopted.

In Figure 3-10 the diagonals' DCR values are provided as bullet points along the building elevation, while Figure 3-11 shows the percentage of diagonals with DCR>1, i.e. of overstressed elements. It can be observed that the number of overstressed elements is generally small, less than 5 % for patterns 60°, 70°, 80°, VA1 and VA3; for the patterns VA2, VD1 and VD2 a larger percentage of diagonals (more than 10%) fail the strength check. The patterns 60°, 70°, 80°, VA2, DV1 and DV2 have overstressed elements concentrated at upper modules (in percentage of 4.6%, 6,1%, 0.8%, 18%, 10.8% and 10.5%, respectively) while the overstressed elements in the model VA3 are the ones located at the base (4.9%). As reported in Chapter 1, unlike what normally occurs in the case of other structural systems for tall buildings, the strength

requirements are not at all negligible compared to stiffness requirements, and frequently governs the sizing process of diagonals.

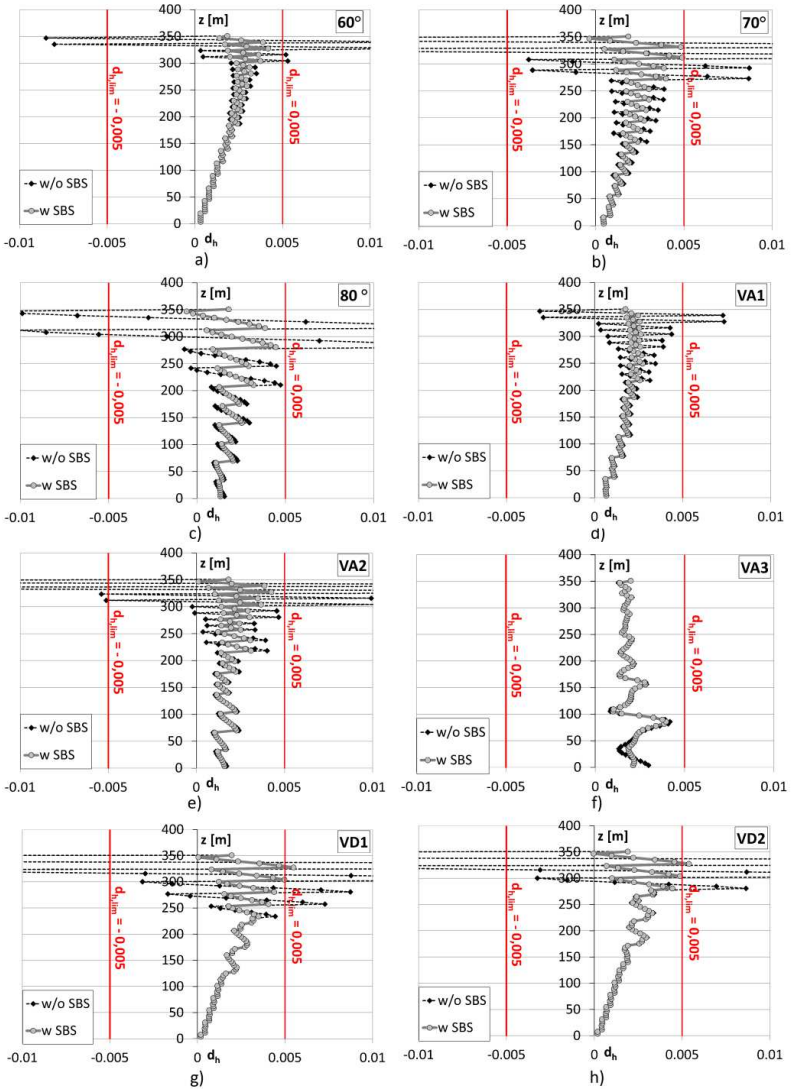

Figure 3-8 Interstory drift under wind forces. a) 60°; b) 70°; c) 80° ; d) VA1; e) VA2; f) VA3; g) VD1

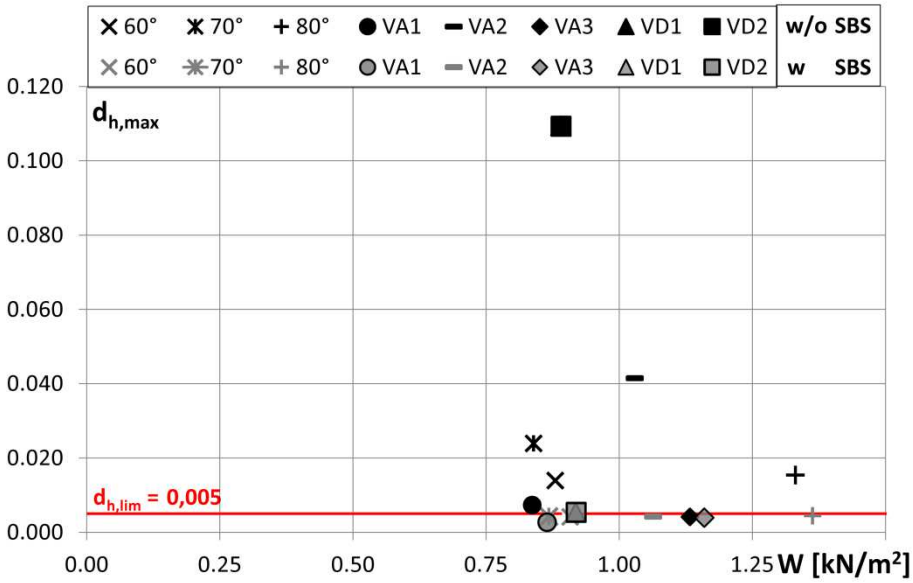

Figure 3-9 Maximum interstory drift under wind loads as a function of the unit structural weight

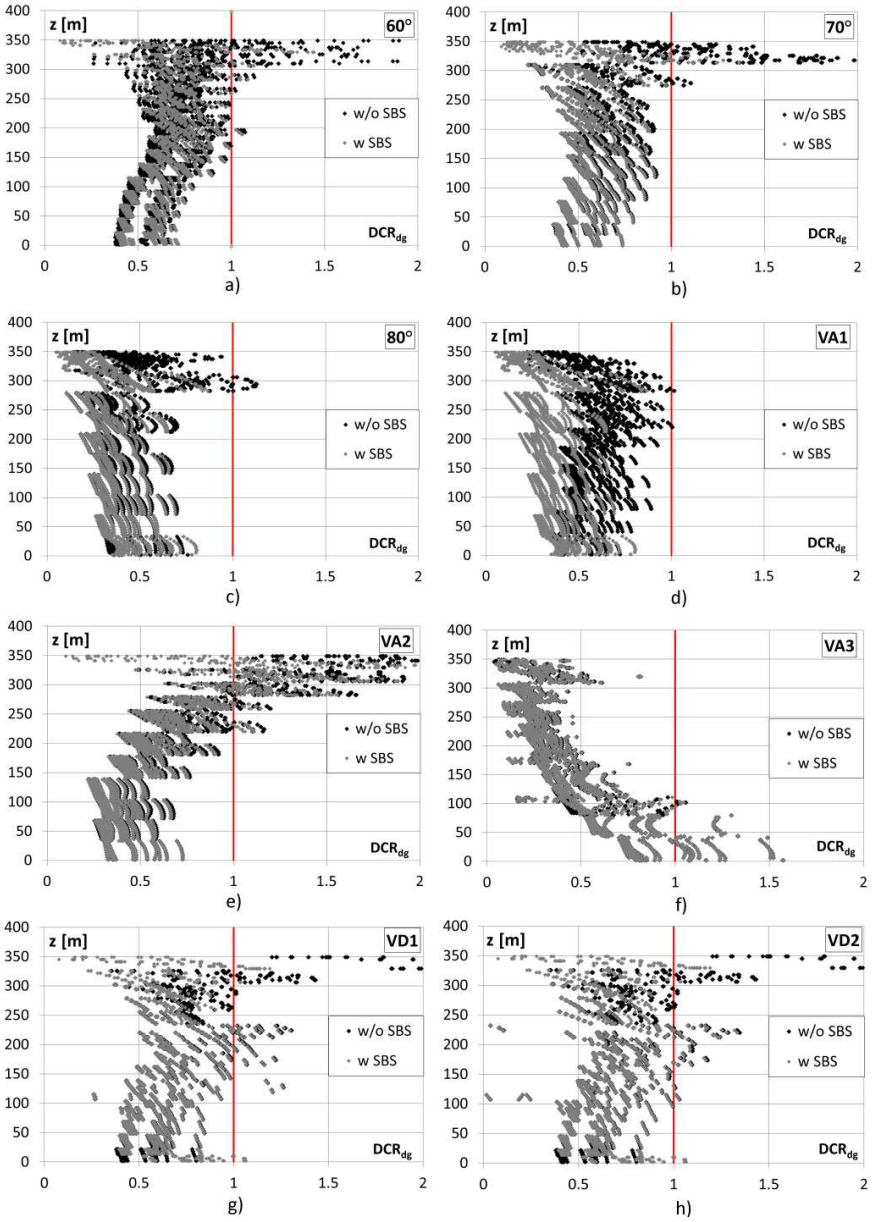

Figure 3-10 Demand to capacity ratio (DCR) under gravity loads plus wind loads.) 60°; b) 70°; c) 80° ; d) VA1; e) VA2; f) VA3; g) VD1

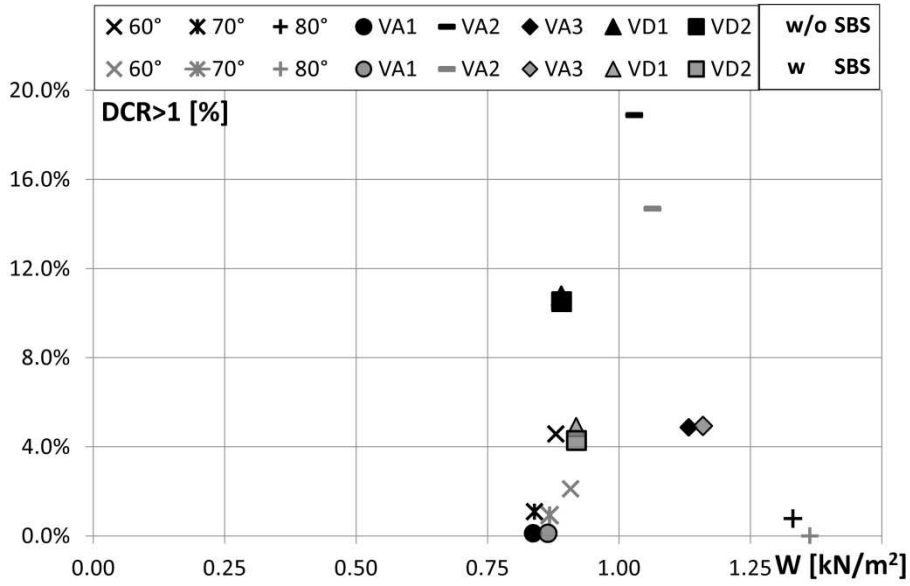

Figure 3-11 Percentage of overstressed diagonals (DCR>1) as a function of the unit structural weight

3.7 Design refinement: secondary bracing system - SBS

The onset of local deformations within the module height requires the addition of a properly designed secondary bracing system (SBS). The behavior and the design procedure of the SBS will be analyzed and described in details in the following Chapter4. Anyway, at this point it useful to underline that the SBS limits the local deformation in order to avoid serviceability problems in architectural finishes, but does not affect the structure global behavior under lateral load, being the lateral stiffness of the building almost the same with and without it [1], [27]. The addition of a SBS allows to transfer the horizontal forces to the vertical truss panel points (i.e. to the diagrid nodes) by means of a load path involving the axial stiffness of the SBS members instead of the flexural stiffness of the diagrid mega-diagonal elements. The secondary bracing

system also has the important function of stabilizing the columns of the gravity load resisting system (core columns) at the intermediate levels comprised between two panel points.

For each diagrid building designed in this paper, a SBS consisting of four concentric braced frames along the two orthogonal building direction has been designed (Figure 3-12); a twofold design criterion has been adopted (see Chapter 4 and Montuori, 2013c) : (i) to comply with the imposed drift limitations, and (ii) to stabilize the core gravity columns [38], [51], [2].

In Figure 3-7 the diagrams of the bending moment and axial force in the upper diagonals of the 70° diagrid pattern are shown for the cases without (Figure 3-7a) and with SBS (Figure 3-7b). It can be clearly observed that (i) the introduction of the SBS strongly reduces the flexural engagement of the diagonals, going from values of bending moment of 290 kNm to 22 kNm; (ii) the modification of the load path activated for transferring the horizontal forces to the diagonal panel points, showing the involvement of the axial behavior of the SBS members instead of the flexural behavior of the diagrid members.

The results of the structural analyses carried out on the building models equipped with the SBS are shown in terms of horizontal displacements in Figure 3-5 and Figure 3-6 (grey lines and grey points). As previously stated, it can be observed that the secondary bracing system does not affect the global behavior of the structure, i.e. the top displacements and the deformed shapes of the building structures are almost the same with and without SBS. Conversely, a dramatic reduction of the local deformations is obtained (Figure 3-8 and Figure 3-9, grey lines and points), since the interstory drifts within the single diagrid modules remarkably decrease and all patterns satisfy the design limit.

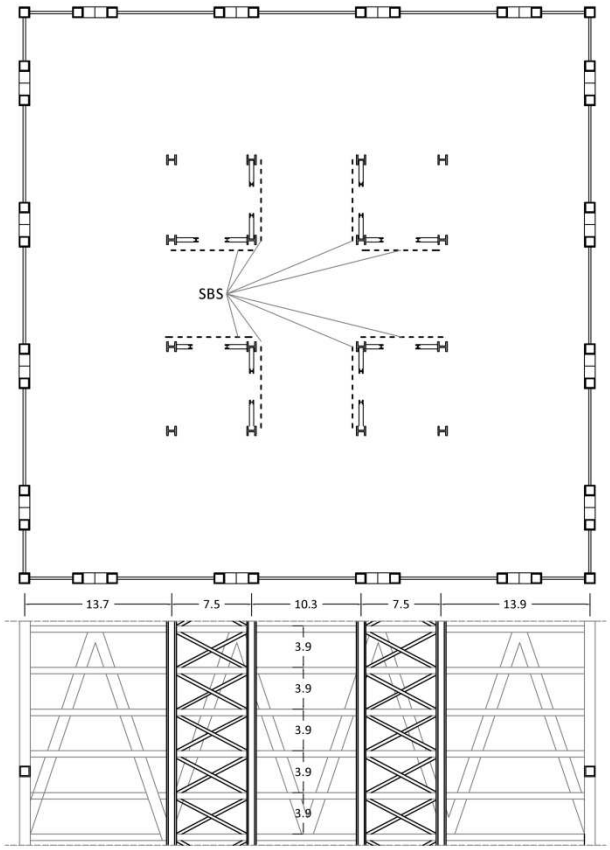

Figure 3-12 Secondary bracing systems, plan location and geometry

In Figure 3-13a the unit structural weights of the diagrid patterns (with and without SBS) is provided as a bar chart; the values depicted by the bars have been obtained by dividing the total weight of the steel members composing the diagrid structure by the gross floor area of the building. The comparison within each couple of bars (with and without SBS) allows to assess the modest increase of structural weight due to introduction of the SBS, about 3% for all patterns. Therefore it can be stated that the secondary bracing systems greatly improve the structural

behavior of the diagrid buildings (Figure 3-6 and Figure 3-9) against a slight increase of the structural weight.

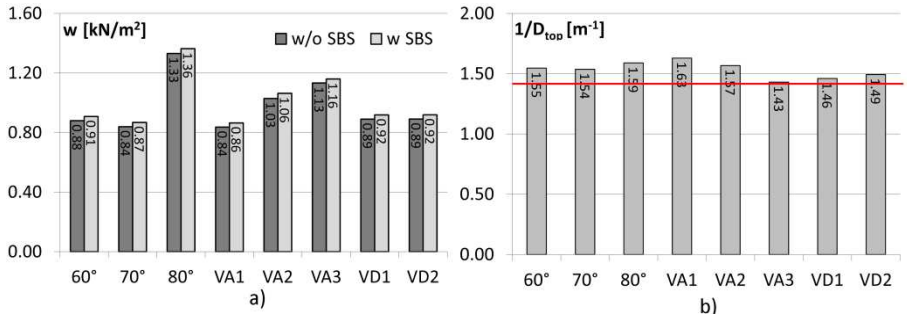

Figure 3-13 a) Unit steel weight without (black bars) and with (grey bars) secondary bracing system; b) Stiffness parameter (Inverse of the building top drift)

3.8 Structural Efficiency And Design Optimization Of The Different Patterns

The comparison between the unit structural weights of the diagrid buildings, already provided in Figure 3-13a, allows to identify the most efficient diagrid patterns, namely the design solution which meets the performance requirements with the minimum structural weight.

On this comparative basis, the most efficient solutions are the regular pattern with θ=70° and the variable angle pattern VA1, both characterized by steel weight equal to 0.84 kN/m^2 (w/o SBS); however the solutions 60°, VD1 and VD2 are only slightly heavier than the previous ones, with an increase of steel weight within 10% (5%, 6.4% and 6.5% respectively for the solutions 60°, VD1 and VD2). On the contrary the patterns VA2, VA3 and 80° are not likewise efficient, with weight increase beyond 20% (23%, 35% and 59%, respectively for the solutions VA2, VA3 and 80°).

A more refined parameter of the structural efficiency explicitly needs to account for the building lateral stiffness; a simple measure of the lateral stiffness is the inverse of the building top drift, provided in Figure 3-13b for the different patterns; the bar chart shows that two of the heaviest patterns, i.e. 80° and VA2, have a lateral stiffness remarkably higher than the other patterns, and much larger than the minimum required, corresponding to the horizontal line. Therefore, by putting together the results of Figure 3-13a and b, it can be envisaged that the diagrid structures in these two patterns might be further optimized, with some appreciable weight reduction.

The results of Figure 3-13a and b are actually putted together in Figure 3-14: here the ratio of lateral stiffness to structural weight is reported; it allows for better appreciating the outcomes of the parametric design, i.e. the structural efficiency of each diagrid pattern coupled to the adequacy of the implemented design procedure.

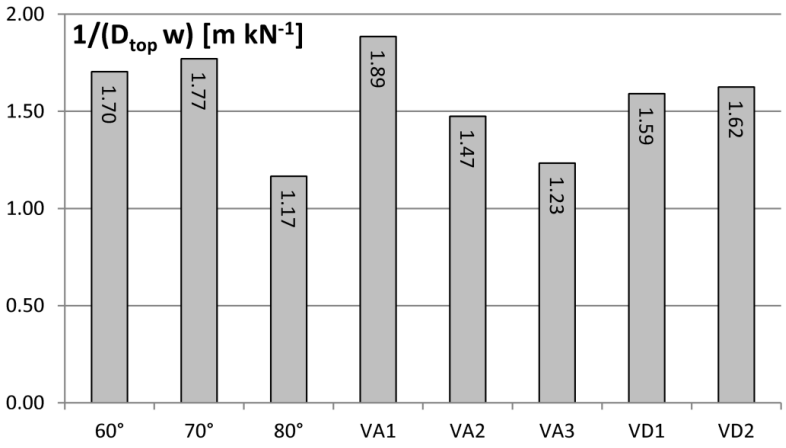

Figure 3-14 Efficiency parameter (inverse of the building top drift multiplied by the unit steel weight of diagrid)

In line with observations already made in terms of structural weight and stiffness, the patterns VA1, 70° and 60° show the highest values of the efficiency parameter, while 80° and VA3 are the less efficient patterns.
As already noticed, some patterns might be further optimized, with some appreciable weight reduction and efficiency increase. In other words, the structural efficiency seems to be affected not only by the pattern geometry but also by the relevant design procedure. A rough measure of the expected margin for design refinement is proposed in Figure 3-15, where three bars are provided for each patterns: the former two bars (black and grey bars) respectively represent the structural weight of the designed solution and the structural weight multiplied by $D_{top}H/500$ (i.e. the top displacement normalized to the limit value); quite trivially it can be stated that the larger the difference in each couple of bars, the larger the margin for optimizing the pattern design. From the bar chart it can be envisaged that the diagrid structures of some heaviest patterns, i.e. 80° and VA2, might be further optimized, with some appreciable weight reduction (about 10%); on the contrary, similar design improvements cannot be anticipated for the pattern VA3.
In order to check the expected improvements, an iterative optimization process of the models has been carried out; in particular the cross sections of the diagonals have been gradually reduced, allowing for the top displacement approaching the design value of H/500 as close as possible.

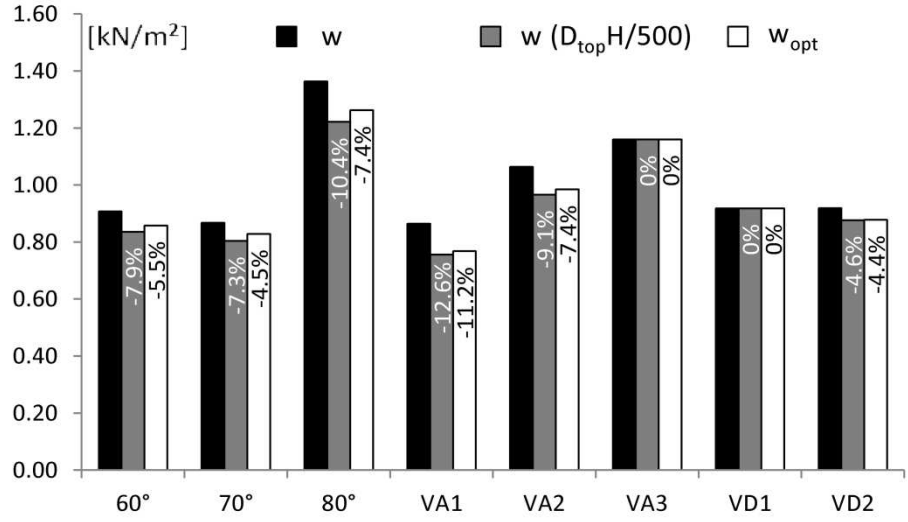

Figure 3-15 Comparison between unit steel weight of diagrid (black bars), unit steel weight multiplied by $D_{top}H/500$ (grey bars) and unit steel weight for the optimized solutions (white bars)

The white bars in the chart of Figure 3-15 provide the structural weight of the optimized solutions, and can be directly compared to the prediction made by means of the parameter $wD_{top}H/500$ (grey bars). In general, the trend of the expected improvement is confirmed, though the actual weight reduction has been obtained to a lesser extent. The optimization process has led to significant weight reduction for the models 80° and VA2 (- 7.4 %), but the maximum effect is registered for the VA1 pattern (-11%), with a final minimum weight equal to 0,77 kN/m^2; slight reductions have been obtained for the patterns 60°, 70°, VD2 (in the range -4.5,-5.5 %), and almost no modifications for the patterns VA3 and VD1.

Finally, the comparison among structural efficiencies evaluated for the optimized patterns is provided in Figure 3-16, showing that the VA1 model has become the most efficient one; the regular patterns 60° and

70°, as well as the variable patterns VA2, VD1 and VD2, all show similar efficiencies, contrary to the models 80° and VA3.

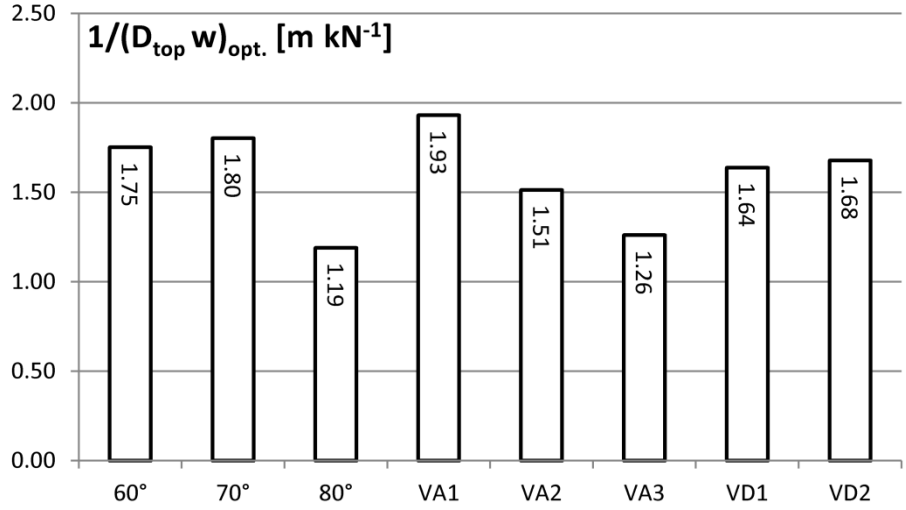

Figure 3-16 Efficiency parameter (inverse of the building top drift multiplied by the unit steel weight of diagrid) for the optimized solutions

3.9 Conclusive remarks

This chapter represents a first step of the exploration of both uniform and non uniform diagrid patterns and of defining adequate design criteria. In particular in this chapter, eight alternative geometrical patterns of diagrid structures have been generated, designed, optimized and comparatively assessed from the structural point of view; the parametric design has been carried out on a 90-story building, characterized by an aspect ratio H/L equal to 6,62.

Regular patterns, obtained by means of uniform vertical tessellation of a constant base unit, as well as patterns characterized by variable angle (VA) and variable density (VD) have been considered. The configurations herein considered all rely on the triangle module as a giant

order, thus, varying the module and the tessellation strategy from one configuration to the other, it is possible to obtain different visual articulation of the building façade through solutions that are almost comparable in terms of structural performance.

Handy and quick analytical tools for preliminary sizing of diagrid members are proposed where the geometrical and mechanical parameters which govern the load path, resisting mechanisms and deformation modes, are clearly identified; this allows for the complete control of the structural response and for the fast assessment of the sensitivity to changes/modifications.

The alternative structural solutions have been also refined and optimized in an usual, iterative manner, through standard finite elements analysis, in the same way as in more traditional structural designs. However the attention is mainly focused to procedures for the preliminary design, which avoid to leap blindly from the phase of geometrical pattern generation to phase of computer structural analyses.

The structural assessment of the alternative diagrid solutions has shown that several patterns can be considered equally efficient, i.e. exhibit similar values of structural weight and of building top drift, suggesting that different geometrical arrangements of diagonal members, designed for the same stiffness and strength requirements, give rise to similar values of global material consumption.

The importance of checking the local strength demand in the diagonal elements, as already observed in previous chapter, has been confirmed. In particular, all patterns except one have a percentage around 5% of diagonal members characterized by DCR larger than 1 under design loads.

The need for secondary stability system (SBS) for reducing the interstory drifts and stabilizing the core gravity columns at intermediate floor levels has emerged from the structural response of the diagrid patterns,

particularly the ones characterized by the tallest diagrid modules and/or the most flexible diagonal members. With this regard it has been shown that ordinary concentric braced frames located in the interior core are sufficient for drastically reducing the interstory drifts, with a very slight increase (3%) of the structural weight.

The conceptual framework established in this paper for dealing with diagrid structures essentially allows the designer to outline a range of structural configurations, and merely use the computer to fine tune them. In fact, being diagrids inherently efficient systems, the simplified procedures let the designer guess with a reasonable confidence what to expect from more rigorous and sophisticated analyses, and take the designer 90% of the way towards an optimized solution. For this reason both the design procedures and the results in terms of structural efficiency here provided can be helpful for structural designers involved in exploring patterns solutions for diagrids, and contemporarily, can enlarge the freedom and unchain the inventiveness of architects willing to exploit the expressive potentials of diagrids.

4 Secondary bracing systems for diagrid structures in tall buildings

In this chapter a framework for assessing the "local" structural issues in the design of diagrid tall buildings is reported, and a methodology for establishing the need for a specific secondary bracing system (SBS) as a function of the diagrid geometry is presented. Further, design criteria for secondary bracing systems are worked out and applied to some 90 story building models, characterized by perimeter diagrid structures with different module height and diagonal cross sections. The outcomes of the proposed simplified procedures, both for assessing SBS necessity and for the consequent SBS member design, have been compared to the structural response of the diagrid building models, obtained without and with SBS, demonstrating both the accuracy of the proposed formulations and the primary importance of the discussed local questions. In fact, all analyzed diagrid models exhibited problems concerning stability of interior columns (i.e. multi-storey buckling modes) and/or local flexibility (excessive interstory drift); the above local problems are completely solved after the introduction of a SBS at the central core location, and, against a modest increase of structural weight (about 3%), any flexural engagements in the diagrid member is eliminated.

4.1 Introduction

As frequently happens in the field of tall building design, it can be observed that the research lags behind the advanced state of the practice:

despite the wide use of this structural solution, remarkably little formal research is conducting by academic institutions on diagrid structures and relevant behavior, design and analysis issues.

An important question related to the design of diagrid buildings has not received adequate attention so far, namely the need for bracing of the multiple-story diagrid module. In the previous chapters, it has been observed that, though the diagrid structure provides the required lateral stiffness to the building under wind loads, large interstory drifts arise at floor levels located within the diagrid module, particularly the ones characterized by the steepest angles (i.e. the tallest diagrid modules) and/or the most flexible diagonal members.

From an overview of recent realizations and projects of diagrid structures, partially reported in [25], it seems that only the 30 St. Mary Axe, characterized by a module 2-storey tall, has an interior core structure designed as a simple frame, merely resisting gravity loads. All other buildings, with diagrid module extending over 4 to 6 storey and more, have a core structure that, while sharing the global stiffness and strength demand in a tube-in-tube configuration, also provide local floor-to-floor restraints to the diagonal members, thus avoiding flexural engagement along the member length, and preserving the purely axial behavior in the diagrid structure.

However, the extraordinary efficiency of diagrid described in the previous Chapters would always allow for a pure tube configuration, with core structure only resisting gravity loads, and diagonalized façade providing the global stiffness and strength to resist lateral loads. But this structural choice requires the need of addressing the "local" behavior of the structural members within the module height, which can extend several floors apart; the problem is twofold, and, involving both the perimeter diagrid members and the interior core columns, requires: (i) to reduce or avoid the flexural deformations of the diagonal members along

their length, and (ii) to stabilize the core gravity columns at intermediate floor levels. Similar structural issues arise in other lateral load resisting systems for tall buildings, whenever mega-bracing elements spanning over several floors are employed: this is the case of tube configurations characterized by mega-diagonals, namely the braced tube, as well as exoskeleton mega-structures [47], [1]. However the case of diagrid is unique due to the complete absence of vertical columns in façade.

Therefore the aim of this chapter is to provide a contribution towards filling the gap between the advanced state of practice and the research state of art, specifically focusing on the above structural issues that seem nor secondary neither negligible in the design process. This could encourage the applications of diagrid in purely-tube configurations, thus allowing for feasible, efficient and material-saving solutions.

In this chapter a thorough evaluation of the local behavior of diagonal members and gravity columns within the diagrid module height are provided, and a methodology for establishing the need for a specific secondary bracing system as a function of the diagrid geometry is presented. Further, design criteria for secondary bracings are derived both for controlling diagonal flexural deformations and gravity column buckling; the application of the above formulations to some 90 story building models, characterized by perimeter diagrid structures with different module height and diagonal cross sections, allows for comprehensive discussion on design implications of secondary bracings.

4.2 Statement of the structural issues

The structural behavior of systems with mega-diagonals could be assimilated to a vertical truss with panel points (diagrid nodes) located multiple floors apart; in Figure 4-1a a typical diagrid system is sketched,

with a 3-storey-high triangle module. The diagrid structure ensures the global stiffness and strength of the overall building only engaging the diagonal members in a purely axial behaviour (i.e. tension/compression internal forces and extension/shortening deformations), and fully braces the interior gravity columns for stability only at panel points. The intermediate floors, marked with asterisks in Figure 4-1a, are not laterally restrained by the global behavior of the diagrid system; more precisely, if diagonals are continuous throughout the module height, the floors would derive a certain degree of lateral stiffness only from the flexural stiffness of the diagonals (Figure 4-1b).

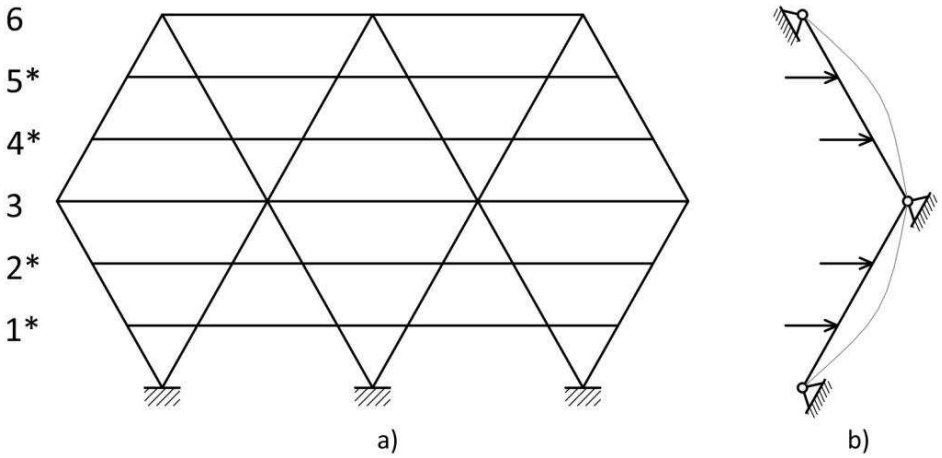

Figure 4-1 Sketch of a typical diagrid system; b) Static scheme of mega-diagonal elements between panel points

This particular behavior has important consequences.

First of all, the global lateral system, that guarantees the building stiffness and strength under horizontal loads, is not able to guarantee as well lateral stability of interior gravity columns between the panel points: the lateral restraint is given at regular (multiple floor) intervals, therefore the two requirements of resisting lateral loads and stabilizing columns

become somewhat separated. As in the case of other mega-bracing structures, "the problem is one of overall story stability with all columns buckling simultaneously in a multy-story mode between the mega-brace point" [1].

The second important local issue of mega-bracing configurations concerns the flexural deformations of the mega-diagonals along their length, between panel points, that arise while restraining intermediate floors. As a consequence, local deflections within the module augment lateral displacements deriving from the global deformation mode of the diagrid structure. Depending on the number of mega-diagonals on building façade, on the mega-diagonal cross section, and on the module height, the local deformations between the panel points could produce very large interstory drifts, and cause serviceability problems in architectural elements such as claddings, floor finishes and partitions.

These two problems, i.e. gravity column stability and diagonal flexural engagement, are strictly related and concern the local lateral flexibility of the structure; both could be solved according to different approaches [38], [47], [1].

The first solution consists in leaving the intermediate floors laterally restrained by the flexural stiffness of mega-diagonals only, and accounting for this in the design of gravity columns and other components, i.e. designing the gravity columns as they were braced only at the panel points of the diagrid, and sizing the diagrid members with enough flexural stiffness to control interstory drifts. This approach, however, may lead to quite large cross sections for columns and diagonals, especially for very tall buildings.

The second solution [Nair, 1988] is to add structural members between the panel points of the overall bracing system: examples of local bracing members placed within the diagrid module are provided in Figure 4-2a (dashed lines); similar configurations, though designed for other than

structural purposes, have been proposed for the Hypergreen tower [11], designed by architect Jacques Ferrier in partnership with Lafarge Company (Figure 4-2b). This solution however interacts with the aesthetics of the building, compromising the clarity and regularity of the diagrid, thus requires a decision shared with the architectural and façade designer.

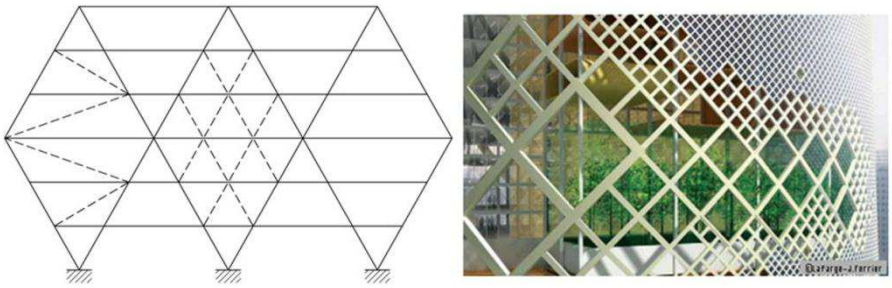

Figure 4-2 a) Examples of local bracings placed within the diagrid module; b) The structural façade of the Hypergreen

The third solution is the addition of a specific secondary bracing system, separated from the primary diagrid structures and acting between the module panel points, with the dual function of: (i) stabilizing gravity columns at the intermediate levels, and (ii) transferring the horizontal forces applied at these intermediate levels to the diagrid nodes, thus excluding the involvement of diagonal bending behaviour.

A framework for addressing the above structural issues in the design of diagrid tall buildings is presented in the following. First, a simplified method is suggested for assessing the viability of the first solution above delineated, i.e. for examining the local behaviour of diagrid buildings and accounting for the flexural demand on the diagonal members deriving from the lack of single floor restraint; the method eventually reveals if a

specific structural system is strictly necessary for preventing multi-storey instability of gravity columns and excessive deformations within the diagrid module. Then, a design procedure for secondary bracing systems (SBS) is formulated and applied to some diagrid building models; the structural behaviour of the buildings with and without SBS is compared and discussed, and design implications are emphasized.

4.3 Need for SBS (Is your diagrid suitably braced?)

Within the module height, the diagrid members provide a partial lateral restraint as a function of their flexural stiffness; this contribution could be or not sufficient to brace the internal columns, activating a single floor buckling mode, and to limit interstory drifts, thus preventing serviceability problems. Simplified calculations for quantifying the diagonal stiffness contribution within the diagrid module are very important in order to decide if a secondary bracing system is necessary or not.

4.3.1 Stability

The bracing effect provided by diagonals on interior gravity columns can be evaluated idealizing the system constituted by diagonals and columns as a so called "lean-on" system; according to the classification of bracing systems given by [16], in this configuration some "leaning" pin-ended columns (namely, the gravity columns located in the building service core) rely for stability purpose on other adjacent members with nonzero lateral stiffness (namely, the diagrid members). The leaning columns and the adjacent bracing members are tied or linked together, such that buckling of one column requires all columns and adjacent members to buckle with the same lateral displacement.

Considering the lean-on structural configuration in Figure 4-3a, the element A represents the megadiagonals while the element B represents the core gravity columns; two principal buckling modes are possible for this structure arrangement: the global sway (multiple floors) mode, and the local non -sway (single floor) mode. The buckling capacity of the system associated to each mode can be calculated accounting for the capacities of the structural elements (leaning-on and bracing elements) involved in the mode.

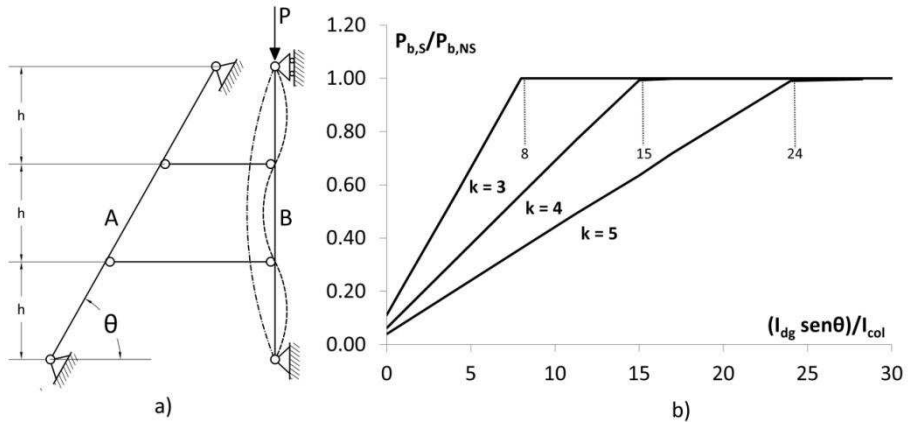

Figure 4-3a) Lean-on configuration of mega-diagonals (A) and core gravity columns (B) ; b) Ratio between the sway buckling load ($P_{b,S}$) and the no-sway buckling load ($P_{b,NS}$) vs. ratio between inertia moment of diagonal and column

If the bracing element A is very slender, its contribution to the system can be neglected and the system will buckle in the sway mode, shown by the dot-dash line in Figure 4-3a; the associated buckling load $P_{cr,col,S}$ is given by the sum of the buckling capacities of the n_{col} columns extending over k stories, i.e.:

$$P_{crit,col,S} = \frac{\pi^2 \cdot E \cdot n_{col} I_{col}}{(k h_{\text{int}})^2} \tag{4.1}$$

where, in the hypothesis that all columns have the same cross section, I_{col} is the minimum moment of inertia of the column section, k is the number of floors between two consecutive panel points (i.e.: k=3 in Figure 4-3a), h_{int} is the interstory height.

If the bracing element A is not very slender, its contribution to the buckling capacity in the sway mode is not negligible; therefore the sway buckling capacity of the system is augmented by this contribution, and is given by the sum of $P_{crit,col,S}$, as calculated by equation 4.1, plus the buckling capacities of the diagonals $P_{cr,dg}$, i.e.:

$$P_{crit,dg} = \frac{\pi^2 \cdot E \cdot sen\theta \cdot (I_{zz} n_w + I_{yy} n_f)}{(k \cdot h \cdot sen\theta)^2} = \frac{\pi^2 \cdot E \cdot (I_{zz} n_w + I_{yy} n_f)}{(k \cdot h)^2 \cdot sen\theta} \tag{4.2}$$

where: n_w and n_f are the number of diagonals, respectively on the web and flange building façades; I_{zz} and I_{yy} are the inertia moments of the diagonals respectively along the zz and the yy directions (if the local axis zz of the diagonals sections is oriented along the building perimeter); θ is the diagonal angle. For the sake of simplification, square hollow sections are considered for diagonals, for which $I_{dg} = I_{zz} = I_{yy}$, and the equation 4.2 becomes:

$$P_{cr,dg} = \frac{\pi^2 \cdot E \cdot n_{dg} \cdot I_{dg}}{(k \cdot h_{int})^2 \cdot sen\theta} \tag{4.3}$$

with $n_{dg} = (n_{d,w} + n_{d,f})$ total number of mega-diagonals along the building perimeter.

Therefore the sway buckling load of the lean-on system is given by:

$$P_{b,S} = P_{cr,col,S} + P_{cr,dg} =$$
$$\frac{\pi^2 \cdot E \cdot n_{col} I_{col}}{(kh_{\text{int}})^2} + \frac{\pi^2 \cdot E \cdot (I_{zz} n_w + I_{yy} n_f)}{(k \cdot h_{\text{int}})^2 \cdot sen\theta} \tag{4.4}$$

If the bracing element A is sufficiently stiff, buckling is controlled by the non-sway mode, shown by the dashed line in Figure 4-3a, with associated capacity equal to:

$$P_{b,NS} = P_{cr,col,NS} = \frac{\pi^2 \cdot E \cdot n_{col} I_{col}}{h_{\text{int}}^2} \tag{4.5}$$

Quite trivially, the occurrence of this buckling mode implies that the system capacity in the sway mode, $P_{b,S}$ (eq. 4.4), is larger than the non-sway buckling load $P_{b,NS}$ (eq. 4.5), that, as already said, only happens if the bracing is "sufficiently" stiff; therefore, equating the buckling capacities of the two modes, $P_{b,S} = P_{b,NS}$, i.e.:

$$\frac{\pi^2 \cdot E \cdot n_{col} \cdot I_{col}}{(k \cdot h_{\text{int}})^2} + \frac{\pi^2 \cdot E \cdot n_{dg} \cdot I_{dg}}{(k \cdot h_{\text{int}})^2 \cdot sen\theta} = \frac{\pi^2 \cdot E \cdot n_{col} \cdot I_{col}}{h_{\text{int}}^2} \tag{4.6}$$

the statement "sufficiently stiff" can be quantified, and therefore the condition of non-sway buckling occurrence can be established:

$$n_{dg} I_{dg} > (k^2 - 1) \cdot sen\theta \cdot n_{col} \cdot I_{col} \tag{4.7}$$

In order to check this procedure, finite element analysis have been carried out on three models, respectively characterized by k=3, 4, 5. The

results, reported in Figure 4-3b, confirm the prediction accuracy of eq. 4.7: they show that the sway buckling load $P_{b,S}$ linearly increases with I_{dg}, and the internal columns buckle in the non-sway mode when I_{dg} senθ/I_{col} is greater than 8, 15 and 24, respectively for k=3, 4 and 5.
Therefore, once the diagrid structure has been designed as the primary lateral load system of the building, the equation (4.7) could be used to find out if the SBS is necessary or not for the stability of internal columns. If $n_{dg} \cdot I_{dg}$ is less than $(k^2-1) \cdot \text{sen}\theta \cdot n_{dg} \cdot I_{col}$, then the internal columns buckle in a sway mode; in this case, either the internal columns have to be designed for more than one-story buckling length, or an internal system of secondary bracing is necessary.

4.3.2 Interstory drift

In order to evaluate if the flexural stiffness of mega-diagonals is enough to avoid serviceability problems, the interstory drift (δ) must be used as the structural performance parameter; in particular the interstory drift experienced by the structure should be less than a specified value (δ_{lim}):

$$\delta_{\text{lim}} = h / \eta \tag{4.8}$$

where η is a factor mainly depending on the cladding type and connections (eg. β=200 for rigid claddings rigidly connected to structure).
In the case of diagrid structures, the interstory drift could be seen as the sum of two contributions, respectively due to the global deformation of the building (δ_{glob} in Figure 4-4a) and to the local flexural deformation of the diagonals between the panel points (δ_{loc} in Figure 4-4a):

$$\delta_{\lim} = \delta_{glob} + \delta_{loc.} = h_{\text{int}} / \eta \tag{4.9}$$

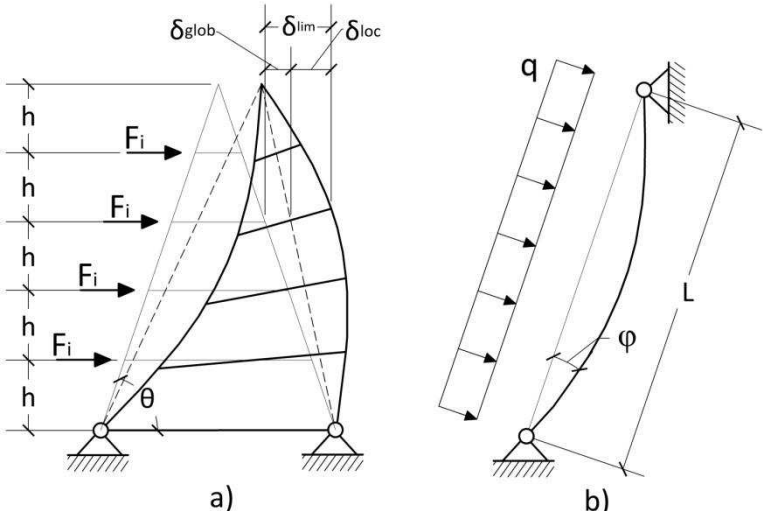

Figure 4-4 a) Lateral deformation of diagrid module b) Static scheme of the diagrid diagonals under horizontal forces

The global stiffness requirements for tall building design are frequently specified in terms of maximum displacement at building top, set equal to H/ε, where H is the building height and ε is usually assumed equal to 500. Considering a simplified linear shape for the building deformed configuration, then also δ_{glob}=h/500, and:

$$\delta_{loc} = \delta_{\lim} - \delta_{glob} = \frac{(500 - \eta) h_{\text{int}}}{500\eta} \tag{4.10}$$

The structural behavior of the diagonals between the panel points could be idealized as a simply supported beam (Figure 4-4b), with hinged end restraints corresponding to the panel points, uniform load acting along the span L (corresponding to the horizontal forces acting at the

intermediate floors, i.e. $q = sen\theta \sum_{i=1}^{k-1} F_i / L$), and beam stiffness related to the flexural stiffness of the diagonal member. The maximum rotation occurring at hinge end restraint is:

$$\varphi = \frac{\left(\sum_{i=1}^{k-1} F_i \right) \cdot sin\theta \cdot L^2}{24 E I_{dg} n_{dg}} \tag{4.11}$$

The maximum local interstory drift defined by equation (4.10) can be easily expressed as a limitation for the beam rotation:

$$\frac{\delta_{loc}}{h_{\text{int}}} = \varphi = \frac{\left(\sum_{i=1}^{k-1} F_i \right) \cdot sin\theta \cdot L^2}{24 \cdot E \cdot I_{dg} \cdot n_{dg}} < \frac{(500 - \alpha)}{500 \cdot \alpha} \tag{4.12}$$

The equation (4.12) could be used for establishing if the SBS is necessary or not for local drift purpose, once the primary structural system (mega-diagonal cross sections) has been designed for global stiffness requirements (top building drift not exceeding H/500). Conversely, the same relationship can be used as a design tool, i.e. for deriving the minimum inertia moment ($I_{dg,min}$) of diagonal section that satisfies the interstory drift limitation:

$$I_{dg,\min} = \frac{\left(\sum_{i=1}^{k-1} F_i \right) \cdot sin\theta \cdot L^2}{24 \cdot E \cdot n_{dg}} \cdot \frac{500 \cdot \alpha}{(500 - \alpha)} \tag{4.13}$$

From the equations (4.7) and (4.13) it is evident that the need for the SBS only depends on diagrid geometry: fixed the module width (i.e. the number of diagonals along the building façade, n_{dg}), diagrids with high value of the angle θ have longer diagonals (L) and lower flexural stiffness; conversely, adopting smaller values for θ, the number of floors between the panel points and the length of the diagonal decrease, thus the flexural stiffness of diagonals could be enough to satisfy the conditions (4.7) and (4.12). This is the case of the 30 St. Mary Axe, London – also known as the Swiss Re building – where the triangular modules are two story high; in fact it is the only diagrid building without interior core structure and/or SBS.

4.4 Design of secondary bracing systems (SBS)

4.4.1 Generals remarks

Once the need for SBS has been assessed, the bracing of the intermediate floors between the panel points of the diagrid could be realised by means of limited modifications to the simple frame of the service core, namely either rigid connections at beam-column joints or triangulation of the structural framework, thus obtaining either a moment resisting frame MRF or a concentric braced frame CBF.

It is worth noticing that a substantial difference does exist between CBFs / MRFs utilised as primary lateral load system and the same structures working as SBSs: while in common MRFs and CBFs a lateral restraint is only present at the base (Figure 4-5a and c), in SBSs both bottom and top restraints are present at the mega-module points, thus only the intermediate levels can sideway (Figure 4-5b and d); in addition, and perhaps more importantly, while common CBFs or MRFs carry lateral

loads along the overall building height, the SBS only works on the module height and carry lateral loads only within the zones between two module panel points. In other words the SBS is a "local" structural system, with both base and top lateral restraints, and height equal to the module height; of course the SBS extends throughout the full height of the building, but it is globally given by the vertical stacking of single structures, each working on a limited number of stories (namely, the number of stories of one module).

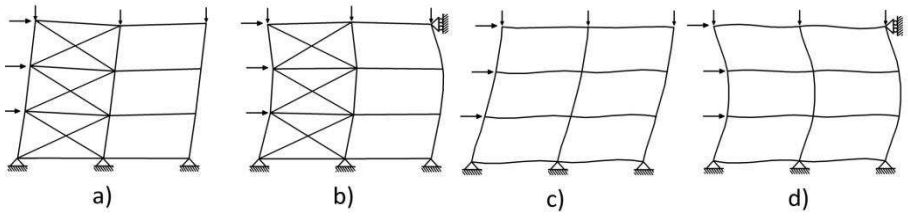

Figure 4-5 Deformed configuration under horizontal forces for a) common CBF; b) Secondary Bracing System CBF; c) common MRF; d) Secondary Bracing System MRF

Considering the peculiarity of SBSs, in the following some procedures suggested in the literature for stability bracings design are briefly reviewed and reworked out for ready-to-use formulae applicable to the specific case of SBS in diagrid buildings; in addition, the problem of local flexural deformations arising in the diagrid members within the module is examined and a specific design criterion for SBS able to control interstory drifts is formally derived.

4.4.2 Stability design procedure

The problem of SBS stability design concerns the definition of the stiffness requirements for generic SBS in order to prevent multiple story buckling of columns in simple frame structures, as well as the definition

of the strength demand on the SBS members deriving from the bracing function. This subject is of fundamental importance in the field of structural steelwork, and has been widely discussed in the relevant literature, starting from the seminal paper by Winter [50], and subsequently in design oriented papers by Yura [51] and Nair [38], with the major results having been included in design codes, starting from 1999 [2], [3].

As in the previous section, the problem concerns the stability of the pin-ended gravity columns, usually located in the service core of the building; but, differently from the previous section, where the interaction between the gravity columns and the perimeter diagrid was idealised by means of a lean-on system, here the focus is on the structural interaction between the columns and the SBS; this bracing scheme corresponds to the so-called "relative" bracing system, where, according to [16], [17] the displacements at one braced point are related to the displacements at any other braced point.

In a single story brace (Figure 4-6a) the diagonal connects the top column to a fixed support; thus, this structure is equivalent to the simple scheme depicted in Figure 4-6b (a bar infinitely rigid, hinged at the bottom and supported by a spring at the top); analysing the buckling behaviour of this scheme, Timoshenko [46] derives the value of the spring stiffness which corresponds to the buckling mode of the fully restrained bar, β_{id}:

$$\beta_{id} = \frac{P_{cr,col,NS}}{h_{\text{int}}} = \frac{\pi^2 EI}{h_{\text{int}}^3} \tag{4.14}$$

where, according to the notation adopted in section 4.3.1, $P_{cr,col,NS}$ is the buckling load of the fully braced column and h_{int} is the column length, corresponding to the interstory height of the building. If the spring

stiffness β is less than β_{id}, the buckling load of the column will be less then $P_{cr,col,NS}$ and the column will buckle involving displacement at the column top; if β is greater than β_{id} the buckling load will be equal to $P_{cr,col,NS}$. This approach is valid in the hypothesis of "ideal" column (perfectly straight, simple compressed, etc.).

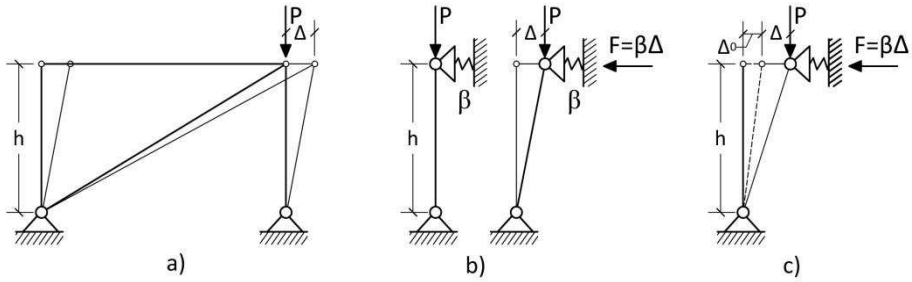

Figure 4-6 a) Horizontal deformation of a single story brace; b) Structural scheme equivalent to single story brace; c) Structural scheme equivalent to single story brace considering initial imperfections

Starting from the previous formulation, Winter [50] provides a simple method for dealing with the case of "real", imperfect columns, with the aim of calculating strength and rigidity required to the support for the so-called "full bracing" condition. The reference model is characterized by an initial crookedness Δ_0, representing a global imperfection accounting for both mechanical and geometrical imperfections (Figure 4-6c). As a compression load P is applied, the column will experience an additional displacement Δ, and the spring reacts with an horizontal force F equal to βΔ; the value of β which restrains the column buckling in a single-story mode, appointed as $\beta_{req,b}$, can be obtained from the rotation equilibrium about the column base:

$$P_{cr,col,NS} \cdot (\Delta_0 + \Delta) - \beta_{req,b} \cdot \Delta \cdot h = 0 \tag{4.15}$$

which gives:

$$\beta_{req,b} = \frac{P_{cr,col,NS} \cdot (\Delta_0 + \Delta)}{\Delta \cdot L} \tag{4.16}$$

For the ideal column (i.e. $\Delta_0 = 0$), $\beta_{req,b}$ is equal to $P_{cr,col,NS}/h$, which corresponds to the value β_{id} obtained in the theoretical case of the perfectly-straight elastically-supported column (equation 4.14). In order to define the relationship between the spring stiffness and the column buckling strength P_b, the equation (4.15) can be written in terms of total displacement ($\Delta_T = \Delta + \Delta_0$) and spring stiffness β:

$$P_b \cdot \Delta_T - \beta \cdot h \cdot (\Delta_T - \Delta_0) = 0 \tag{4.17}$$

multiplying and dividing by the ideal stiffness defined in equation (4.14)

$$\frac{P_b}{P_{cr,col,NS}} = \frac{\beta}{\beta_{id}} \cdot \left[\frac{(\Delta_T - \Delta_0)}{\Delta_T} \right] = \frac{\beta}{\beta_{id}} \cdot \left[1 - \frac{1}{\Delta_T / \Delta_0} \right] \tag{4.18}$$

The relationship between $P_b/P_{cr,col,NS}$ and Δ_T/Δ_0 is depicted in Figure 4-7 for different values of the ratio β/β_{id}. For $\beta=\beta_{id}$ (grey curve), when P_b approaches $P_{cr,col,NS}$, the top displacement of the column becomes very large, that, in turn, leads to very large brace forces (i.e.: $F=\beta\Delta$). The increase of β beyond β_{id} ($\beta>\beta_{id}$) leads to smaller displacements at the top

of the column and, consequently, to smaller values for F (the larger the brace stiffness, the smaller the brace force).

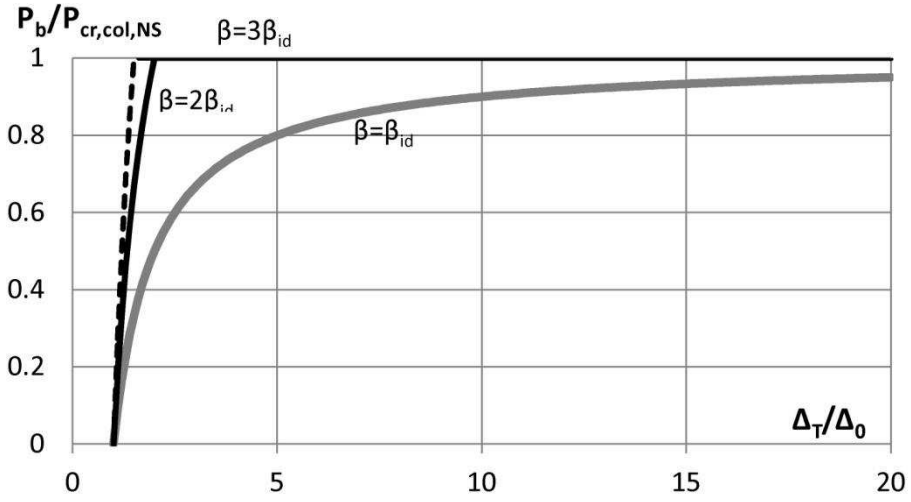

Figure 4-7 Ratio between the system buckling load (P_b) and the columns buckling load ($P_{cr,col,NS}$) vs. ratio between the total and the initial crookedness (Δ_0)

In the case of multi-degree-of-freedom systems, as is the case of the SBS of k stories, Zhang et al. [54] demonstrated that the equation (4.16) for the required stiffness as well as the above discussion, still hold, regardless the number of brace points.

Design recommendations and codes concerning the stability bracing [2] are based on the previous concepts, and the relevant provisions assume, more or less implicitly, a brace stiffness at least twice the ideal stiffness and an out-of plumbness Δ_0=h/500. Accordingly, the required braced force is obtained as:

$$F_{br} = \beta_{req,b}\Delta = 2\beta_{id}\Delta_0 = 2P_{cr,col,NS}\frac{\Delta_0}{h_{\text{int}}} = 0.004P_{cr,col,NS} \tag{4.19}$$

Given this force, it is possible to design the SBS members (diagonals of the CBF) in order to stabilize the interior gravity columns of a buildings employing perimeter diagrid as lateral load resisting system.

4.4.3 Interstory drift design procedure

In the design procedure of SBS with the purpose of limiting the local share of interstory drift, the starting point is the definition of δ_{loc}, as given by eq. 4.10. For a conservative and simple approach, the contribution of the diagonal flexural stiffness is neglected; according to this assumption, the local deflection between the panel points is only related to the lateral stiffness of the SBS, which can be expressed as:

$$\beta_{req,d} = \frac{\left(\sum_{i=1}^{k-1} F_i\right)}{2\delta_{\text{lim},loc}} \tag{4.20}$$

where F_i are the horizontal forces acting on the building at the intermediate floors between the panel points. Substituting equation (4.10) in (4.20):

$$\beta_{req,d} = \frac{250\cdot\eta\cdot\left(\sum_{i=1}^{k-1} F_i\right)}{(500-\eta)\cdot h_{\text{int}}} \tag{4.21}$$

The above formula provides the lateral stiffness required for SBS, i.e. the stiffness that the interior CBFs/MRFs of k levels should exhibit in order to contain the interstory drift within the limit h/η.

4.5 Design applications

In this section the accuracy and reliability of the criteria for establishing the need for SBS (equation 4.7 and 4.13) and of the relevant design formulae worked out (equations 4.19 and 4.21), are assessed; for this purpose, the three diagrid regular structures, designed as stand-alone lateral load resisting systems in Chapter 3, are considered.

4.5.1 Building model

As reported in Chapter 3, the reference building model has 90 storey, a square plan 53x53 m, with a central core 25,4x25,4 m; the total height is 351 m, with interstory height equal to 3.9 m. The overall building geometry and the floor framing plan are depicted in Figure 4-8; the dead load is 7 kN/m^2, including the weight of the floor steel structure, of the internal partitions and the external claddings. The live load has been assumed equal to 4 kN/m^2. The horizontal load due to wind pressure has been calculated according to ASCE-7 05 provisions [ASCE 2006], considering wind speed equal to 50 m/s (110 mph) (see Table 4-1).

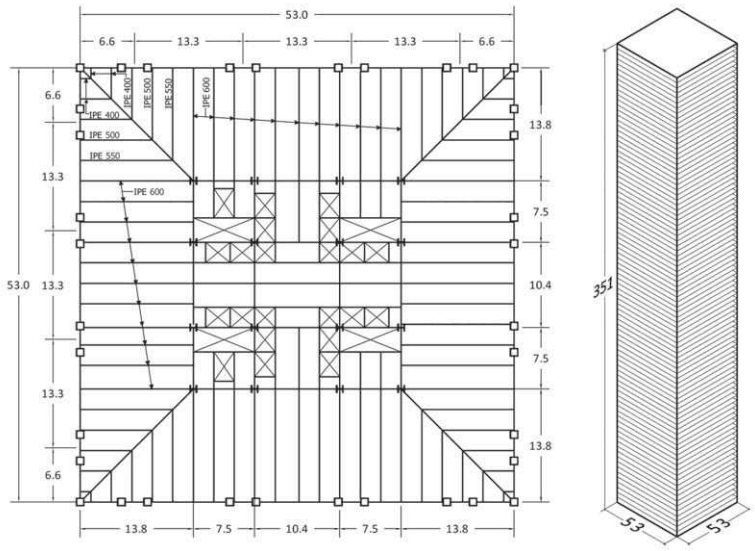

Figure 4-8 Building model: overall dimensions and floor framing plan

GRAVITY LOAD [kN/m^2]	
Dead	7
Live	4
HORIZONTAL LOAD – WIND	
Base shear [MN]	69,4
Overturning moment [MN m]	13043,2

Table 4-1 Design loads

The steel material used both for the horizontal floor structures and for the vertical structures (exterior diagrid and interior core gravity columns) is S275, with f_{yk} = 275 N/mm^2; for the framing floor structure, beams IPE 600 (depth 600mm, width 220mm) spaced at 2.5 m, have been selected to support a composite steel deck (total thickness 110 mm); for

the diagrid structures and interior core columns, members with built-up box sections have been thoroughly adopted.

The design criterion for sizing the cross-sections of the diagonals is based on global stiffness requirements (see Chapter 3), namely limitation of the building top drift under design wind loads within H/500; no specific caution in limitation of interstory drift has been adopted in the design process. The cross sections adopted for the diagonal members in the three diagrid configurations are provided in table 4-2.

4.5.2 Checking the need for SBS

Concerning the stability issue of internal columns, the need for SBS have been evaluated applying equation 4.7; in particular the ratio $n_{dg}I_{dg}sen\theta/n_{col}I_{cl}$ has been calculated and compared to the relevant limit (k^2-1), as shown in Figure 4-10a, b, c for the three diagrid configurations. The results suggest that for $\theta=60°$ and $k=3$ (Figure 4-10a), only the upper modules have value of diagonal inertia lower than the minimum required for fully bracing the internal columns, while both models with $\theta=70°$, $k=5$, and with $\theta=80°$, $k=9$, have almost all diagonal members with inertia less than the minimum required.

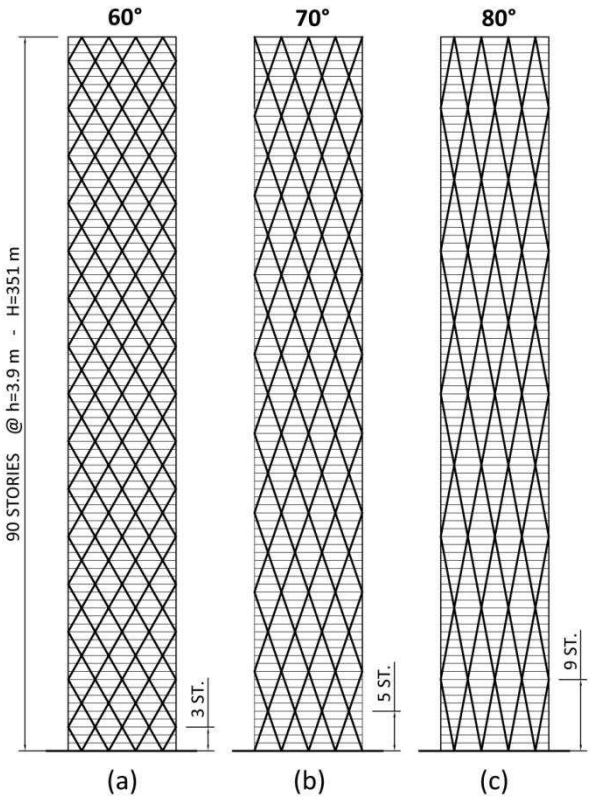

Figure 4-9 Structural patterns: a) 60°; b) 70°; c) 80°

Concerning the interstory drift issue, equations 4.12 and 4.13 have been utilized to establish the need for SBS. The graphs of Figure 4-11 provide the values of the local interstory drift calculated for each diagrid pattern with equation 4.12 (black solid lines and black dots), along with the adopted local limit value, δ_{loc} = 1/300 (red vertical line). It is worth noticing that the inertia of diagonal sections and the height of the diagrid module strongly affect the values of interstory drift: since the diagonal sections decrease from the building bottom to top, while the module height is constant along the building height, then the interstory drifts

rapidly increase with height; therefore all diagrid patterns (60°, 70°, 80°) exhibit interstory drift values at upper modules beyond the design limit. These graphs seem significant in their simplicity, showing that a SBS is strictly necessary for the patterns with diagonal angles equal to 70° and 80°, while in the diagrid with diagonals at 60°, a small increase of the diagonal cross sections, particularly at upper modules, could be sufficient to reduce local problems. Furthermore it is worthy to note that the typical "local" behavior of SBS allows to use it only where it is needed throughout the building height (i.e. at the upper module for θ=60°)

Mod.	**60°**	**70°**	**80°**
1	1200x115	1200 x105	1300 x125
2	1100 x110	1000 x100	1100x120
3	1100x95	800x100	1000x95
4	1000x90	800x 75	800x 65
5	1000x75	600x 90	600x 35
6	800x 80	600x 65	
7	800x 65	600x 50	
8	800x 50	400x 45	
9	600x 55	300x 20	
10	600x 50		
11	600x 40		
12	600x 30		
13	600x 25		
14	400x 20		
15	300x 10		

Table 4-2 Built up box cross sections for diagonals

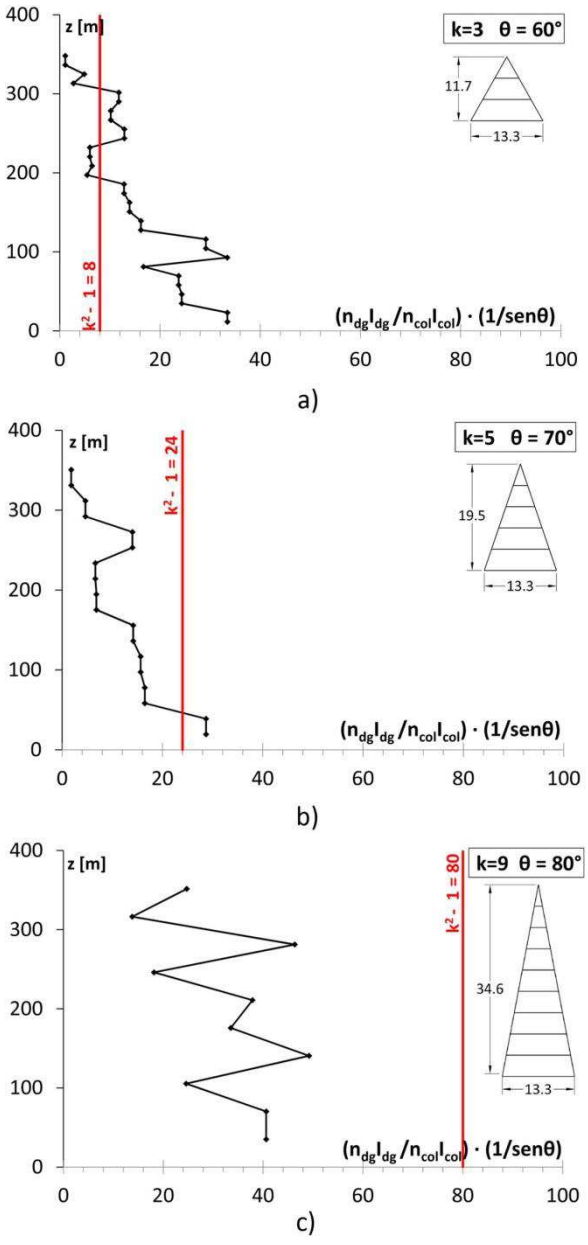

Figure 4-10 Value of $n_{dg}I_{dg}sen\theta/n_{col}I_{cl}$ vs. building height for structural patterns a) 60° ; b) 70°; c) 80°

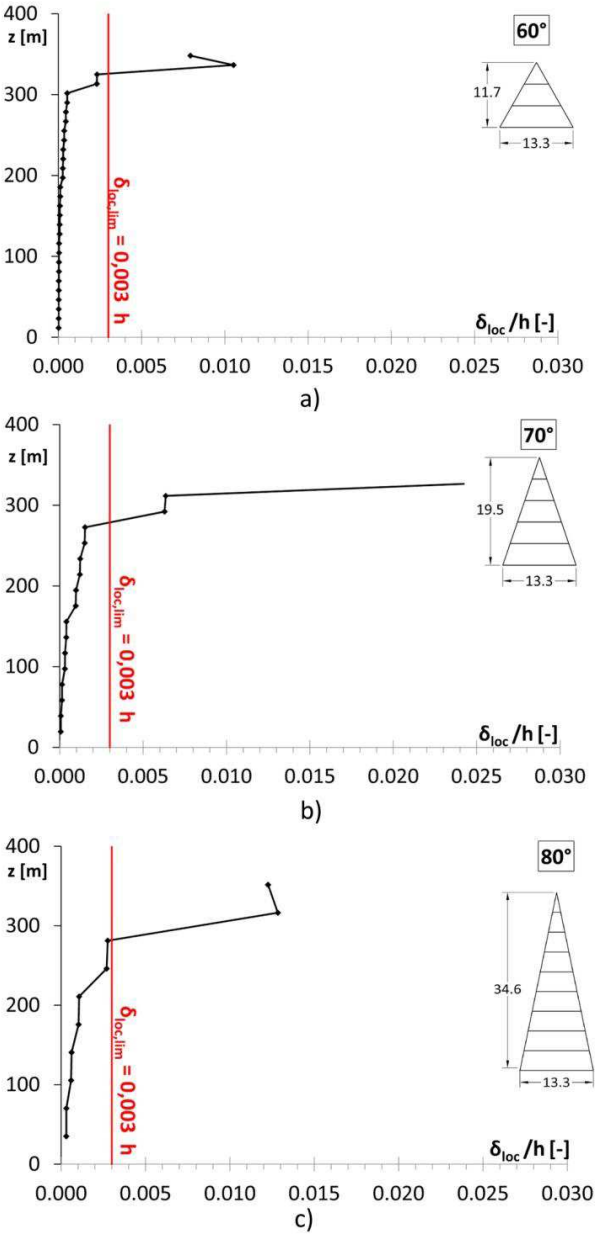

Figure 4-11 Local interstory drift vs. building height for structural patterns a) 60° ; b) 70°; c) 80°

4.5.3 SBS design

For each diagrid building, a SBS consisting of four concentric braced frames along two orthogonal building directions has been designed (Figure 4-12); the twofold design criterion has been adopted for (i) stabilizing the core gravity columns (equation 4.19) and (ii) complying with the imposed drift limitations (equation 4.21).

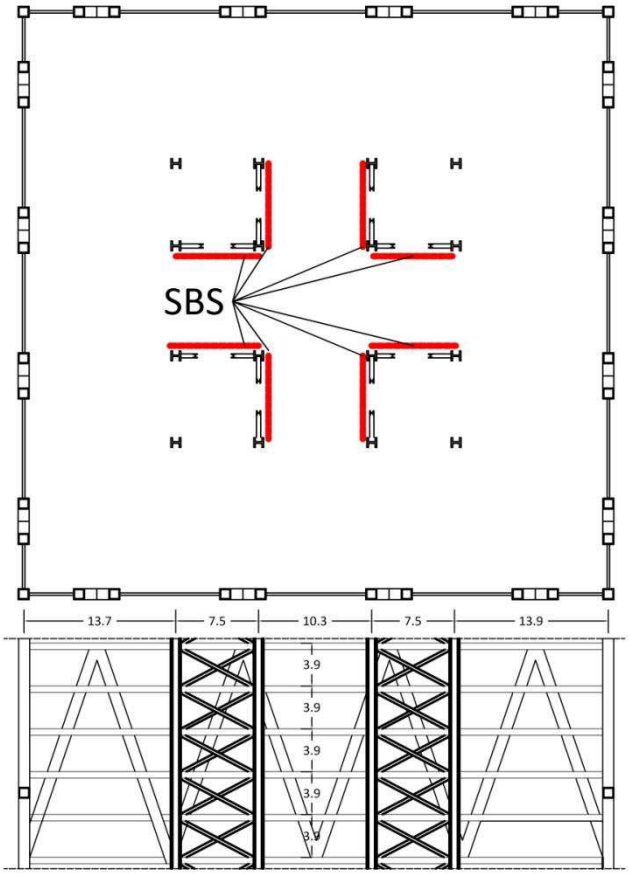

Figure 4-12 Secondary bracing systems, plan location and geometry

The graphs in Figure 4-13 report the comparison between the cross section areas for CBF diagonals obtained considering the stability requirements (solid lines and black dots) and the local interstory drift requirements (dashed lines and grey dots). It can be observed that the section areas obtained for stability requirements are almost the same for all the patterns, solely depending on the gravity load and SBS geometry; conversely, the sections deriving from deflection control are highly affected by the diagrid geometry, and in particular by the number of floors between the module panel points. It is worth noticing that while stability requirements usually are predominant over drift, SBSs designed for stability only could be not sufficient to control interstory drift at the upper modules, particularly for diagrid with steeper angles.
In Figure 4-14 the unit structural weight of the diagrid patterns (with and without SBS) is provided as a bar chart; the values depicted by the bars have been obtained by dividing the total weight of the steel members composing the diagrid structure by the gross floor area of the building. The comparison within each couple of bars (with and without SBS) allows to assess the modest increase of structural weight due to introduction of the SBS, about 3% for all patterns. Therefore it can be stated that a slight increase of the structural weight can lead to significant improvement of the structural behavior of diagrid buildings.

4.6 FEM analysis

In order to evaluate the consistency of the design procedure based on the simplified calculations presented in the previous sections, the diagrid buildings have been analyzed using FEM numerical models with SAP2000 program (Figure 4-15). Static analyses, with and without P-Δ effects, have been carried out the building models under factored gravity

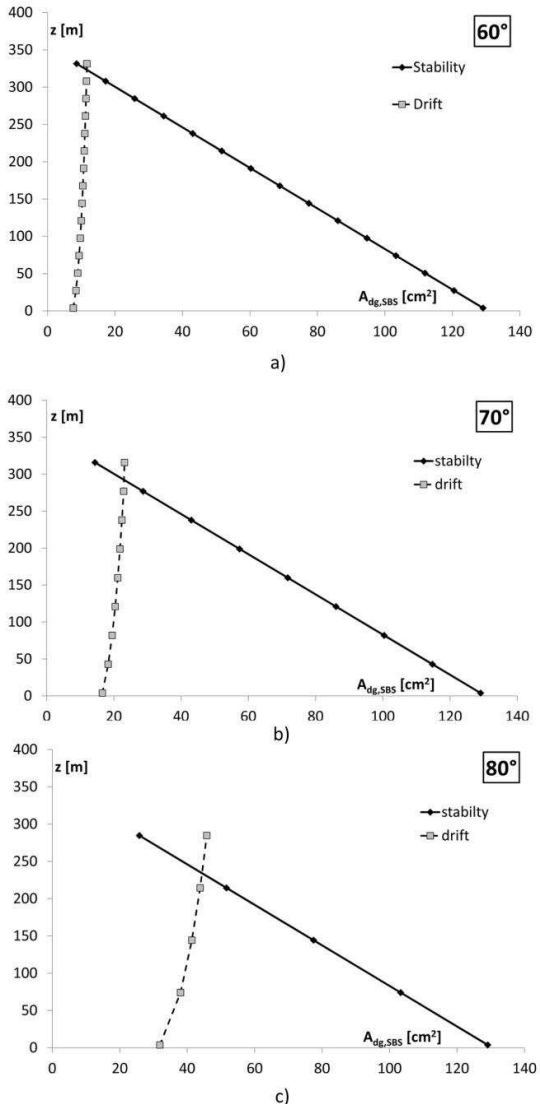

Figure 4-13 Comparison between the cross section areas for CBF diagonals obtained considering the stability requirements (solid lines and black dots) and the local interstory drift requirements (dashed lines and grey dots) in function of the building height. a) 60°; b) 70° ; c) 80°

and wind loads, as specified in Table 4-1. Two configurations, with and without SBS, have been considered for each diagrid building.

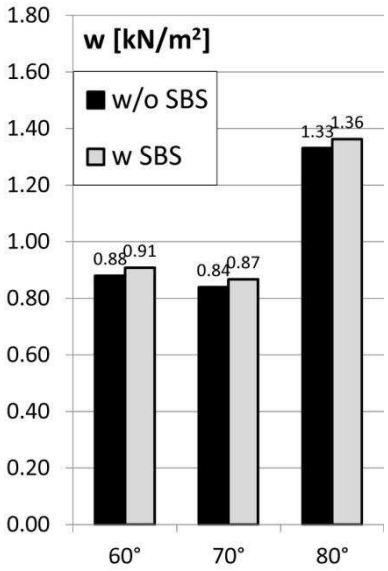

Figure 4-14 Unit structural weight of the diagrid patterns with and without SBS

The analysis results are reported in the following, in terms of lateral displacements, interstory drifts, buckling modes and eigenvalues.

The charts in Figure 4-16 provide the deflection characteristics of the diagrid buildings, without and with SBS, under wind load; in particular Figure 4-16a, c, e, show the lateral displacements as a function of the building height, while the charts in Figure 4-16b, d, f, show the interstory drift ratios ($d_h=\delta/h$). From the comparison of the displacement values (Figure 4-16a, c, e), it is evident that the SBS does not affect the global stiffness of the building, since the top displacement is the same without (black dashed lines) and with SBS (grey solid lines). On the contrary, an overt effect of the SBS can be observed by looking more closely at deformed configurations: models without SBS exhibit large lateral displacements at floors between the panel points, due to the low local stiffness, only given by the flexural stiffness of diagonals. Conversely, in

the models with SBS the lateral stiffness between the panel points is given by the axial stiffness of the SBS diagonals, thus the local deformation is significantly reduced.

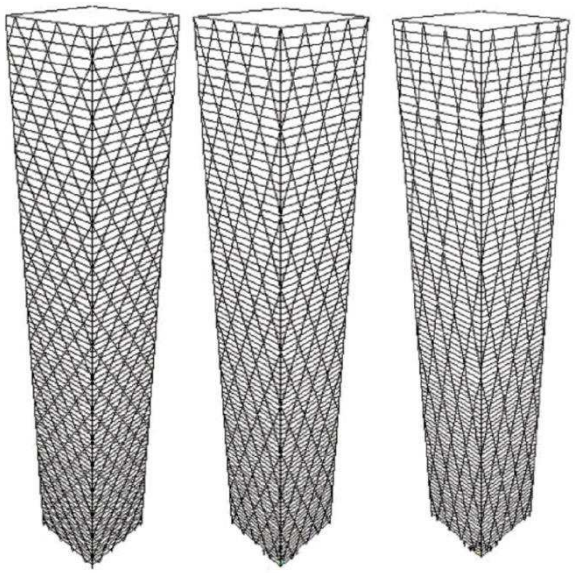

Figure 4-15 3D view of finite element models obtained with SAP2000 for a) 60°; b) 70°; c) 80°

This effect can be better appreciated by analyzing and comparing the results in terms of interstory drift for the structures without and with SBS, given in Figure 4-16b, d, f. All diagrid solutions without SBS (black lines and dots) do not respect the design limit of h/200, particularly at the upper levels, where the diagonal cross sections are smaller; the addition of the SBSs leads the interstory drift values (grey lines and dots) within the assumed limit, for all diagrid patterns.

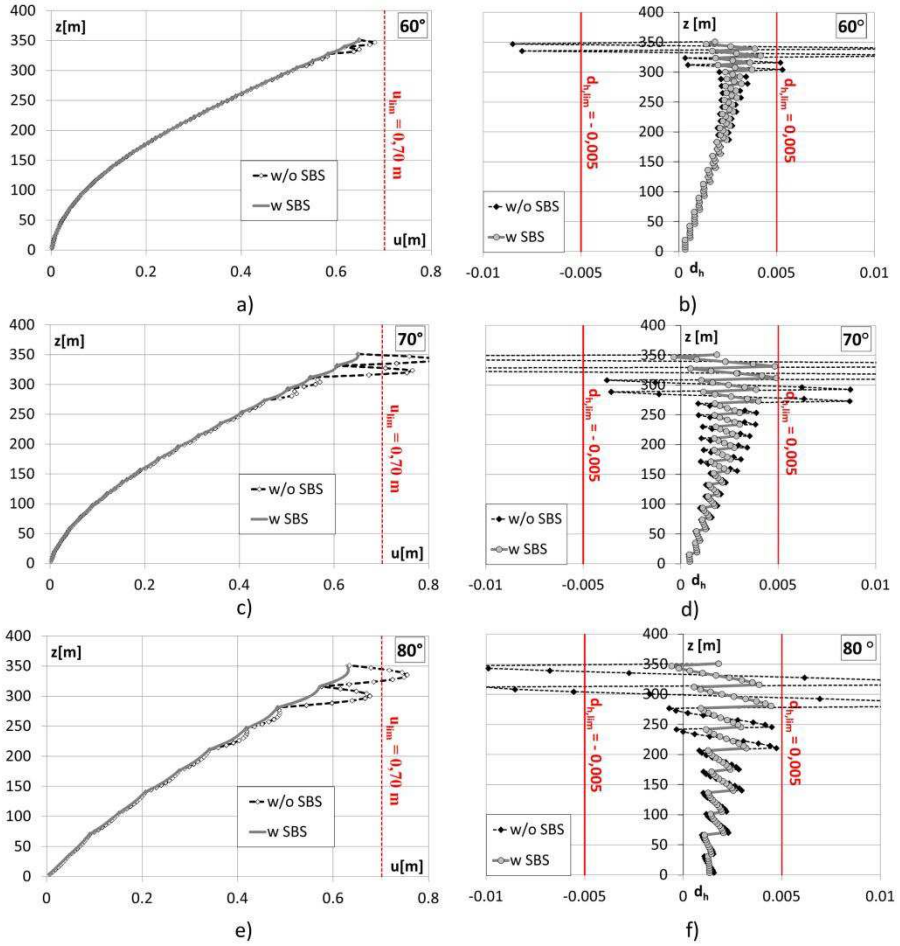

Figure 4-16 Lateral displacements under wind forces a) 60°; c) 70°; e) 80°. Interstory drift under wind forces b) 60°; d) 70°; f) 80°

These results are consistent with the ones obtained by means of the simplified approach (equation 4.13), already shown in Figure 4-11. In Table 4-3 the comparison between the maximum values of interstory drift derived from FEM analysis and from equation 4.12 is explicitly provided, showing errors always within 4%.

Considering the stability issue, an elastic eingenvalue analysis has been carried out for each diagrid building, on both model without and with SBS. In all three cases, buckling of the core gravity columns without SBS occurs in the one-module mode, involving three, five and nine stories, respectively, for the diagrid building with θ equal to 60°, 70°, and 80° (Figure 4-17 a, c, e). In all three cases, as well, the introduction of the SBS modifies the first buckling mode in a single-story mode (Figure 4-17b, d, f), that occurs at the same story level, exclusively depending on the gravity loads and on the column cross sections. Also the eingenvalue under factored loads is almost the same for the three buildings with SBS (4.43-4.86), increasing from 2.87 to 4.86 for θ= 60°, from 1.05 to 4.43 for θ= 71, from 1.37 to 4.44 for θ= 80°.

On the basis of the above comparisons, the proposed simplified procedures, both for assessing SBS necessity and for the consequent SBS member design, can be considered accurate and reliable.

	FEM RESULTS [δ/h]	**EQUATION 12** [δ/h]	**ERROR** [%]
60°	0.014	0.015	-4%
70°	0.032	0.032	0%
80°	0.015	0.015	4%

Table 4-3 Comparison between the maximum values of interstory drift derived from FEM analysis and from equation 12

4.7 Design implications and conclusive remarks

Diagrid structures represent very efficient tubular solutions for tall buildings since address global strength and stiffness demands under wind loads engaging the axial behaviour of the diagonal members. However

some peculiar "local" aspects of the structural behaviour arise within the single triangle module, which typically extends over multiple floors, and concern the involvement of the diagonal flexural stiffness for bracing the floors within the module height; despite the term "local" utilised for appointing them, these structural issues are nor secondary neither negligible in the design process.

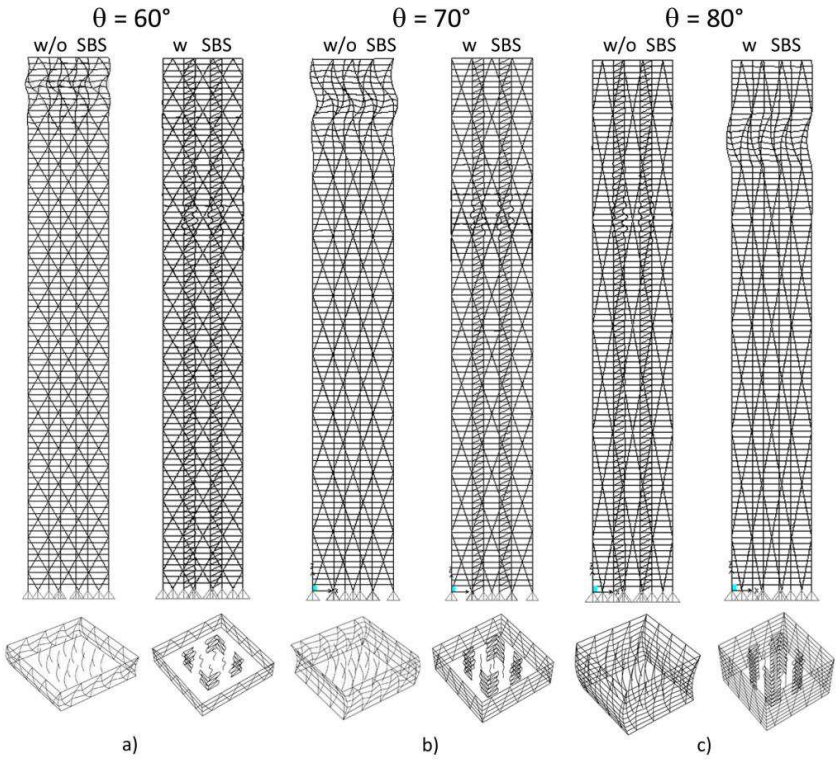

Figure 4-17 Results of the elastic eingenvalue analyses for model with and without SBS a) 60°; b) 70°; c) 80°

In this chapter a framework for assessing the above structural issues in the design of diagrid tall buildings is defined, and a methodology for establishing the need for a specific secondary bracing is presented.

Further, design criteria for SBS are worked out and applied to some 90 story building models, characterized by perimeter diagrid structures with different module height and diagonal cross sections. The outcomes of the proposed simplified procedures, both for assessing SBS necessity and for the consequent SBS member design, have been compared to the structural response of the diagrid building models, obtained without and with SBS, demonstrating both the accuracy of the proposed formulations and the primary importance of the discussed local questions. In fact, all analyzed diagrid models exhibited problems concerning stability of interior columns (i.e. multi-storey buckling modes) and/or local flexibility (excessive interstory drift); the above local problems are completely solved after the introduction of a SBS at the central core location, and, against a modest increase of structural weight (about 3%), any flexural engagements in the diagrid member is eliminated.

The above results have interesting design implications. An overview of the current practice indeed has shown that the majority of diagrid buildings are not stand-alone systems, but present a core structural system that, while sharing the global stiffness and strength demand in a tube-in-tube configuration, also provide local floor-to-floor restraints to the diagonal members, thus avoiding flexural engagement along the member length, and preserving the purely axial behaviour in the diagrid structure. However, the extraordinary efficiency of diagrid would suggest a tube configuration, with core structure only resisting gravity loads, and SBS avoiding the occurrence of the local flexibility effects. Considering that the SBS entails a very slight increase in structural steel consumption against the much larger quantities that would be required for a full-height rigid core structure, an inversion of the current design practice can be suggested, encouraging applications of diagrid in purely tubular configurations, as feasible, efficient and material-saving solutions.

5 Hexagrid - Hexagonal tube structures for tall buildings: patterns, modeling, design

This chapter provides a first insight on tube configurations based on the hexagonal shape (Hexagrid) for tall buildings. The idea is to investigate the mechanical properties of Hexagrid to assess their applicability in tall buildings, and to compare their potential efficiency to the more popular diagrid systems.

For the above purposes, a general homogenization approach has been established for dealing with any structural patterns, and a methodology for characterizing the structural patterns from the mechanical point of view has been developed and specified for hexagrids and diagrids. Then on the basis of a simple stiffness criterion, a design procedure has been proposed and applied to a tall building case study, and several structural solutions (both hexagrids and diagrids) have been designed and assessed by varying the major geometrical parameters of the patterns.

5.1 Introduction

A first example of actual applications of hexagonal grid at the mega-scale is the Sinosteel building (Figure 5-1-a), briefly described in the following; additional conceptual examples of hexagrid structures have also been proposed (Figure 5-1-b).

The Sino Steel International Plaza [15] designed by MAD Architects and China Construction Design International, is the first tall building which utilizes the hexagonal grid pattern for the tube structure.

The design concept combines geometry, structure and cultural symbolism as a repetitive motif. The façade is made up of five standardized units of hexagonal openings, which flow across the building in a naturally evolving pattern, and animate the façade, creating an ever-changing image of the building from each different perspective. The Tower has a height above ground level of 351 meters, 90 stories, plan dimension of the standard floor 53x53 m; the height-to-width ratio is 6.6. The tower has a central concrete core in addition to the exterior hexagrid tube. In the lower part (1^{st}– 42^{nd} floors) the diagonal members of the hexagrid have steel rectangular hollow sections (RHS), filled by concrete for the first four floors, while the upper part (50^{th}– 83^{rd} floors) the façade is a diagrid structure made of steel RHS members; the transition zone between the lower hexagrid and the upper diagrid (43^{rd}-49^{th} floors) is an irregular grid, made of steel RHS members (Figure 5-2). The hexagrid is characterized by diagonal angle of 60° in the central part of the façades, in order to maximize the structural shear capacity, and of 71° in the corner zones, in order to increase locally the axial stiffness and strength, necessary to counteract the global flexural demand. The upper diagrid structure has diagonal members inclined of 56°.

Hexagon-based patterns are currently being examined as tube structural grids for tall buildings. Objects of the study are both regular and non-regular patterns: the former are patterns made by uniform tessellation of (i) horizontal hexagonal cells, appointed as horizontal hexagrids (i.e. hexagonal patterns made only by horizontal and diagonal structural members), (ii) vertical hexagonal cells, appointed as vertical hexagrids (i.e. hexagonal patterns made only by vertical and diagonal structural members), (iii) horizontal and vertical hexagonal cells, appointed as mixed horizontal/vertical hexagrids (i.e. hexagonal patterns made by specific arrangements of horizontal and vertical cells along elevation); the non regular patterns are either based on Voronoi diagrams, or on mixed hexagrid/Voronoi patterns.

(a) (b)

Figure 5-1 Examples of Hexagrid building a) Sinosteel building, (from www.i-mad.com); b) Nanotower (from www.archicentral.com)

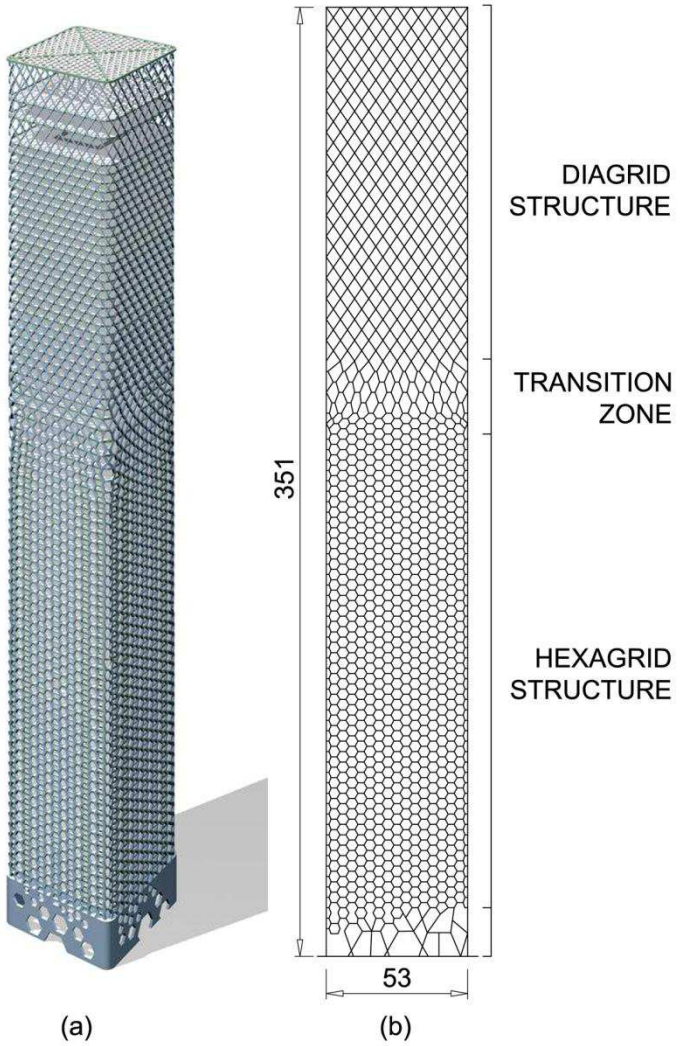

Figure 5-2 Sinosteel Building structural configuration a) 3D view; b) façade (from www.i-mad.com)

This chapter is focused to regular horizontal hexagrid patterns, namely structural assemblage of horizontal and diagonal structural members creating hexagonal frames. Major aims are to investigate the structural

properties of hexagonal structures, to assess their applicability in tall buildings and to compare their potential efficiency to more popular diagrid systems already described and studied in the previous chapters. For these purposes, first a simple stiffness based design criterion is set up for the preliminary design of tube structural configuration of tall buildings, and a general homogenization approach is established for dealing with any structural patterns; then a methodology for characterizing the structural patterns from the mechanical point of view is developed, and specified for horizontal hexagrids; finally, the homogenized stiffness design criterion is applied to a tall building case study, and several alternatives are proposed and assessed by varying some geometrical parameters of the hexagrid pattern.

A strict focus on specific building design issues (interaction with floor framing structures, need for secondary stability system, etc.), constructional aspects (complexity of connections, reasonable number of different member lengths, etc.), and coordination with architectural program, is maintained for ensuring feasible solutions. In particular a thorough assessment of the effect of rigid diaphragm action at floor levels on the grid global properties is carried out, and some simplified models which account for this effect are developed. Further, diagrid configurations are adopted as benchmarks throughout the study, for performance, buildability and efficiency assessments and comparisons. Finally, vertical hexagrids are also considered for some preliminary comparisons.

5.2 Stiffness design criterion and homogenization approach for tall building structural patterns

In order to define a straightforward criterion for the preliminary design of a tall building, "The Idea", i.e. the fundamental conceptual simplification, is that it can be considered as a cantilever beam; as such, it

is globally determinant, the approximate total actions on the tower, overturning moment and shear, are known a priori and the global deformation is a combination of flexural and shear modes [7], i.e.:

$$\delta_{tot} = \delta_{bending} + \delta_{shear} = \frac{q \cdot H^4}{8 \cdot EI} + \frac{q \cdot H^2}{2 \cdot GA} \cdot \mathrm{K} \qquad \textbf{(5.1)}$$

where H is the beam length (i.e. the building height), A and I are respectively the area and the moment of inertia of the beam cross section, E and G are respectively the axial and shear moduli and K is the shear modification factor.

Therefore a stiffness based criterion for preliminary sizing the cross section (area and inertia) of the equivalent beam consists in setting a maximum value for the top displacement, e.g.:

$$\delta_{\max} = \frac{H}{500} = \delta_{tot} \qquad \textbf{(5.2)}$$

The ideal cross section for a cantilever beam is a hollow section, which translates the tube configuration in the conceptual model of giant beam cantilevering from the ground. The four building façades act as two flanges and two webs of the hollow cross section, the formers mainly resisting bending moment through axial tension and compression, the latter providing shear resistance.

Being each façade usually made of a grid of structural members (eg. rectangular grid for frame tubes, triangular grid for diagrids, hexagonal grid for hexagrids) instead of solid panels, an appropriate procedure for taking into account the discrete nature of the structural grid acting as flanges and webs of beam cross section should be defined in order to preserve the conceptual scheme of equivalent cantilever beam (Figure

5-3); in other words, in the formula (5.1) appropriate values $(EI)_{grid}$ and $(GA)_{grid}$ should be substituted to EI and GA:

$$\delta_{tot} = \delta_{bending} + \delta_{shear} = \frac{q \cdot H^4}{8 \cdot (EI)_{grid}} + \frac{q \cdot H^2}{2 \cdot (GA)_{grid}} \cdot \chi \qquad \textbf{(5.3)}$$

This type of approach is proposed by [24], with a methodology for dealing with frame tube panels as equivalent orthotropic membranes, so that the framed tube could be analyzed as a continuous structure.

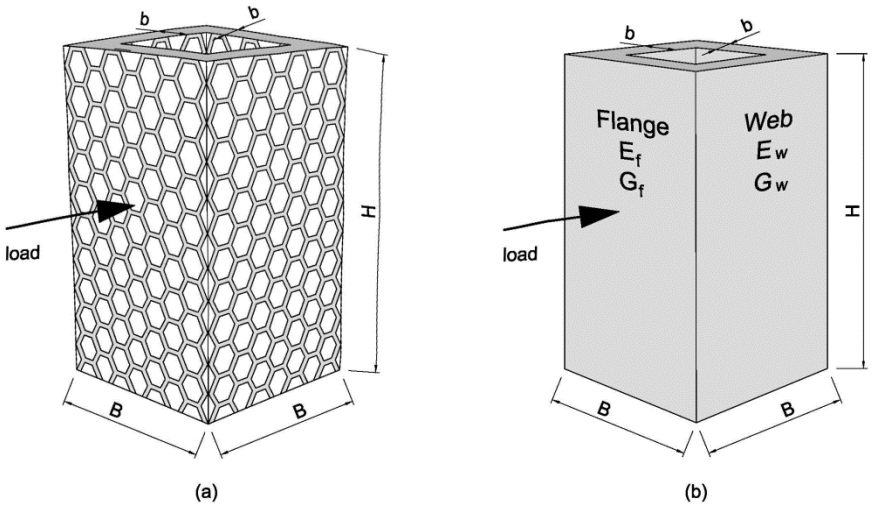

Figure 5-3 Orthotropic Membrane tube analogy: a) structural grid; b) equivalent solid

A more general methodology is proposed for dealing with grid-like structures: the idea is to idealize whichever grid as a continuous depleted medium, characterized by penalized mechanical properties, according to the classical micromechanical approach based on homogenization methods. In fact a plane periodic structure made up of an isotropic linearly elastic material and possessing a certain degree of symmetry

behaves macroscopically as an isotropic material; the macroscopic properties of the structure are called the effective properties, and depend on both the mechanical properties of the solid matrix and on the micro-structural features of the grid, namely topology, density, and orientation.

Basically, the procedure consists in evaluating the effective axial and shear moduli of the grid, which account for the geometric and elastic properties of structural members as well as for the geometrical pattern of the grid, and expressing them as:

$$E_{grid} = \frac{E^*_1}{E_s} \cdot E_s \qquad \textbf{(5.4)}$$

$$G_{grid} = \frac{G^*_{12}}{G_s} \cdot G_s \qquad \textbf{(5.5)}$$

where: E^*_1/E_s and G^*_{12}/G_s are appointed as axial and shear stiffness modification factors, respectively; E_s and G_s are the Young and shear modulus of the solid material utilized for the structural members of the grid.

These modification factors can be seen as additional material properties of the corresponding solid that take into account the geometrical pattern of the grid, the type of connection among members, the geometrical properties of the member cross sections.

Once the modification factors for the axial stiffness E^*_1/E_s and for the racking shear stiffness G^*_{12}/G_s are evaluated, the standard formulae defined for a solid tube can be utilized for calculating the horizontal deflections of the homogenized grid tube (eq. 5.3); that is, the stiffness based design criterion for a tube tall building (eq. 5.2) can be specified substituting EI and GA with EI_{grid} and GA_{grid}, respectively, and the

member cross section properties required for satisfying the limit deflection can be obtained.

The starting point of this procedure is the mechanical study of the Representative Volume Element (RVE), which is defined as the smallest homogeneous material volume which macroscopic constitutive relationships must be referred to [39]. In any specific grid structure, therefore, it is preliminarily necessary to identify the unit, repetitive sub-assemblage of beam elements, here appointed as unit cell: the unit cells should be chosen in a way that there are no elements on the edges and can be arrayed in two directions to form an infinite grid, without overlap and gaps. Once the unit cell is identified, the relevant structural model (i.e. the RVE) should be defined.

In [48], taking the Water Cube as an example, this approach has been successfully applied to foam-like macrostructures made of interconnected beam elements; more recently the authors have developed the analytical procedure for dealing with sandwich plates of depleted material, made by recursive patterns of a base unit (RVE), and a design procedure for such type of long-span weight efficient structures have been proposed. Both applications have confirmed the potentials of classical micromechanical-based strategies for the design and assessment of mega-scale civil structures, generated by complex, non-conventional patterns.

In this paper, two different configurations of regular structural grids, namely hexagonal and triangular, are considered; in particular, for the hexagrid, the attention is mainly focused to horizontal hexagonal grids, though vertical hexagrids are considered as terms of comparison in the design applications.

5.3 Hexagrid and diagrid patterns: geometry, module, unit cell and relative density

In order to evaluate the geometry, the mechanical behavior and the structural efficiency of the considered patterns, three distinct unitary "entities" have been considered (i) the module, (ii) the unit cell and (iii) the RVE.

The module is the frame shape, i.e. the geometrical arrangement of the structural members giving a visual representation of the pattern (hexagon for hexagrid and triangle for diagrid, Figure 5-4); anyway the replication of the module gives rise to overlaps of the edges, so that the overall geometry cannot be obtained by simply copying the module. For this reason it is necessary to identify the unit cell, defined as the geometric unity that through replication allows to obtain the overall geometrical pattern without overlaps or gaps (Figure 5-4).

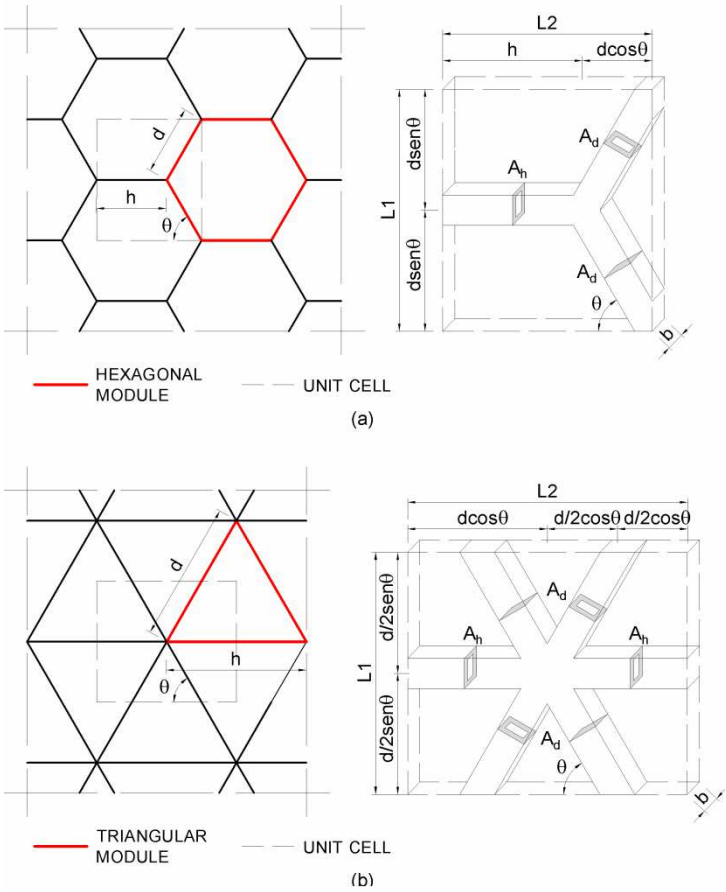

Figure 5-4 Modules, unit cells and volume occupied by solid material in the Unit Cell respectively for a) Horizontal Hexagrid; b) Diagrid

Considering the unit cells, an important scalar geometrical quantity is the Relative Density (ρ), namely the ratio of the volume occupied by the solid material, ρ^*, to the total volume of the cell, ρ_{vol} :

$$\rho = \frac{\rho^*}{\rho_{vol}} = \frac{\sum_{i=1}^{n} l_i \cdot A_{.i}}{L_1 \cdot L_2 \cdot b} \qquad \textbf{(5.6)}$$

Where: n is the total number of beams, l_i and A_i are respectively the length and the section area of beams , L_1 and L_2 are respectively the dimensions of the unit cell along x_1 and x_2 directions, b is the thickness of the unit cell. This expression of ρ is specialized for Hexagrid (ρ_H) and Diagrid (ρ_D) in the following equations (5.7) and (5.88), respectively.

$$\rho_H = \frac{(h_{hex} \cdot A_h) + (2 \cdot d_{hex} \cdot A_d)}{\left[(h_{hex} + d_{hex} \cos\theta) \cdot (2 \cdot d_{hex} sen\theta)\right] \cdot b} \quad \textbf{(5.7)}$$

$$\rho_D = \frac{A_d + \cos\theta \cdot A_h}{d_{hex} \cdot \cos\theta \cdot sen\theta \cdot b} \quad \textbf{(5.8)}$$

Where: h_{hex} and d_{hex} are respectively the lengths of the horizontal and diagonal beams, A_h and A_d are respectively the cross sectional areas of the horizontal and diagonal beams, θ is the angle between the diagonal element and the horizontal axis.

The relative density could be used for assessing the efficiency of the different grids; in particular dividing the stiffness of the grid by their relevant value of ρ, a measure of the grid efficiency can be obtained.

While the unit cells represents the repetitive unit from the geometric point of view, the RVE represents the structural idealization of the unit cell, that only can be established by anticipating the deformation modes and internal forces arising in the unit cell as a part of the global grid. For this purpose, in the following paragraph, infinite hexagon and triangle grids, under both uniaxial compression and shear deformations, are tested and the relevant RVEs are derived.

5.4 RVEs and stiffness modification factors

The Elastic Axial Modulus (E^*_1) is defined as the ratio of the uniaxial normal stress, σ, divided by the uniaxial strain, ε, in the loaded direction in the elastic range. Normal stress is the average normal force, F_1, acting perpendicularly on a surface per unit cross-sectional area (Bxb). Strain is the shortening, or lengthening, Δx_1, of the reference specimen (the RVE) divided by the initial length, L, in the loaded direction.

$$E^*_1 = \frac{\sigma}{\varepsilon} = \frac{\frac{F_1}{B \cdot b}}{\frac{\Delta x_1}{L}} \tag{5.9}$$

Uniaxial compressions test on RVE is performed as illustrated in Figure 5-5a; in particular the displacements of the nodes on the bottom edge along x_1-axis and the displacements of the nodes on the left edge along the x_2-axis are constrained.

The Shear Modulus (G^*_{12}) represents the elastic modulus used to describe the relationship between the deformation parallel to the loaded surface of a RVE due to a shear force applied parallel to one face of the RVE. It is the ratio of the shear stress, τ, divided by the shear strain, γ. The shear stress is the force, F_2, applied parallel to a face, divided by the cross-sectional area, (Bxb). The shear strain is defined as the transverse displacement, Δx_2, divided by the initial length, L.

$$G^*_{12} = \frac{\tau}{\gamma} = \frac{\frac{F_2}{B \cdot b}}{\frac{\Delta x_2}{L}} \tag{5.10}$$

The test shear on RVE is performed as illustrated in Figure 5-5b. In particular the displacements along the x_1 axis of nodes on the bottom and on the top edges are constrained.

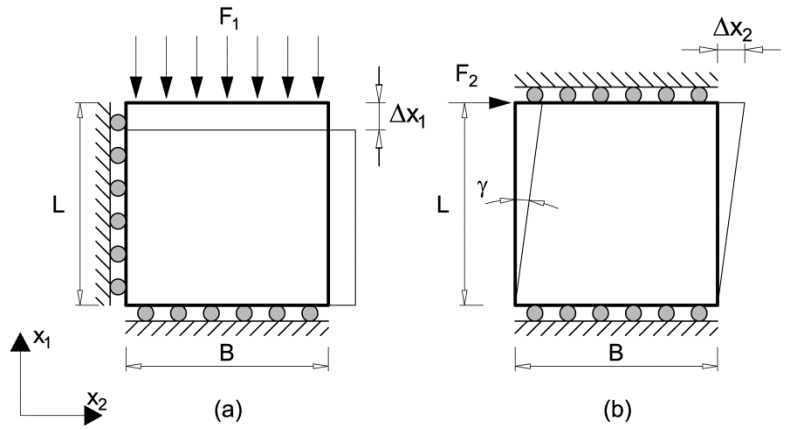

Figure 5-5 Restrains and external loads considered for a) Uniaxial compression test; b) Shear test

The method proposed by [12] is initially adopted for defining the above stiffness modification factors of hexagrid and diagrid structures. Then a refined method is proposed and utilized for taking into account the rigid diaphragm action of the floors structure that, restraining the lateral expansion of the structural grid under axial compression loads, results in a non negligible stiffening effect. The approach for taking into account the rigid diaphragm action is discussed in paragraph 5.6.

5.4.1 Axial stiffness modification factor - Hexagrid

The vertical deformation and the internal forces diagrams of an infinite horizontal hexagon grid under uniaxial compression are shown in Figure 5-6. From these diagrams some information on the member deformation modes and local resisting mechanisms can be deduced.

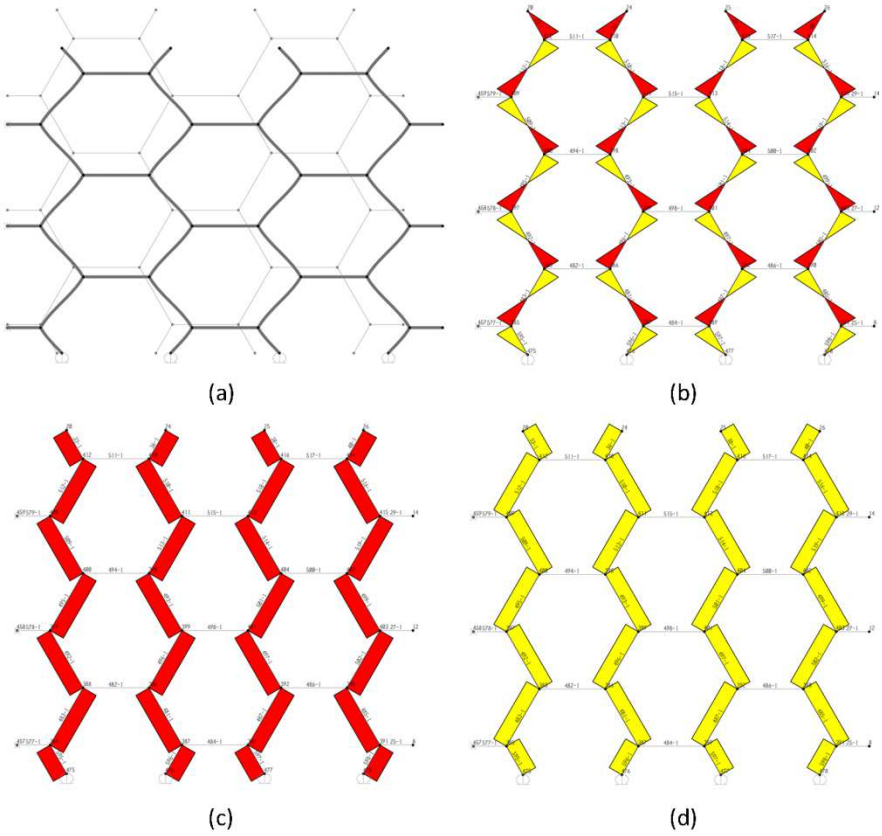

Figure 5-6 Uniaxial compression test for Horizontal Hexagrid panel a) deformed configuration (scale factor 200); b) moment diagram; c) axial forces diagram; d) shear forces diagram

Basically, it is evident that the hexagonal pattern, characterized by a low connectivity of the joints, is a bending-dominated structure [5], since the global deformation of the grid involves bending deflections of the diagonal members.Considering the unit cell, made of one horizontal member and two diagonal members, it can be observed that the horizontal member has no bending moments, axial forces, shears, while

in the diagonal elements double curvature moment, with point of contraflexure at mid-length, is present.

On the basis of the above observations, the mechanical model of the geometric unit cell is defined for obtaining deformations and forces that develop in the structural members of the grid. With the purpose of calculating the axial stiffness modification factor, hinges are introduced at members mid-length (Figure 5-7). The schematization of the concept is translated into the RVE.

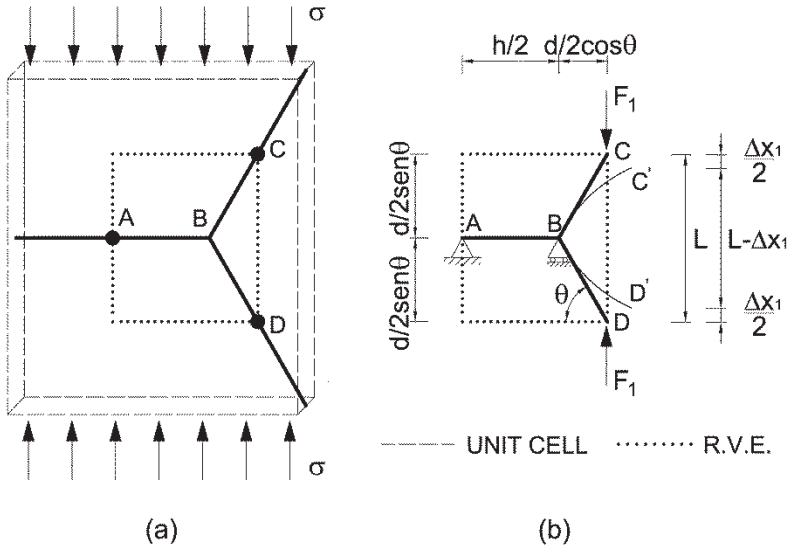

Figure 5-7 Uniaxial compression test, definition of the RVE for Horizontal Hexagrid

Then, the global axial deformation the RVE is given by the contributions of local bending, axial and shear deformations of the RVE structural elements (two half diagonals and one half horizontal). Therefore the stiffness of the grid in X_1 direction, E^*_1, normalised to the Young's modulus of the member solid material E_s, is given by:

$$\frac{E^*_1}{E_s} = \frac{12 I_d sen\theta A_d}{(h_{hex} + d_{hex}\cos\theta) b\left[\cos^2\theta(d^2_{hex} A_d + 24 I_d \chi(1+\nu)) + 12 sen^2\theta I_d\right]} \quad \textbf{(5.11)}$$

5.4.2 Axial stiffness modification factor - Diagrid

As a comparison, the analogous evaluation is carried out for the diagrid. While the hexagrid is a bending-dominated structural pattern, the triangular grid is an axial force-dominated structure, thanks to the higher connectivity of joints (6 members meeting at a diagrid joint, against 3 members meeting at a hexagrid joint); further, being the triangle shape statically determinant, pinned connections are considered at grid nodes. The vertical deformation and the axial force diagrams of an infinite triangular grid under uniaxial compression is depicted in Figure 5-8, where it is shown that the global shortening in the X_1 direction only involves member axial deformations, and causes a stretching in the X_2 direction, which produces a tensile reaction forces, F_h, in the horizontal elements.

The RVE of the diagrid is a single triangle; the geometric relationship between the original and the deformed triangle can be derived using the Pythagorean Theorem, and, from this, the strain in X_1 direction and the axial stiffness modification factor can be evaluated (Figure 5-9):

$$\frac{E^*_1}{E_s} = \frac{sen^3\theta A_d A_h}{d_{hex}\cos\theta b A_h + d_{hex}\cos^4\theta b A_d} \quad \textbf{(5.12)}$$

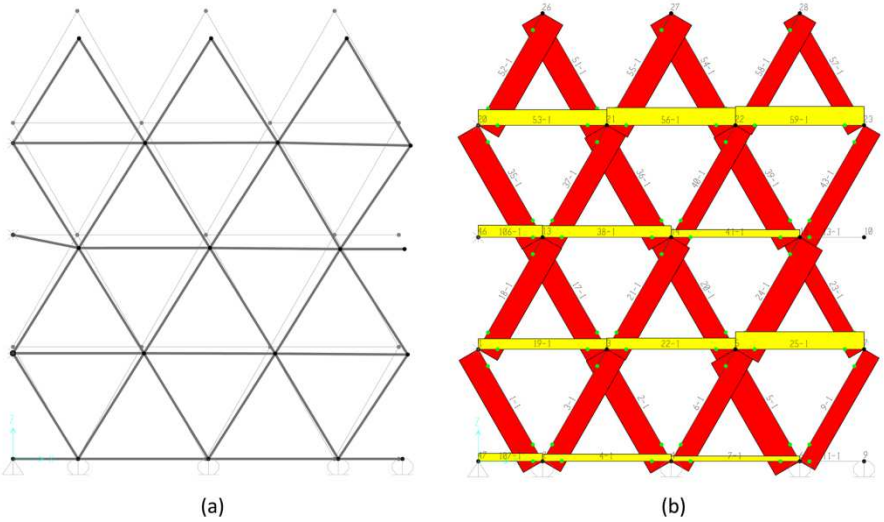

Figure 5-8 Uniaxial compression test for Diagrid panel a) deformed configuration (scale factor 1000); b) axial forces diagram

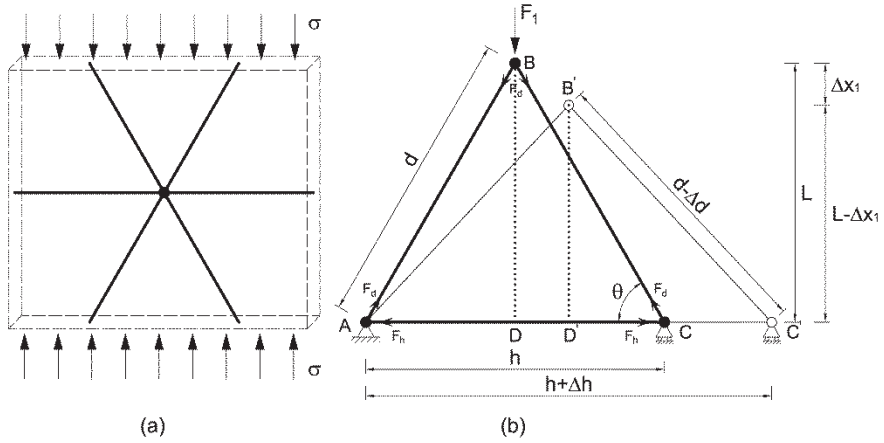

Figure 5-9 Uniaxial compression test, definition of the RVE for Diagrid

5.4.3 Shear stiffness modification factor - Hexagrid

The deformation of an infinite horizontal hexagonal grid under shear load and the relative stress diagrams are shown in Figure 5-10. For regular grids the moments in the horizontal elements are two times the moments in the diagonal elements.

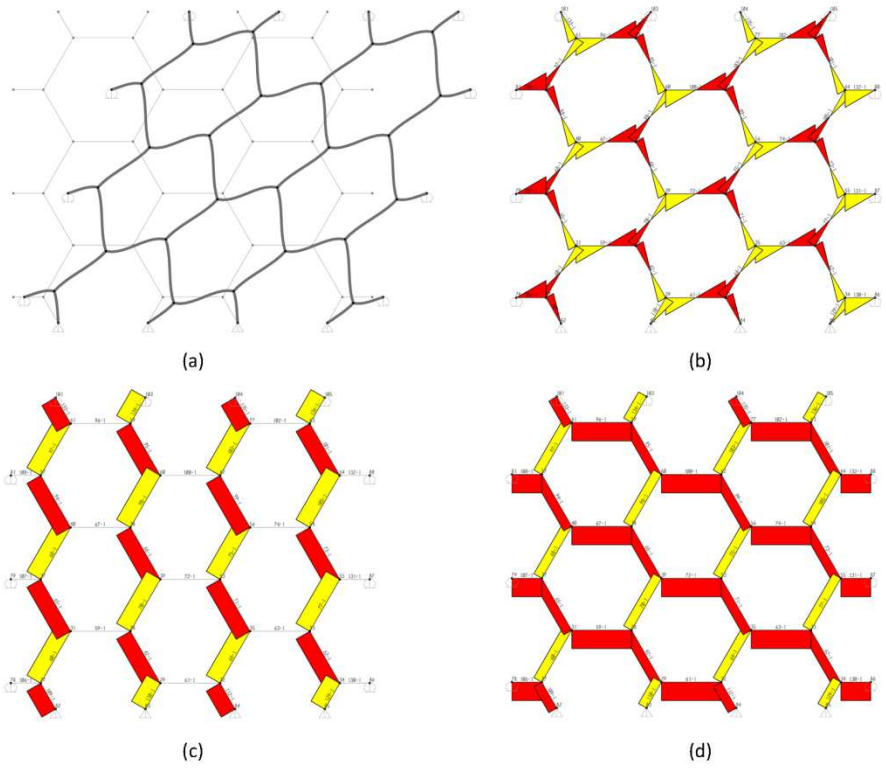

Figure 5-10 Shear test for Horizontal Hexagrid panel a) deformed configuration (scale factor 200); b) moment diagram; c) axial forces diagram; d) shear forces diagram

Just like for the calculation of the axial stiffness factor, hinges are introduced at mid length of the diagonal and horizontal elements, where the bending moments are equal to zero. The schematization is translated

into the mechanical model (RVE) in Figure 5-11, where τ is replaced by a concentrated horizontal load F_2.

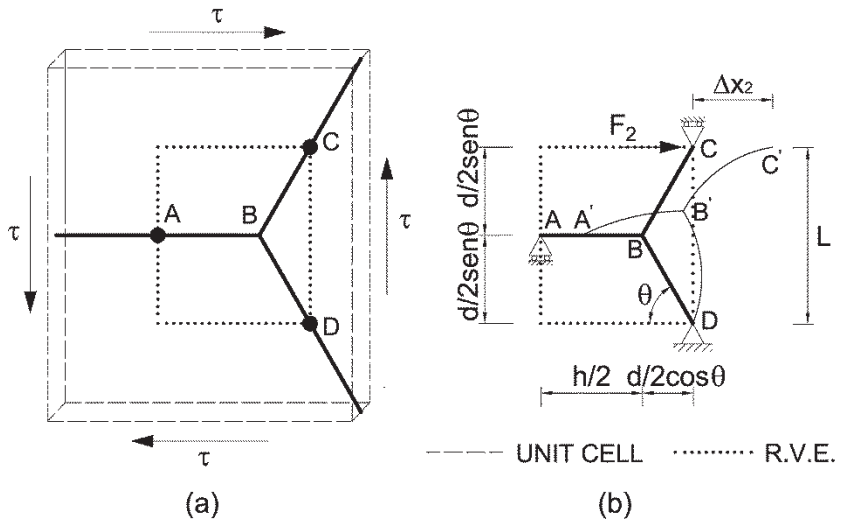

Figure 5-11 Shear test, definition of the RVE for Horizontal Hexagrid

The shear deformation of the unit cell, Δx_2, is caused by shortening of elements subjected to axial forces, shear deformation of elements under shear load and by flexural deflection of elements subjected to bending moments. The shear displacement in X_2 direction, divided by the RVE height, defines the shear strain, γ.

$$\frac{G^*_{12}}{G_s} = \frac{24 \cdot A_d \cdot A_h \cdot I_d \cdot I_h (1+\nu)(h_{hex} + d_{hex}\cos\theta) sen\theta}{\left[\begin{array}{l} 12 \cdot A_h \cdot I_d \cdot I_h \cdot b \cdot \cos\theta (2 \cdot d_{hex} \cdot h_{hex} + (d^2_{hex} + h^2_{hex})\cos\theta) \\ +b \cdot sen^2\theta ((12 \cdot A_h \cdot I_d \cdot I_h \cdot \chi_d (d^2_{hex} + 2 \cdot h^2_{hex}(1+\nu))) \\ +(A_d \cdot d^2_{hex} \cdot h^2_{hex} \cdot (A_h \cdot h_{hex} \cdot (2 \cdot h_{hex} \cdot I_d + d_{hex} \cdot I_h) + 48 \cdot I_d \cdot I_h \cdot \chi_h (1+\nu)))) \end{array}\right]} \quad \textbf{(5.13)}$$

5.4.4 5.4 Shear stiffness modification factor - Diagrid

The shear deformation and the consequent axial force diagrams of an infinite triangular grid are shown in Figure 5-12.

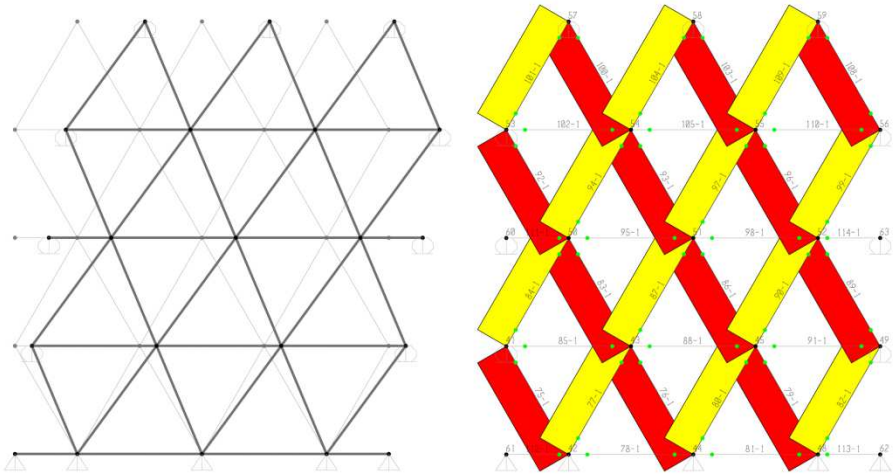

Figure 5-12 Shear test for Diagrid panel a) deformed configuration (scale factor 1000); b) axial forces diagram

Just like in the calculation of the axial stiffness factor, a single triangle is separated from the grid; it is the mechanical model, where τ is replaced by a concentrated horizontal load F_2. The geometric relationship between the original and the deformed triangle, derived using the Pythagorean Theorem (Figure 5-13), allows to express the shear stiffness modification factor as:

$$\frac{G^*_{12}}{G_s} = \frac{2 \cdot A_d \cos\theta \cdot sen\theta \cdot (1+\nu)}{d_{hex} \cdot b} \qquad \textbf{(5.14)}$$

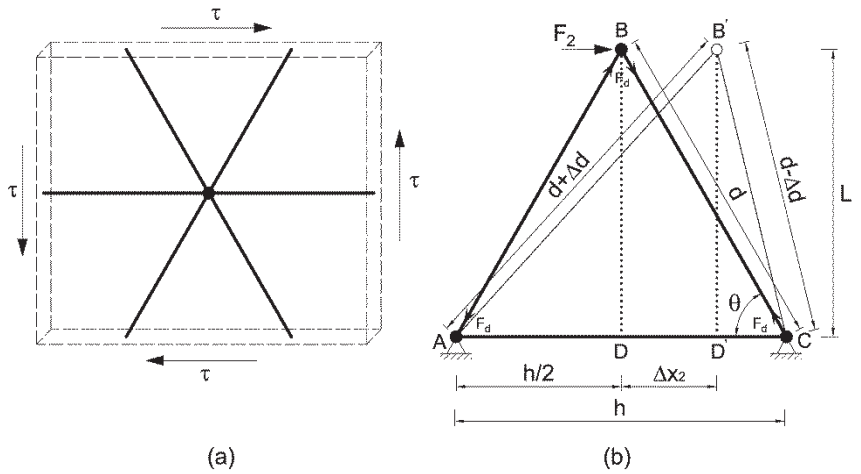

Figure 5-13 Shear test, definition of the RVE for Diagrid

5.5 Effect of the floor rigid diaphragm

The preliminary application of this procedure for analyzing tall building hexagrid structures and the comparison to the numerical results obtained by means of FEM analyses, showed significant errors, around 50%; the main source of this large scatter is related to the effect of the rigid floor diaphragm, which provides an additional restraint in the deformation mode of the RVE and, globally, of the structural grid.

More precisely, the error affects the static model proposed for the computation of E^*_1, and indeed the problem is located to the facades which are perpendicular to the wind direction, which counteract the overturning moment due to the horizontal load as compression/tension flanges. This problem does not affect the facades parallel to the wind direction.

The stiffening action of the floor rigid diaphragm (RD) for hexagrid can be clearly seen in Figure 5-14 where the comparison between the deformed configurations of two panels under vertical forces without (a)

and with (b) RD is depicted. For diagrids this effect is not as significant as for hexagrid, as can be seen in Figure 5-15, where the results obtained for diagrids panels without (a) and with (b) RD are depicted.

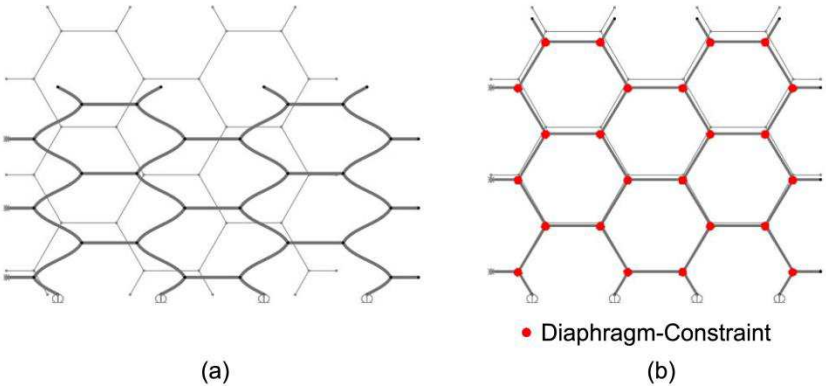

Figure 5-14 Comparison between the deformed configurations of two panels Horizontal Hexagrid under vertical forces a) without Rigid Diaphragm ; b) with Rigid Diaphragm

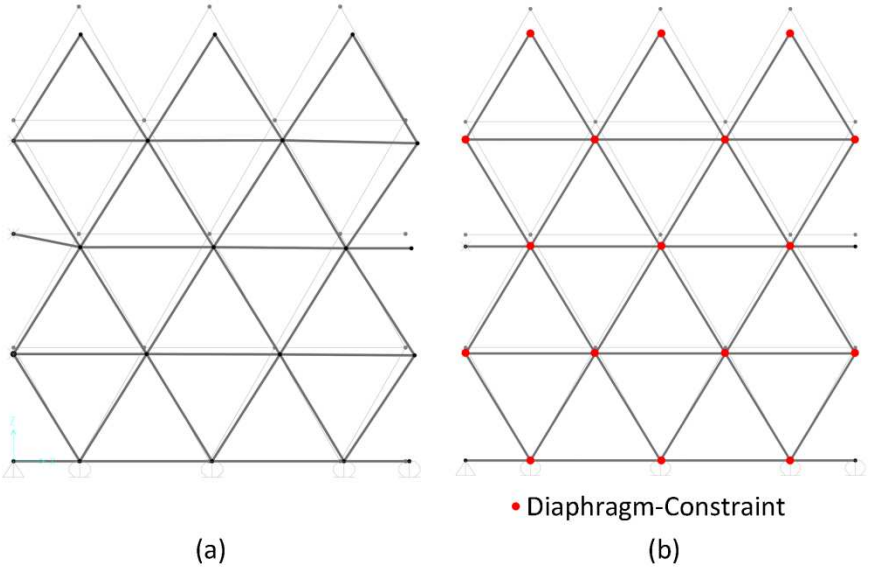

Figure 5-15 Comparison between the deformed configurations of two panels diagrid under vertical forces a) without Rigid Diaphragm ; b) with Rigid Diaphragm

Considering the grid façades of a tube structure, the stiffening effect due to the rigid diaphragm (RD) action can be clearly appreciated by observing the vertical deformed configurations for hexagrids with different number of RDs along elevation, i.e.: (a) RD only at the building top level; (b) RD at every 9th level; (c) RD at every floor (Figure 5-16). The comparison among the deformation modes suggests an analogy with the behaviour of laminated elastomeric bearings: the stiffening effect of RD on the vertical deformation of building structural grid is analogous to the confinement exercised by the steel interlayer shims on the lateral bulging of the rubber layers, which is accounted for through the primary shape factor S_1, which, in turn, strongly affects the vertical stiffness of the isolator.

On the basis of the above considerations, two procedures have been outlined for dealing with this problem and improving the accuracy in the evaluation of the vertical stiffness modification factor: the former is based on the definition of a new, appropriate mechanical model which explicitly takes into account the RD effect (appointed as Modified RVE Approach (MRA)); the latter utilizes the analogy with Isolator deformation mode and the concept of primary shape factor (appointed as Isolator Analogy Approach (IAA)). In the following, for the sake of brevity, only the first approach is illustrated and applied to hexagrid and diagrid structures.

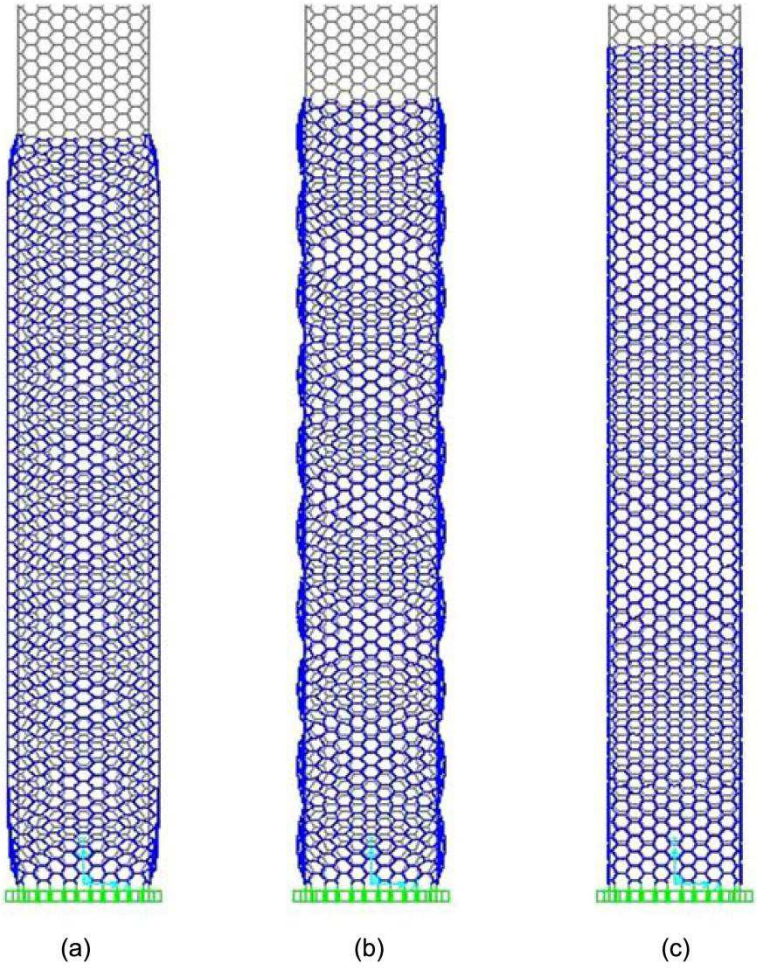

Figure 5-16 Deformed configurations for Horizontal Hexagrid building model with different number of RDs a) RD only at the top; b) RD at every 9th floor; c) RD at every floor

5.6 Modified RVE

This approach, simply modifies the RVE in order to account for the RD additional restraint; of course, the modified RVE strongly depends on

the module height, namely on the number of floors (and of rigid diaphragm constraints) present along the unit cell. In the following, this approach is explicitly developed for two different cell heights cell, i.e. equal to interstory height ($H_{unit\ cell}$= H_{level}) and equal to two interstory height ($H_{unit\ cell}$= $2H_{level}$), which respectively correspond to: H_{RVE} = L = $H_{level}/2$; H_{RVE} = L = H_{level}. Obviously the following equations for the normalized vertical module can be obtained also for hexagrid with different cell heights (i.e. H_{RVE} = L = 2 or 3 H_{level}).

5.6.1 Hexagrid– Unit cell equal to interstory height

When the height of the unit cell is equal to the interstory height, the RD constraint partially blocks the horizontal dilatations of the module, namely the horizontal displacements of the joints marked with solid circles in Figure 5-17; therefore the ends of the diagonal members in the RVE cannot experience horizontal displacements and should be accordingly restrained.

The normalized vertical stiffness for the above structural model is computed through the following relationship:

$$\frac{E_{\perp}^{*}}{E_s} = \frac{\dfrac{1}{(h_{hex} + d_{hex}\cos\theta)b}}{\left[\dfrac{1}{A_d sen\theta} + \dfrac{\cos^2\theta\left(\dfrac{d_{hex}^2}{12I_d} + \dfrac{2\chi(1+\nu)}{A_d} - \dfrac{1}{A_d}\right)}{A_d sen\theta\left(\dfrac{d_{hex}^2 sen^2\theta}{12I_d} + \dfrac{2\chi(1+\nu)sen^2\theta}{A_d} + \dfrac{\cos\theta sen\theta}{A_d} + \dfrac{2}{A_h}\right)} + \dfrac{2h_{hex}\cos^2\theta\left(\dfrac{d_{hex}^2}{12I_d} + \dfrac{2\chi(1+\nu)}{A_d} - \dfrac{1}{A_d}\right)}{A_h d_{hex} sen\theta\left(\dfrac{d_{hex}^2 sen^2\theta}{12I_d} + \dfrac{2\chi(1+\nu)sen^2\theta}{A_d} + \dfrac{\cos\theta sen\theta}{A_d} + \dfrac{2}{A_h}\right)}\right]} \quad \textbf{(5.15)}$$

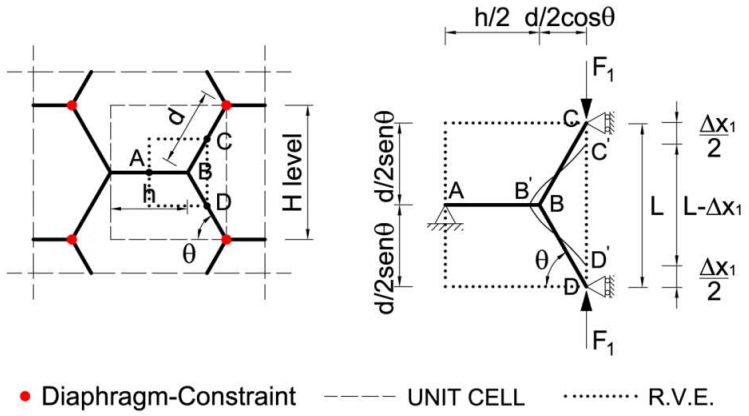

Figure 5-17 Uniaxial compression test, definition of the RVE for Horizontal Hexagrid considering the RD effect for $H_{unitcell}=H_{level}$

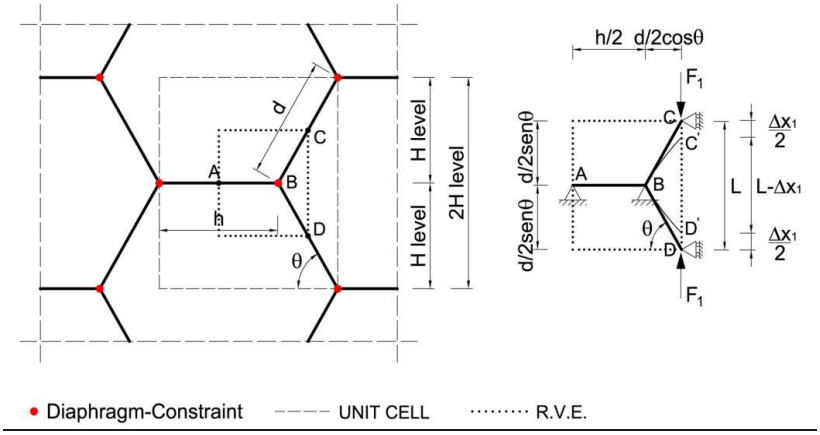

Figure 5-18 Uniaxial compression test, definition of the RVE for Hexagrid considering the RD effect for $H_{unitcell} = 2\ H_{level}$

5.6.1 Hexagrid –Unit cell equal to two interstory height

When the height of the unit cell is twice the interstory height ($2H_{level}$), the RD constraint completely blocks the horizontal dilatations of the module, namely the horizontal displacements of all the joints of the module; therefore the RVE is modified as in Figure 5-18, with the

relationship for calculating the normalised vertical stiffness given by the following equation:

$$\frac{E^*_1}{E_s} = \frac{\dfrac{1}{(h + d\cos\theta)b}}{\left[\dfrac{1}{A_d sen\theta} + \dfrac{\cos\theta\left(\dfrac{d^2}{12I_d} + \dfrac{2\chi(1+\nu)}{A_d} - \dfrac{1}{A_d}\right)}{A_d sen\theta\left(\dfrac{d^2 sen^2\theta}{12I_d\cos\theta} + \dfrac{2\chi(1+\nu)sen^2\theta}{A_d\cos\theta} + \dfrac{\cos\theta}{A_h}\right)}\right]} \qquad \textbf{(5.16)}$$

5.6.2 Diagrid –Unit cell equal to one and two interstory height

As already described in paragraph 5.6, the RD effect for diagrids is not as significant as for hexagrid; the diagrid is indeed an axial force dominated pattern, therefore the structural members of the RVE do not experience any bending deformations, thus the RD stiffening effect does not dramatically modify the deformation modes and the consequent global stiffness. Furthermore, the effect of the RD is independent from the height of the unit cell (i.e. from the number of rigid constraints); therefore, considering the modified RVEs (Figure 5-19 for $H_{unitcell} = H_{level}$; Figure 5-20 for $H_{unitcell} = 2H_{level}$), the (slight) effect of the RD can be accounted for using the following formula:

$$\frac{E^*_1}{E_s} = \frac{sen^3\theta A_d}{d_{hex}\cos\theta b} \qquad \textbf{(5.17)}$$

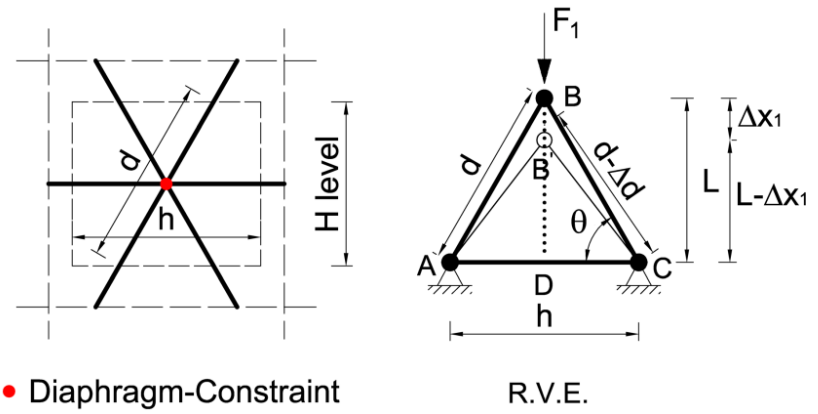

Figure 5-19 Uniaxial compression test, definition of the RVE for Diagrid considering the RD effect for $H_{unitcell}=H_{level}$

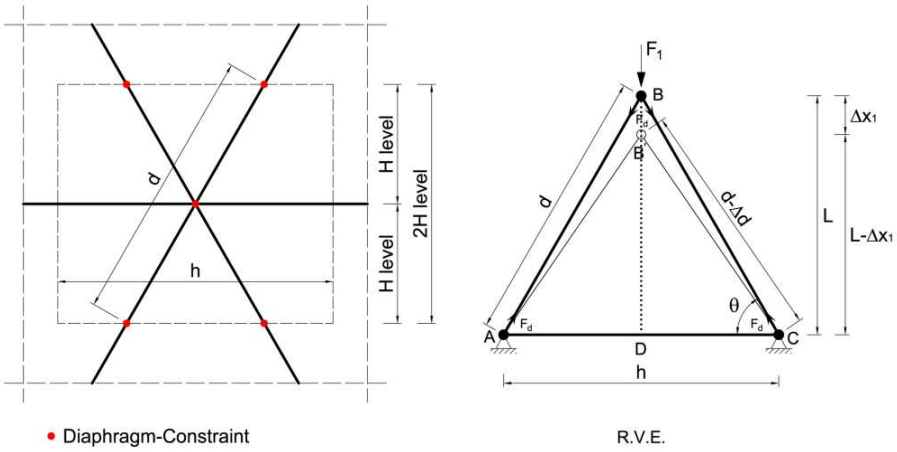

Figure 5-20 Uniaxial compression test, definition of the RVE for Diagrid considering the RD effect for $H_{unitcell} = 2\ H_{level}$

5.7 Design applications and validation of the proposed method

In order to assess the conceptual model and the subsequent design formulae proposed in this chapter, a parametric design application is developed.

The building model utilised for the design applications is characterized by plan dimensions and height equal to the building model used in Chapter 3 and 4, i.e.: height 351 m, 90 stories, interstory height 3.9 m, square plan dimension 53x53 m. A horizontal wind action, modelled as uniform load of 200 kN/m, has been considered in the application of the stiffness design criterion.

Several Hexagrid and Diagrid solutions are worked out for the building model, varying the module height, the diagonal angle, and the type of member cross sections. Concerning the module height, one and two story tall modules have been considered. In order to select the optimal angles for the diagonals, some preliminary parametric analyses have been carried out; in particular, the axial and shear stiffness and the relative density are evaluated according to the variation of the angle in order to assess the grid efficiency. As a result, diagonal angles between 50° and 70° have shown the maximum efficiency, in both cases of Hexagrid (Figure 5-21-a) and Diagrid (Figure 5-21.b). Therefore, for the design applications three values of the diagonal angle, 50°, 60° and 70°, have been chosen. Finally, three different types of steel member cross sections have been considered in the design applications, i.e. square hollow sections and rectangular hollow sections (horizontal and vertical); in each grid, the same cross sections have been adopted for the horizontal and diagonal elements throughout the building height.

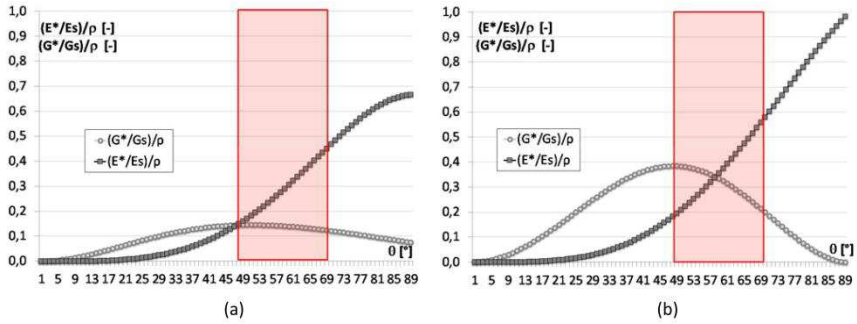

Figure 5-21 Axial and Shear grid stiffness divided by Relative Density versus diagonal angle a) Hexagrid; b) Diagrid

In the following the building models are appointed by means of an acronym defined by a letter (H for hexagrid and D for diagrid), a two-digits number, representing the diagonal angle (50, 60 or 70), a one-digit number for the unit cell height (1 for $H_{unitcell}=H_{level}$ and 2 for $H_{unitcell}= 2H_{level}$), a letter indicating the type of cross sections (s for square hollow section, h and v respectively for horizontal and vertical rectangular cross section) (see: Table 5-1 for hexagrid $H_{unit\ cell}= H_{floor}$; Table 5-2 for hexagrid $H_{unit\ cell}= 2H_{floor}$; Table 5-3 for diagrid $H_{unit\ cell}= H_{floor}$; Table 5-4 for diagrid $H_{unit\ cell}= 2H_{floor}$).

Angle θ [°]	**Hexagonal modules** [n°]	**Section (axbxt)** [mmxmmxmm]		
		s	**h**	**v**
52,4	13	1000x1000x87	1000x650x106	700x1000x124
65	17	700x700x68	700x500x82	500x750x96
76	21	550x550x69	650x400x65	450x750x74

Table 5-1 HexaGrid $H_{unit\ cell}= H_{floor}$

Angle θ [°]	**Hexagonal modules** [n°]	**Section (axbxt)** [mmxmmxmm]		
		s	**h**	**v**
56,8	7	1000x1000x130	1200x700x127	850x1300x131
68,6	9	900x900x101	1150x500x98	750x1200x108
78,8	11	900x900x84	1100x500x84	750x1200x92

Table 5-2 HexaGrid $H_{unit\ cell} = 2H_{floor}$

Angle θ [°]	**Triangle modules** [n°]	**Section (axbxt)** [mmxmmxmm]		
		s	**h**	**v**
53	9	600x600x78	650x400x93	400x650x95
60,5	12	400x400x75	500x300x74	300x500x75
70,3	19	300x300x56	400x200x56	200x400x56

Table 5-3 DiaGrid $H_{unit\ cell} = H_{floor}$

Angle θ [°]	**Triangle modules** [n°]	**Section (axbxt)** [mmxmmxmm]		
		s	**h**	**v**
49,7	4	900x900x139	1000x700x150	700x1000x153
60,5	6	700x700x80	900x500x79	500x900x81
71,2	10	500x500x62	700x350x56	350x700x57

Table 5-4 DiaGrid $H_{unit\ cell} = 2H_{floor}$

Summing up, 36 design solutions have been generated (18 with hexagrid structures and 18 with diagrid structures). The details of the structural designs are synthesized in Figure 5-22 for hexagrid and in Figure 5-23 for diagrid.

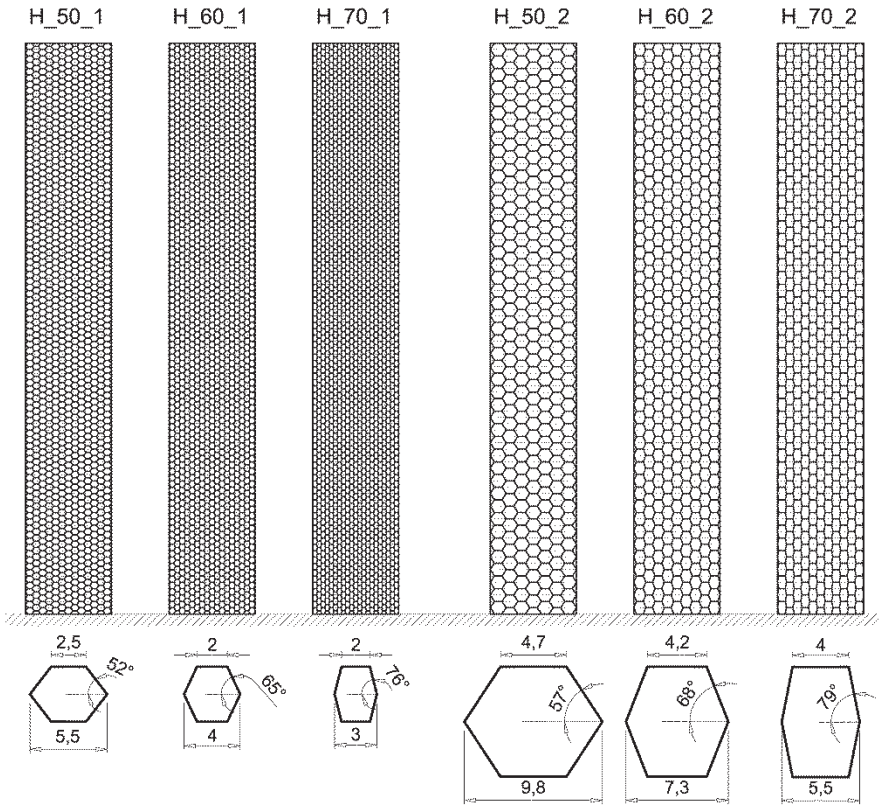

Figure 5-22 Geometrical solutions considered for Horizontal Hexagrid

The procedure has been validated by comparing the lateral displacements obtained by means of FEA of the designed structures, to the target displacements (H/500) adopted in the design procedure (Figure 5-24). Overall, the hand calculations give very satisfying results; the scatters between the displacement computed with the FEM models and those computed with the mathematical relations are always less than 10%.

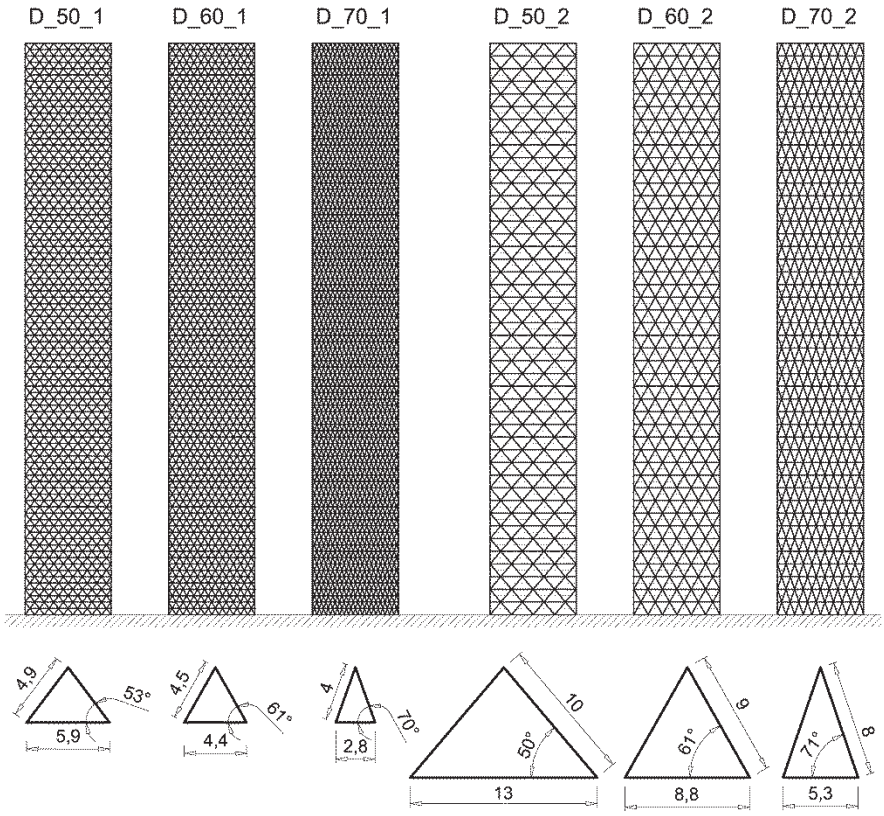

Figure 5-23 Geometrical solutions considered for Diagrid

Considering that hexagrid and diagrid solutions are all designed for the same stiffness requirement, a comparative assessment of the structural efficiency can be made in terms of relative density. The relative density, defined according to equation (5.6), can be directly derived from the geometrical characteristics of the grid, through the formulae (5.7) and (5.8) for hexagrids and diagrids, respectively. However, a parameter of greater interest for building developers and designers is the unit structural weight, i.e. the total structural material quantity divided by the gross area of the building; it is indeed the deciding factor in selecting the

structural system among several possible structural options, at least in the preliminary scheme selection phase [44].

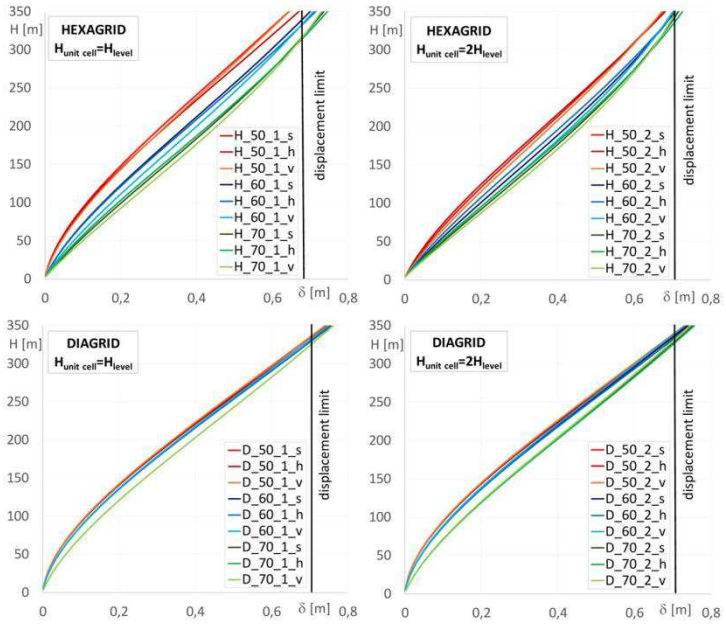

Figure 5-24 Horizontal displacement versus building height

Therefore the structural weight for unit area of diagrids and hexagrids have been computed and compared in Figure 5-25; the first observation that can be done from this figure is that the order of magnitude of the unit structural weight is quite high both for the hexagrid and diagrid solutions, if compared to actual diagrid solutions [25]; however an optimization process should follow this preliminary design stage. Another major observation is that, though the diagrid solutions are always the most weight efficient, the magnitudes of weight for hexagrids and diagrids are quite similar; in particular, considering the possible variations of diagonal angle and cross section, hexagrids and diagrids with comparable values of unit weight can be obtained.

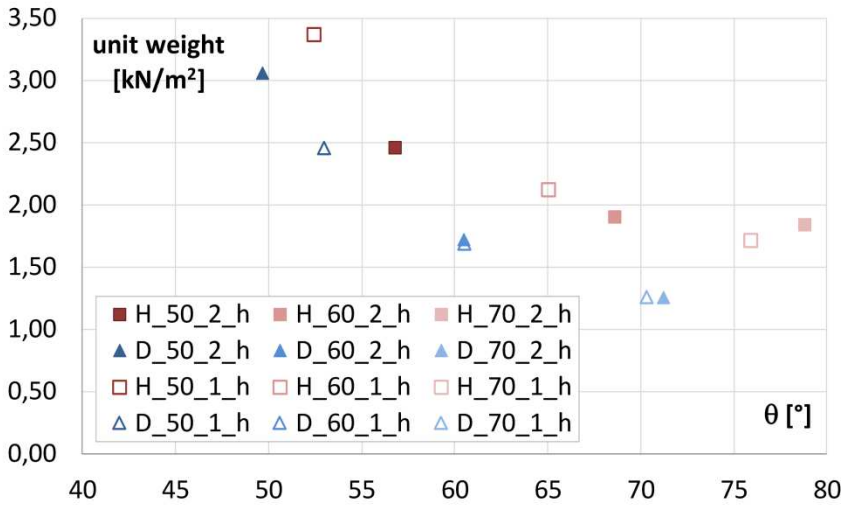

Figure 5-25 Unit weights of the most efficient solution for Horizontal Hexagrid and Diagrid considering $H_{unit\ cell} = H_{level}$ and $H_{unitcell} = 2H_{level}$

5.8 Application and comparison to other patterns – the case of vertical hexagrid

The procedure proposed in the previous paragraphs can be used to deal with any type of structural patterns, and allows for the preliminary comparison among different patterns in terms of weight and efficiency.

In this perspective, a comparison between Horizontal Hexagrid (H_H), Vertical Hexagrid (V_H) and Diagrid (D), is provided in the following; for this purpose, some brief remarks on the mechanical characterization of the Vertical Hexagrid pattern are given.

As already described in paragraph 5.4, also for Vertical Hexagrid three distinct unitary "entities" have been considered: (i) the module, (ii) the unit cell, (iii) the RVE (Figure 5-26). Applying the same procedure

developed for Horizontal Hexagrid and for Diagrid, also in this case it is possible to define the axial and shear stiffness modification factor. The relative density for Vertical Hexagrid is calculated by means the following equation (5.18):

$$\rho_{V\_H} = \frac{(h_{hex} \cdot A_h) + (2 \cdot d_{hex.} \cdot A_d)}{\left[(h + d_{hex} sen\theta) \cdot (2 \cdot d_{hex} \cos\theta)\right] \cdot b} \tag{5.18}$$

As already done for the Horizontal Hexagrid and for the Diagrid, a parametric design application on the same building model is developed for the Vertical Hexagrid, with the module height of the unit cell equal to the interstory height (as proposed for the SinoSteel International Plaza).

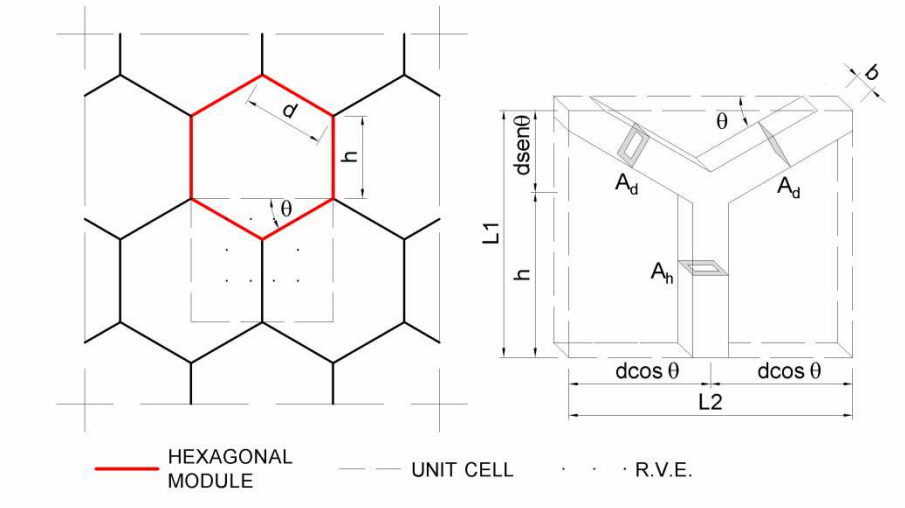

Figure 5-26 Modules, unit cells and volume occupied by solid material in the Unit Cell for Vertical Hexagrid

In addition to the angles considered in paragraph 8 (θ = 50°, 60°, 70°), also θ equal to 30° and 40°, more appropriate for the vertical hexagonal grid, are considered.

The stiffness based criterion is utilised for preliminary sizing of the member cross sections. Summing up, 43 additional design solutions have been generated (13 solutions with Horizontal Hexagrid structures, Table 5-5; 15 solutions with Vertical Hexagrid structures, Table 5-6; 15 solutions with Diagrid structures, Table 5-7). For a fair comparison among the three grid patterns, the same gross dimensions "a" and "b" of the member cross sections have been utilised, while the thickness of the hollow cross sections has been varied as a result of the application of formula (5.3).

Angle θ [°]	**modules** [n°]	**Section (axbxt)** [mmxmmxmm]		
		s	**h**	**v**
31°	7	1500x1500x466	-	-
42°	10	1500x1500x115	1500x1000x131	1000x1500x174
52°	13	1500x1500x52,5	1500x1000x59	1000x1500x72
62°	16	1500x1500x31	1500x1000x35	1000x1500x41
71°	19	1500x1500x21	1500x1000x24	1000x1500x29

Table 5-5 Cross sectional area for Horizontal Hexagrid with $H_{unit\ cell} = H_{floor}$

Angle θ [°]	**modules** [n°]	**Section (axbxt)** [mmxmmxmm]		
		s	**h**	**v**
31°	12	1500x1500x40	1500x1000x48	1000x1500x51
41°	15	1500x1500x24	1500x1000x28	1000x1500x30
51°	19	1500x1500x16	1500x1000x19	1000x1500x21
62°	26	1500x1500x11	1500x1000x13	1000x1500x14
70°	39	1500x1500x8	1500x1000x9	1000x1500x10

Table 5-6 Cross sectional area for Vertical Hexagrid with $H_{unit\ cell} = H_{floor}$

Angle θ [°]	**modules** [n°]	**Section (axbxt)** [mmxmmxmm]		
		s	**h**	**v**
30°	4	1500x1500x301	1500x1000x427	1000x1500x454
41°	6	1500x1500x77	1500x1000x92	1000x1500x95
53°	9	1500x1500x29	1500x1000x34	1000x1500x35
60,5°	12	1500x1500x17	1500x1000x20	1000x1500x21
70°	19	1500x1500x10	1500x1000x11	1000x1500x12

Table 5-7 Cross sectional area for Diagrid with $H_{unit\ cell} = H_{floor}$

The geometric details of the structural grids are synthesized in Figure 5-27 for Horizontal Hexagrid, in Figure 5-28 for Vertical Hexagrid, and in Figure 5-29 for Diagrid.

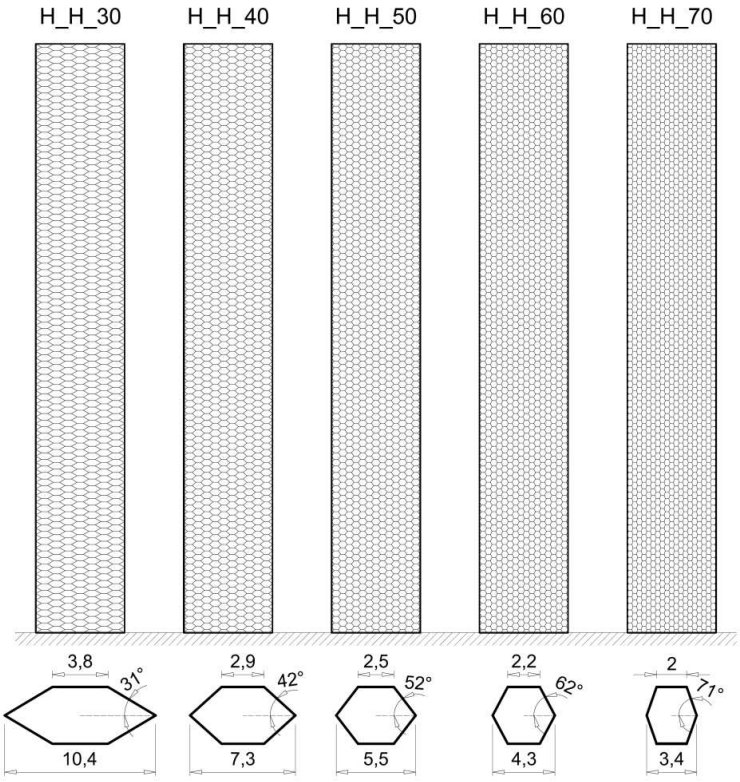

Figure 5-27 Structural grids for comparison – Horizontal Hexagrid

Considering that all solutions are designed for the same stiffness requirement, a first comparative assessment can be made in terms of unit structural weight. Therefore the structural weight for unit area of Horizontal Hexagrid, Vertical Hexagrid and Diagrid have been computed and compared in Figure 5-30. The first observation that can be done from this figure is that for all grid types, the solutions characterized by the lowest structural weights are those with the angle of 70°. For Horizontal Hexagrid and Diagrid the solutions with θ=30 ° give rise to a very large structural weight, since for small diagonal angles, the unit cell is very wide and the structural members are very long.

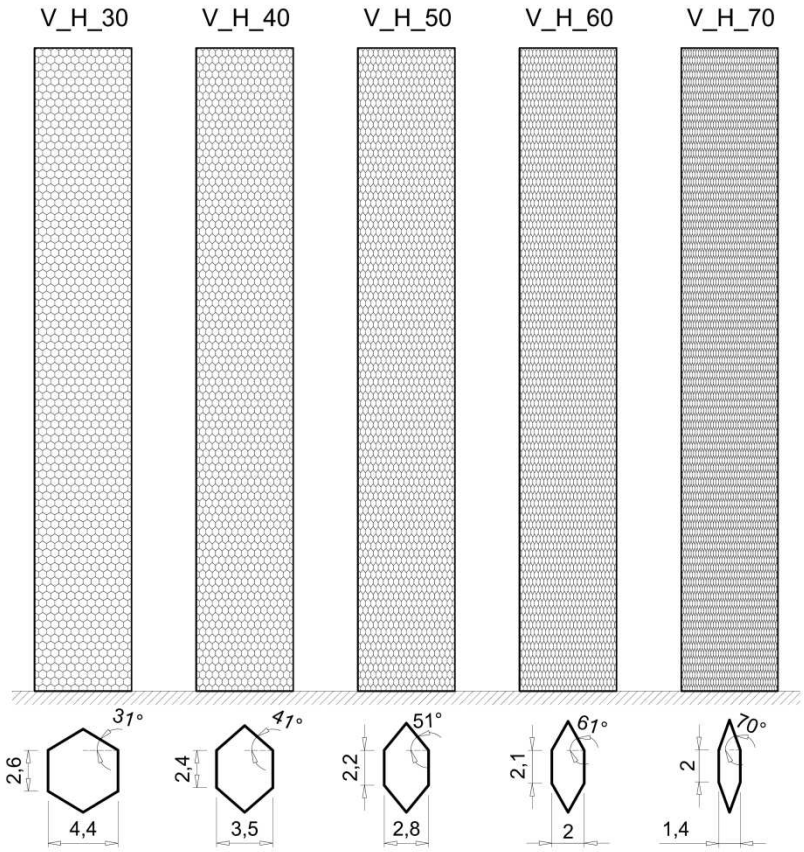

Figure 5-28 Structural grids for comparison – Vertical Hexagrid

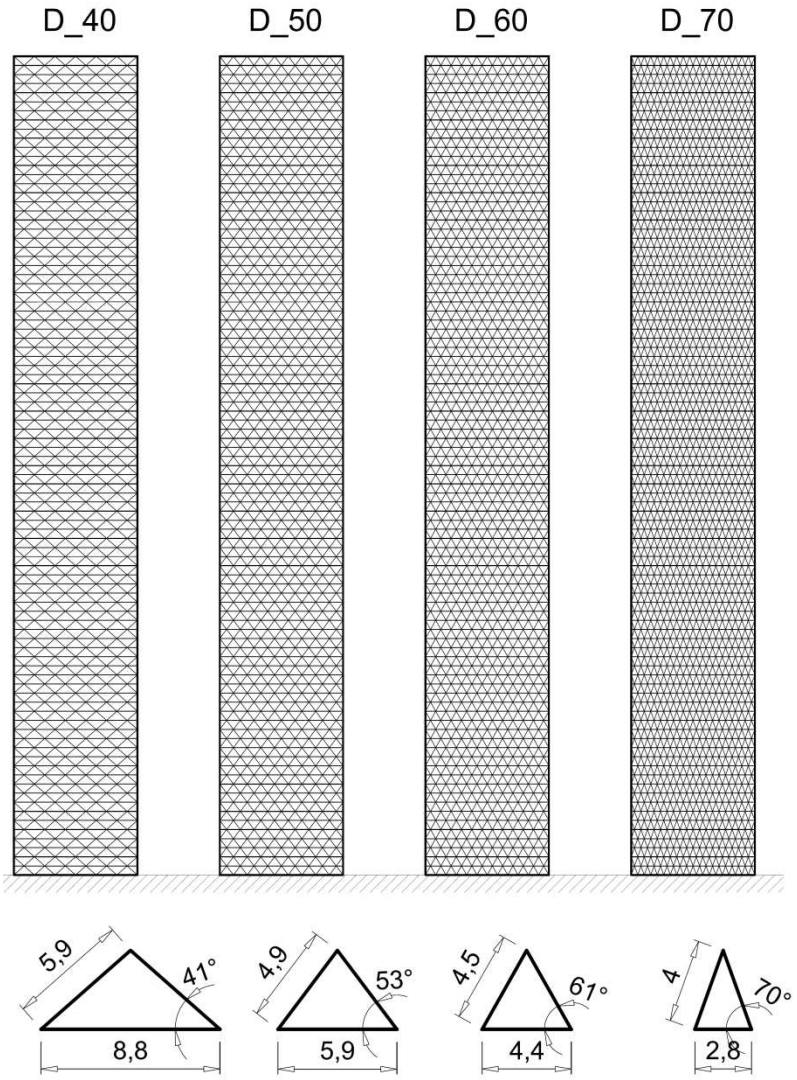

Figure 5-29 Structural grids for comparison – Diagrid

Furthermore, observing the pattern solutions provided in the Figure 5-27, Figure 5-28 and Figure 5-29 it is clear that some solutions (in particular the ones with θ=70°) could be unfeasible for the excessive density of the structural members in façade. In order to take into

account this additional aspect in the comparison among different grids and design solutions, an ad-hoc geometrical parameter is introduced, appointed as "visual density" ρ_v (5.19), defined as:

$$\rho_v = \frac{A^*}{A} = \frac{\sum_{i=1}^{n} l_i \cdot a_i}{L_1 \cdot L_2} \qquad \textbf{(5.19)}$$

Where: A* is the total area of the members used in the grid, A is the area of a surface that has the same outer dimensions as the grid, a_i is the depth of the member section.

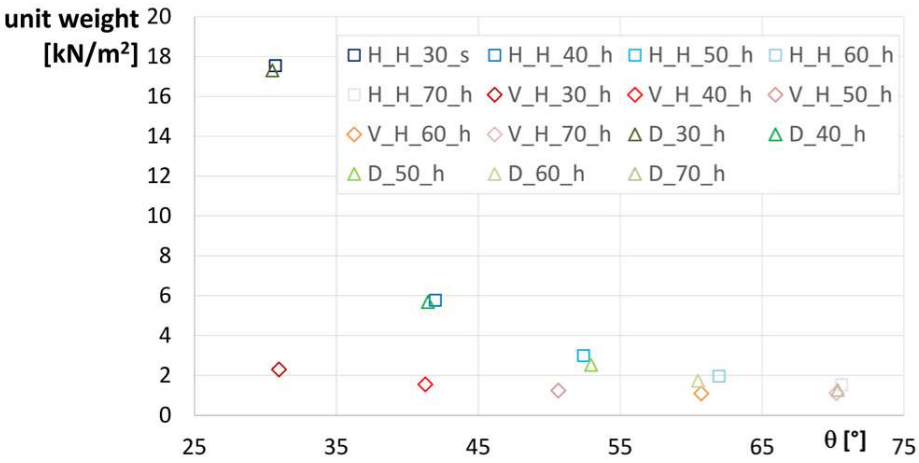

Figure 5-30 Unit weights for Hexagrid, Vertical Hexagrid and Diagrid

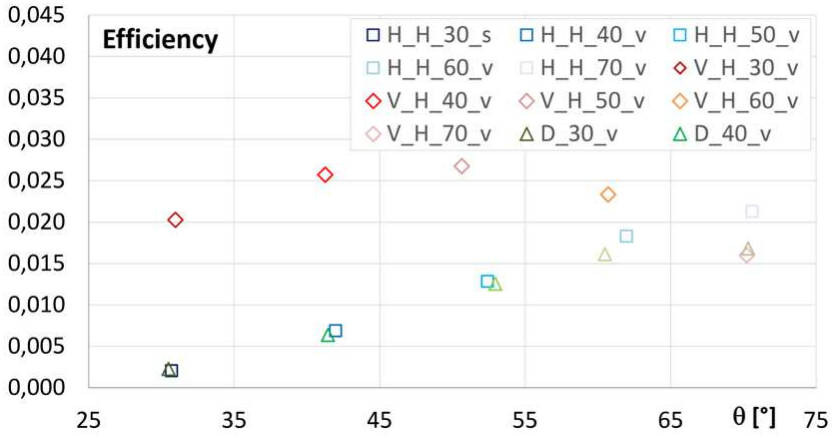

Figure 5-31 Efficiency parameter – Comparison between Horizontal Hexagrid, Vertical Hexagrid and Diagrid

This expression of ρ_v is specialized for Horizontal Hexagrid ρ_{vH_H}, Vertical Hexagrid ρ_{vV_H} and Diagrid ρ_{vD} in the following equations (5.20), (5.21), and (5.22), respectively.

$$\rho_{vH\_H} = \frac{(h_{hex} \cdot a_h) + (2 \cdot d_{hex} \cdot a_d)}{\left[(h_{hex} + d_{hex} \cos\theta) \cdot (2 \cdot d_{hex} sen\theta)\right]} \quad \textbf{(5.20)}$$

$$\rho_{vV\_H} = \frac{(h_{hex} \cdot a_h) + (2 \cdot d_{hex} \cdot a_d)}{\left[(h_{hex} + d_{hex} sen\theta) \cdot (2 \cdot d_{hex} \cos\theta)\right]} \quad \textbf{(5.21)}$$

$$\rho_{vD} = \frac{a_d + \cos\theta \cdot a_h}{d_{hex} \cdot \cos\theta \cdot sen\theta \cdot b} \quad \textbf{(5.22)}$$

A parameter combining the relative density ρ and the visual density ρ_v can be proposed in order to compare the different grids, both in terms

of weight and of grid density. Such parameter is appointed as efficiency of the grid, and defined as (5.23):

$$\textbf{\textit{Efficiency}} = \frac{1}{\rho_v \cdot \rho \cdot b}\left[mm^{-1}\right] \qquad \textbf{(5.23)}$$

In Figure 5-30 this efficiency parameter is provided for the three grid types as a function of the angle θ.

It can be observed that the optimal angle, namely the one that best balances stiffness, weight and visual density, is 40°-50°for the Vertical Hexagrid, while for the Horizontal Hexagrid and the DiaGrid is 60°.

5.9 Conclusive remarks

In the context of a wide research activity on the application of non conventional nature-inspired patterns to structural systems, this chapter provides a first insight on hexagrid tube configurations for tall buildings. The idea is to investigate the mechanical properties of hexagonal grid structures, to assess their applicability in tall buildings, and to compare their potential efficiency to the more popular diagrid systems.

For the above purposes, a general homogenization approach has been established for dealing with any structural patterns, and a methodology for characterizing the structural patterns from the mechanical point of view has been developed and specified for hexagrids and diagrids. Then on the basis of a simple stiffness criterion, a design procedure has been proposed and applied to a tall building case study, and several structural solutions (both hexagrids and diagrids) have been designed and assessed by varying the major geometrical parameters of the patterns.

Some major conclusions that can be derived on the basis of the design/analysis results are:

- The optimal range of diagonal angles, both for diagrids and horizontal hexagrids is 50°-70°; however, an angle of 60° for the diagonal members of both Hexagrid and DiaGrid structures could be the best compromise in terms of stiffness, weight and visual density.
- The optimal angle for the Vertical Hexagrid is in the range 40°-50°.
- The hexagrids, being bending-dominated structures, are inherently less stiff, and consequently, less weight efficient, than diagrids, that are stretch-dominated structures.
- The presence of the floor structure and the consequent rigid diaphragm effect provides a considerable increase of the stiffness of the hexagrid, making it comparable to the diagrid.
- Considering the possible variations of diagonal angle and cross section, hexagrids and diagrids with comparable values of unit weight can be obtained, thus the possibility of structure selection is enlarged.

The very final results of the study herein proposed is a simple hand-calculation method for the approximate analysis and preliminary design of tube structures, which takes into account the characteristics of the patterns through a homogenization procedures, and therefore is applicable to any structural pattern.

The method is suitable for quick evaluations during the preliminary design stage, thus can provide a deep understanding of the effects of varying geometrical and mechanical parameters on the overall structural behavior. Also in the final design stage it can be used for manual checking of the computer analysis results.

The authors believe that the method can be helpful for structural designers involved in exploring tube pattern solutions for tall buildings,

and contemporarily, can enlarge the freedom and unchain the inventiveness of architects willing to exploit the expressive potentials of grid structures.

6 Design of a tall building in Shenzhen, China

The last part of this thesis has been developed at the San Francisco office of the international firm Skidmore, Owings and Merrill, during a four months internship; the active contribution in the design of a tall building structure has been a great opportunity to refine and develop the knowledge on the structural design of tall buildings described in the previous chapters.

The sustainability of tall building structures is having a growing attention worldwide; a sustainable design of a skyscraper should not only care about the consumption of natural resources during the building ordinary life but also try to reduce the amount of structural material. With this aim, in the recent years new structural solutions have been proposed to maximize the structural efficiency; some of them have been described and investigated in the previous chapters.

In the following, an optimized configuration for a perimetral frame of a real tall building is analyzed, firstly evaluating the building performance and issues, and then comparing the optimized structure with more traditional structural solutions.

It has been very interesting to understand how the optimum design (i.e. the most efficient structural solution) can be obtained and modified to mediate with different issues (e.g. architectural requirements, site conditions, client requests, etc.) and how it is necessary to elaborate an integrated design.

6.1 Architectural vision and concept

The overall project comprises two office towers, a serviced apartment building and a retail building. A multi-story bridge structure will connect the taller office tower to the retail building. All buildings share a common basement, two levels deep, that extends over a large portion of the site (Figure 6-4).

The building will be the image of modern Shenzhen (Figure 6-1), with buildings and landscape that perform efficiently and ecologically, providing an exceptional amenity and source of pride for the city and its citizens.

Figure 6-1 City of Shenzhen

The two towers will be as jewels on the skyline of the city (Figure 6-2), while anchoring the project to its site at the urban base. Transforming elegantly from square and massive at the ground to slender and circular at the top (Figure 6-3), the towers respond to the multiple conditions of site, program, systems and structure, and emerge from the earth as beautiful and distinctive icons in the sky.

Figure 6-2 View of the final configuration of the project

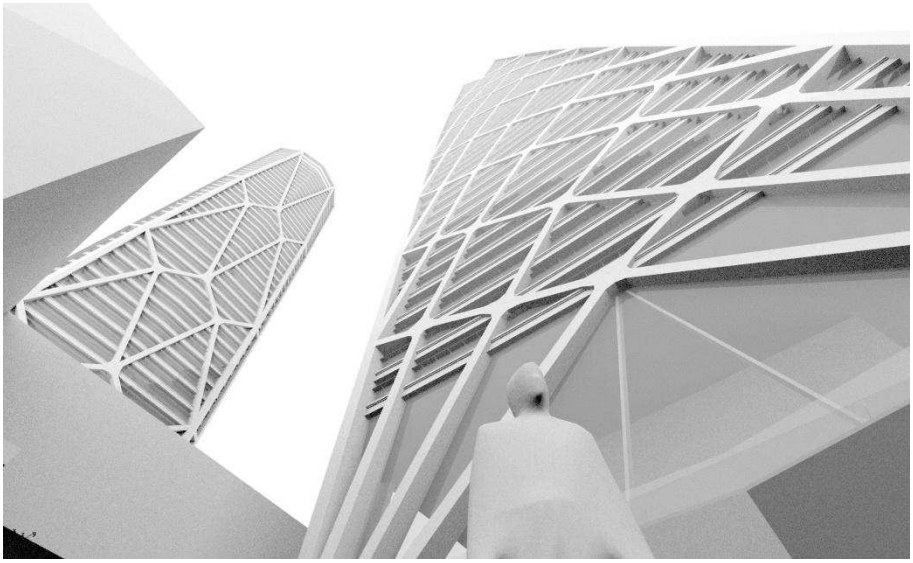

Figure 6-3 View of the two Towers

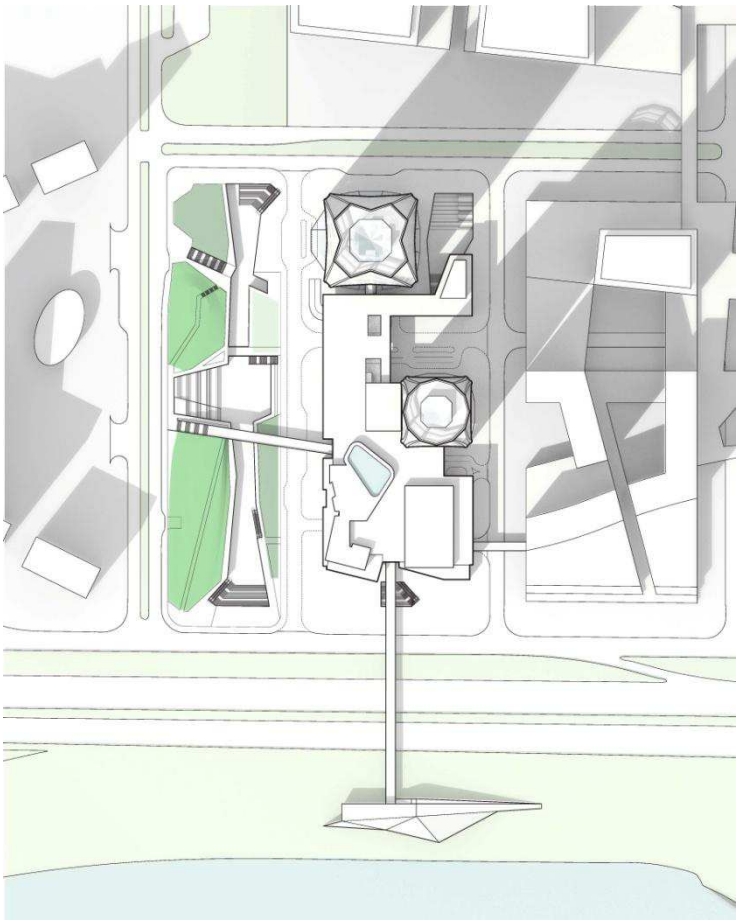

Figure 6-4 Overall plan of the project

6.2 Structural System

The structural lateral system for the office and the hotel tower is conceived as a highly efficient dual system with a reinforced concrete core and a perimeter composite frame. The central core will utilize reinforced concrete shear walls which will typically be located around the mechanical rooms, elevators and stairwells. The shear walls will be connected by reinforced concrete beams.

The analyses described in this chapter are mainly focused on the design and analysis of the Office Tower 1.

6.2.1 Office Tower 1 – OT1

The 68-story office tower is 299.6 m above grade to the main roof, and 312,0 m to the top of parapet with typical floor to floor height of 4.5 m (3.6 m at the upper levels). The tower is typically square in plan (Figure 6-5), but in inward curving (concave) edges that vary in curvature up to height of the building. The tower is symmetrical in plan about both axes, with façades that are curved both in plan and elevation.

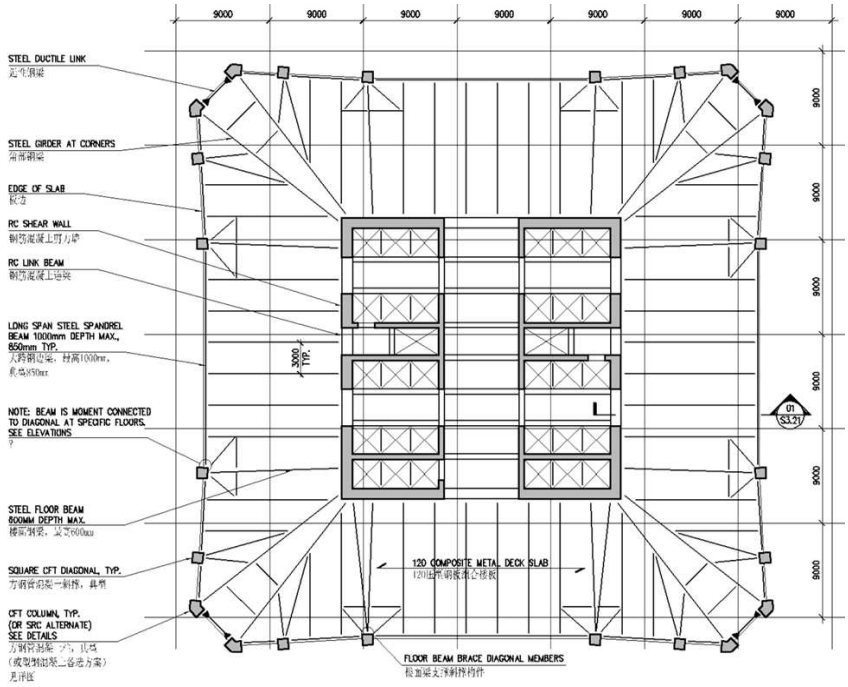

Figure 6-5 Office Tower1 - Typical structural plan

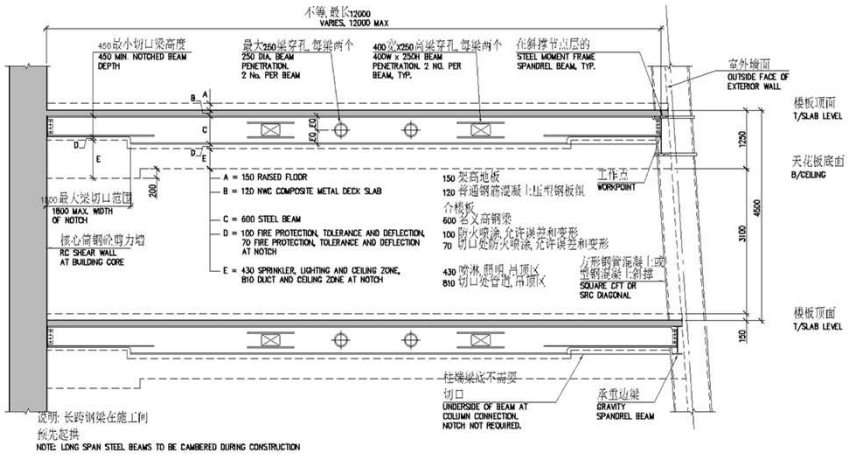

Figure 6-6 Office Tower1 - Structural section

The lateral system consists of a continuous composite steel/concrete braced frame at the building perimeter, and reinforced shear walls within the building core (Figure 6-7). The perimeter braced frame extends from the ground to the top of the parapet, transferring to a system of columns and shear walls below grade coordinated with the basement. The shear wall within the core extends from foundation up to the height of the building, reducing in extent as the size of the core reduces at the upper levels. The shear walls typically range in thickness from 500 mm to 1300 mm and utilize C60 concrete. The perimeter frame is composed of concrete filled rectangular tubes (CFT) which range in size from 700 mm x 700 mm to 1700 mm x 1700 mm. At the four corners of the tower, pairs of adjacent columns at the adjoining façades will be connected by ductile steel moment frame beams (links) at each floor level. Such links will be sized to remain elastic for wind and frequent seismic loading and to yield at the rare seismic event.

The gravity floor framing consists of steel floor framing beams and girders, spanning between the building core and perimeter (Figure 6-6).

The beams support composite metal deck floor slabs, with which they are designed to act compositely. Within the core, the gravity floor framing consists of reinforced concrete beams and slabs.

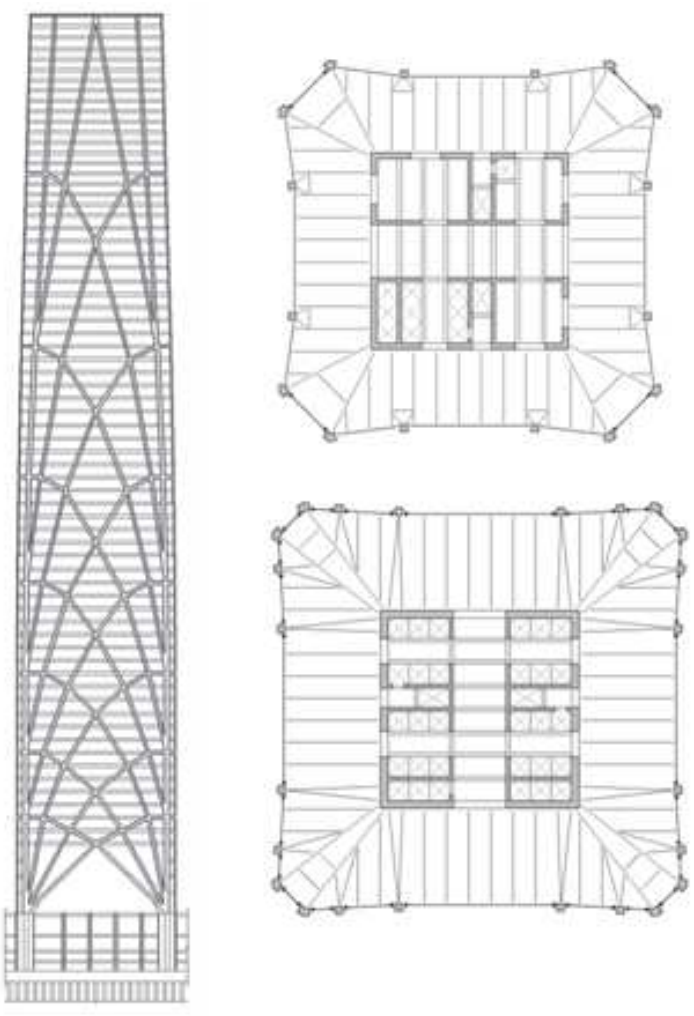

Figure 6-7 Office Tower 1 – Elevation and typical plans

6.2.2 External loads

The gravity loads are calculated considering the floor framing and the occupancy of the floor. The following tables Table 6-1, Table 6-2 and Table 6-3 and Figure 6-8 show the values of the Super Imposed Dead Load (SDL) and Live Load (LL) based on the Chinese Code GN 50009-2012 and their distribution along the building height.

Uniformly Distributed Super Imposed Load (SDL)kN/m^2		
Item	**Load Used**	**Value for Seismic Mass Calculation**
Core	7.7	7.7
Luxury Condo Amenity	4	4
Luxury Sea View	4	4
Mechanical	1.7	1.7
Office	1.1	1.1
Stair	7.7	7.7

Table 6-1 Office Tower 1 –SDL Uniformly distributed

Superimposed Dead Load over area of element kN/m^2		
Item	**Load Used**	**Value for Seismic Mass Calculation**
Exterior Wall	1.25	1.25

Table 6-2 Office Tower 1 – SDL over area of element

Uniformly Distributed Live Load (LL)kN/m^2		
Item	**Load Used**	**Value for Seismic Mass Calculation**
Core	3.5	3.5
Luxury Condo Amenity	2	2
Luxury Sea View	2	2
Mechanical	10	10
Office	3	3
Stair	3.5	3.5

Table 6-3 Office Tower 1 – LL Uniformly distributed

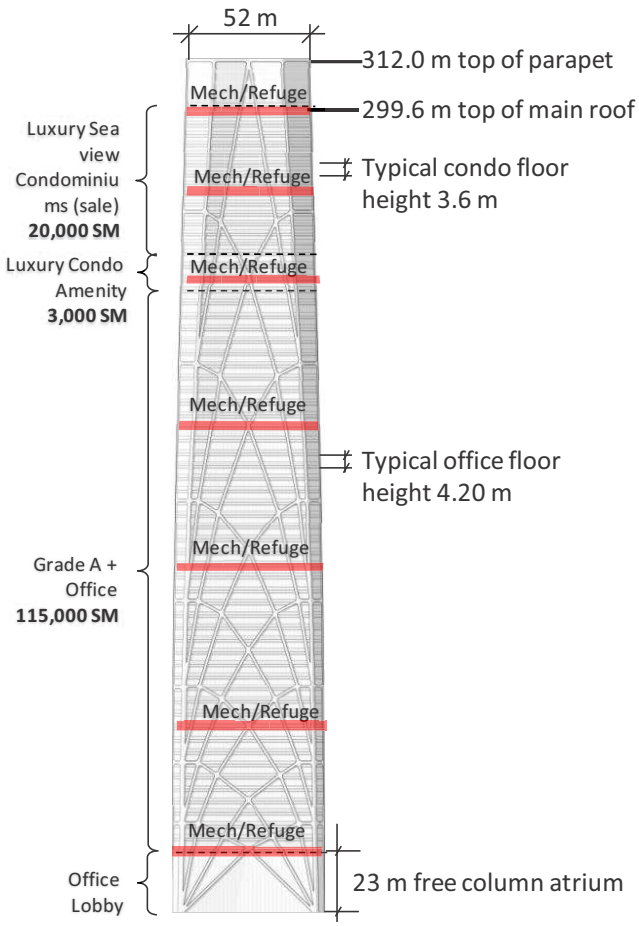

Figure 6-8 OT1 – Building use along the elevation

The wind loads on the building are high due to the sea proximity and to the low roughness of the ground (class A, the worst for the China Code). Considering the recommendation of the China Code for the city of Shenzhen a basic wind pressure for 50 year return equal to 0.75 kPa has been considered.

The building area has a medium seismicity level, i.e. seismic design intensity equal to 7 for the Chinese Code GB 50011. The basic design acceleration is equal to 0.10 g with a characteristic period T_g equal to 0.65

sec. The maximum spectral acceleration is equal to 0.04 g, 0.23 g and 0.5 g respectively for the frequent, the medium and the rare earthquake.

The Figure 6-9a and b reports the comparison between wind and the seismic loads in terms of global shear along x and y respectively; Figure 6-10a and b shows the same comparison in terms of overturning moment. It is clear from the graphs that the wind loads are prevalent and that they will govern the design.

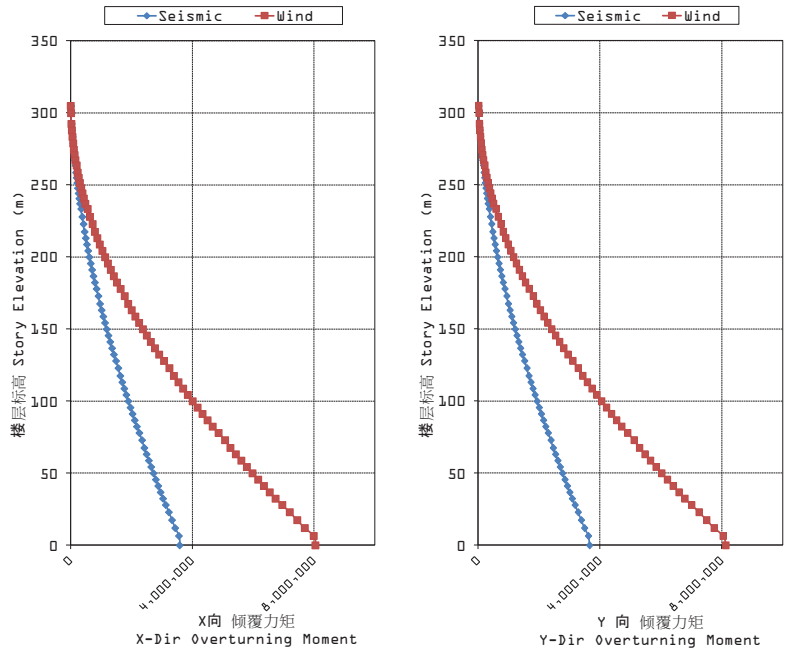

a) b)

Figure 6-9 OT1. Comparison between the seismic (blue lines) and the wind (red lines) shear a) along x, b) along y

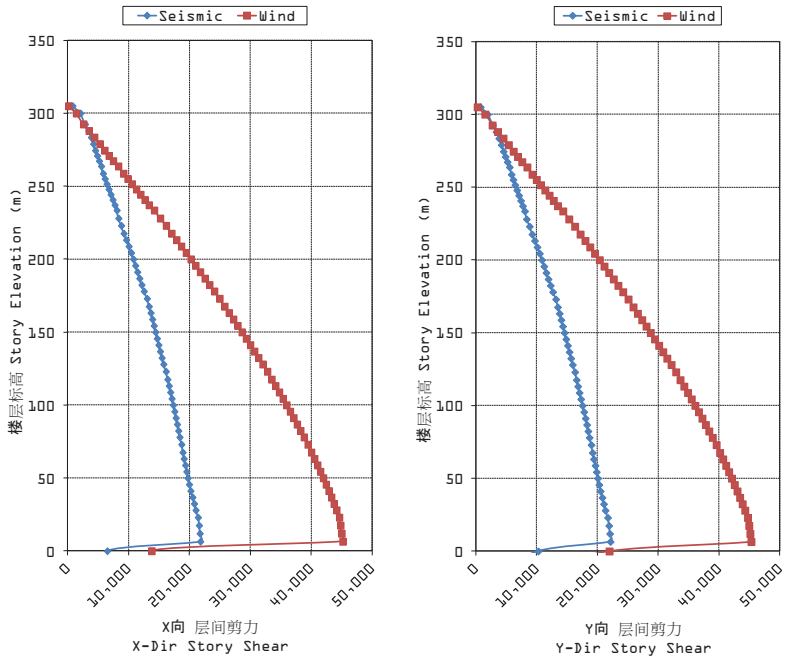

Figure 6-10 OT1 - Comparison between the seismic (blue lines) and the wind (red lines) overturning moment a) along x, b) along y

6.3 Structural analysis OT1 - Special Studies

The Office Tower 1 (OT1) shows unique structural behavior and particular issues; four special studies (described in the following) have been carried out in order to obtain a reliable and efficient structural solution.

The first special study regards the structural function of the central core and the influence of its lateral stiffness on the overall behavior of the building. One of the requests of the architectural design was to have a large 20-storey interior atrium at the top of the building as realized in the Guangzhou International Finance Center (IFC, Figure 6-11). For this

reason, the internal shear walls of the core have to stop at 46th level; furthermore the core should be reduced along the building height, increasing the size and the number of the openings.

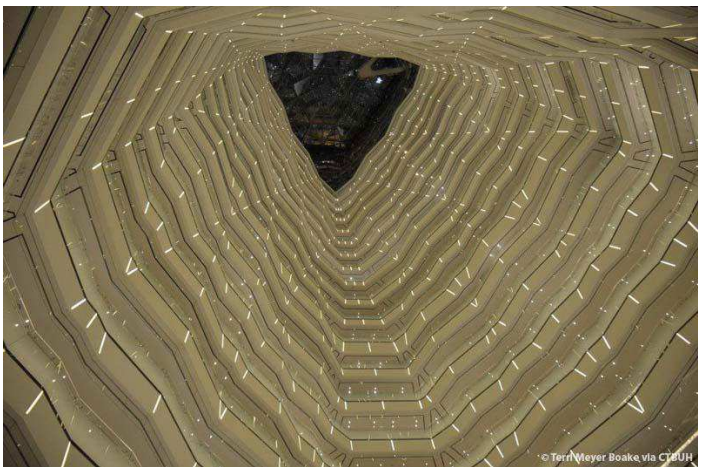

Figure 6-11 Guangzhou International Finance Center top atrium

In order to understand the influence of the stiffness of the core, a "boundary" study has been carried out; in particular considering the same perimeter frame, two "extreme" solutions for the core structure have been defined: i) simple frame with very low horizontal stiffness (solution A, Figure 6-12a), ii) shear walls without reduction and without the atrium at the top (solution B, Figure 6-12b). The structural performances of the two solutions have been evaluated through finite element analysis using the computer code ETABS; as already observed in paragraph 7.2.2 the wind loads control the design; in particular the interstory drift under the frequent wind action can be used as principal response parameter for assessing the global building behavior.

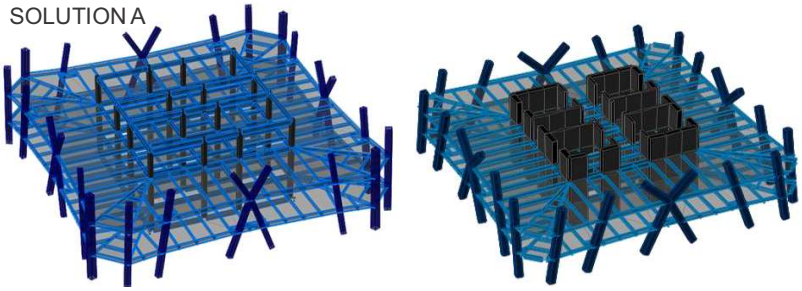

a) b)

Figure 6-12 OT 1. Different structural solution for the central core a) simple frame, b) shear walls and coupling beams

The results of the FE analysis are reported in terms of interstory drift in Figure 6-13a and Figure 6-13b respectively for the solution A and B; the A solution shows the typical behavior of the structures with megadiagonals (see chapter 4). Without a stiff core, at the intermediate floors (i.e. the floors between the "panel points" of the megadiagonals) the horizontal stiffness of the structure is provided by the bending of diagonals. This lack of stiffness causes a local deformability problem (e.g. very high interstory drift) and a stability issue, giving rise to the simultaneous buckling of the central columns in a multy-story mode between the mega-brace point. It is worthy to note that in spite of this local effects, the perimetral optimized diagrid has a high global horizontal stiffness, almost sufficient to counteract the wind actions without any help from the core (Figure 6-13a).

In the second model (Figure 6-13b), the shear walls avoid the local lack of stiffness, acting as a Secondary Bracing System (see Chapter 4). Unlike the SBS described in Chapter 4, the shear walls have a remarkable overall horizontal stiffness, carrying also a good percentage of lateral loads globally.

The Figure 6-14a shows the results of a third solution considering the atrium at the top of the building (i.e. with a simple frame structure in the core above 46th level); above 46th level the structure shows the same local lack of stiffness seen before for the model A. Considering the results of these studies, the final structural configuration for the core (Figure 6-14b and Figure 6-24) represents a compromise between the architectural and the structural requirements; in particular the internal walls in the core stop at level 46th but the perimetral walls continue above level 46th with increasing openings.

Finally it is possible to underline that the shear walls improve substantially the building behavior, not just increasing the overall lateral stiffness but mainly solving the local deformability problems.

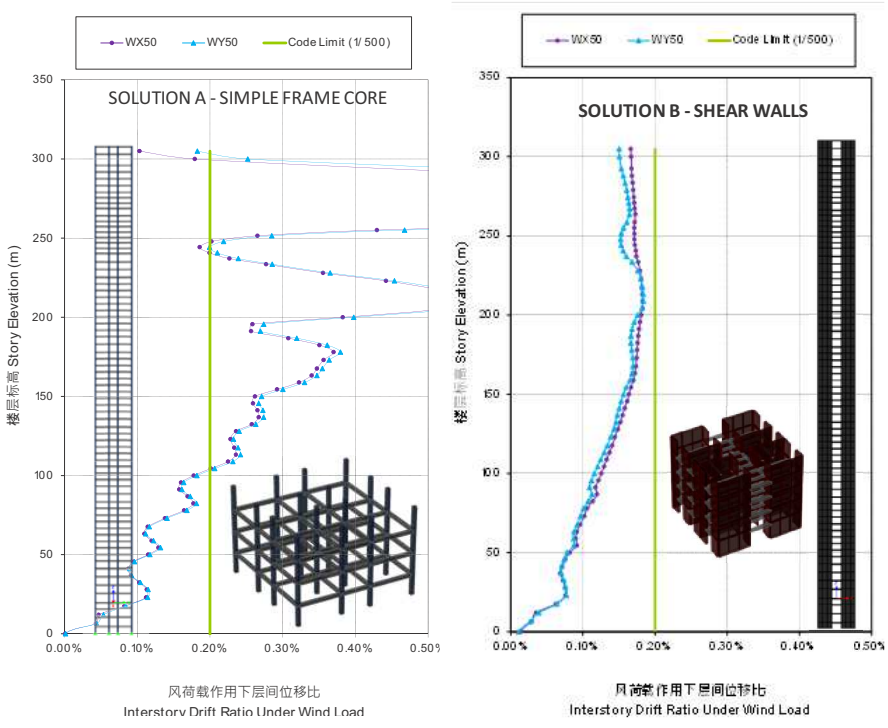

a) b)

Figure 6-13 OT1 - Interstory drift check a) for solution A, b) for solution B

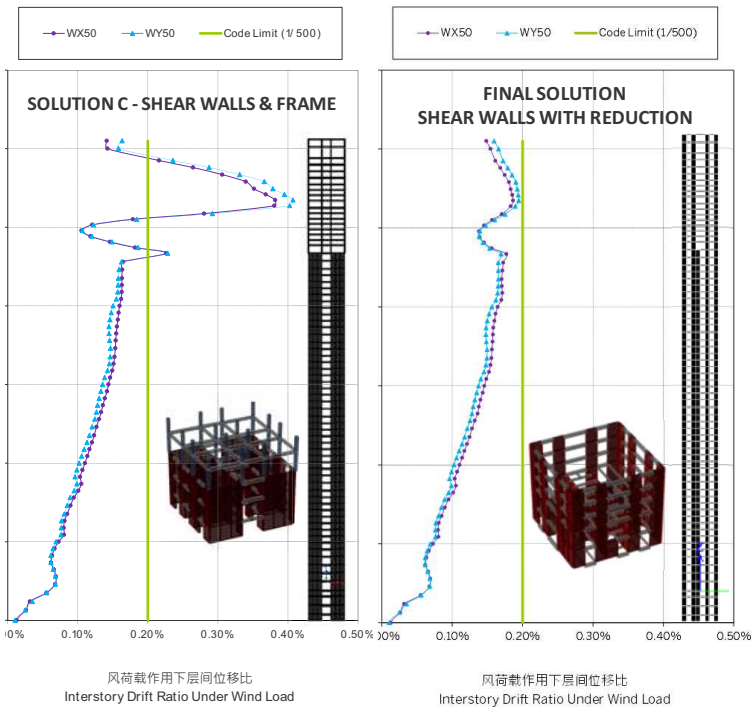

a) b)

Figure 6-14 Office Tower 1 - Interstory drift check a) for solution C, b) for final design.

The second special study concerns the typology of the connections (moment or simple shear, Figure 6-15a and b respectively) between the spandrel beams and the diagrid elements at the building perimeter.

As for the analysis on the core structures, a boundary study has been carried out, defining two extreme cases with the minimum (case D Figure 6-16a) and the maximum (case E Figure 6-16b) number of moment connections for the spandrel beam. The two cases are compared using again as response parameter the interstory drift under wind action; the increase of the horizontal stiffness obtained for the E case (Figure 6-16) is not sufficient to justify the increase of moment

connections with respect to D case (327 and 1585 moment connections for the D and E respectively) in terms of cost and construction time of the structure.

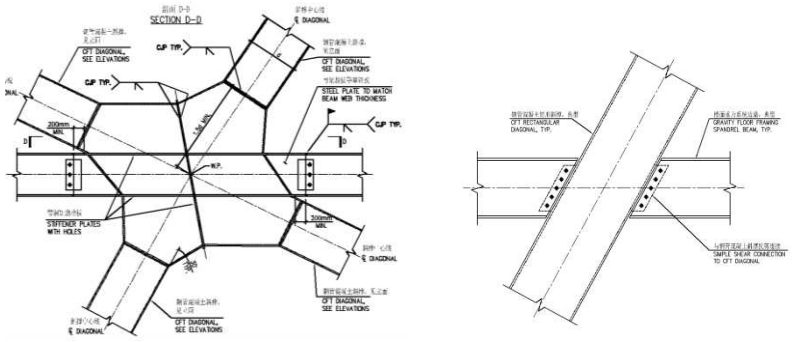

a) b)

Figure 6-15 OT1 - Connection typology between the spandrel beams and the diagrid elements a) moment connection, b) simple shear

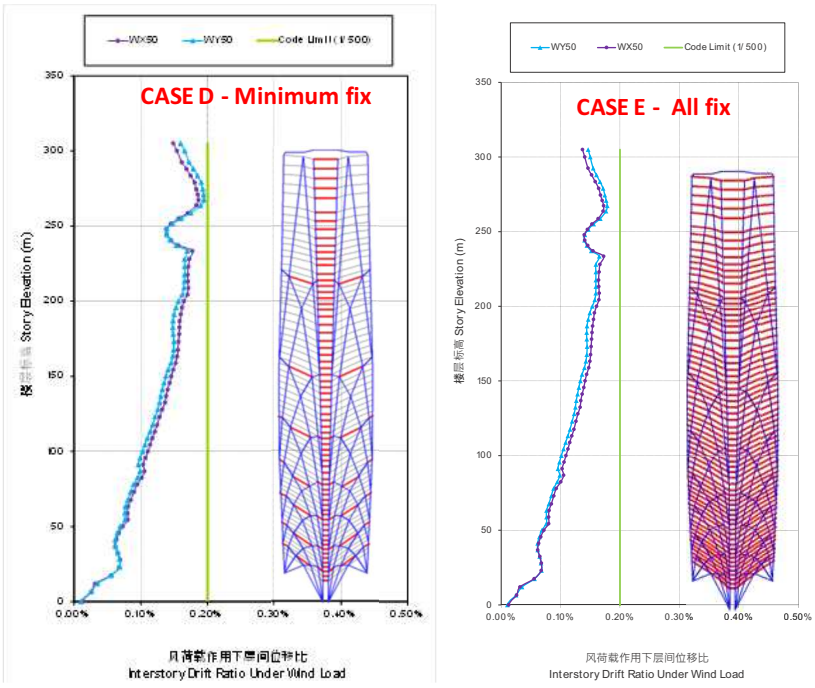

a) b)

Figure 6-16 OT1 - Interstory drift check a) for solution C, b) for final design.

The choice of the connection typology is also related to the peculiar behavior of the diagrid structure under gravity loads, with diagonals in compression and horizontal elements at the base of the triangle module in tension (Figure 6-17a); Figure 6-17b shows with the black line and dots the axial forces in the spandrel beam along the building height. At levels close to the basis of the triangular megamodules, the tension strength of a simple shear connection (vertical red line in Figure 6-17b) is less than the tension forces in the spandrel beam, thus a moment connection must be used to connect the spandrel beam to the diagonals. With this approach, it is possible to select the beam to be moment connected in the final solution (Figure 6-17c).

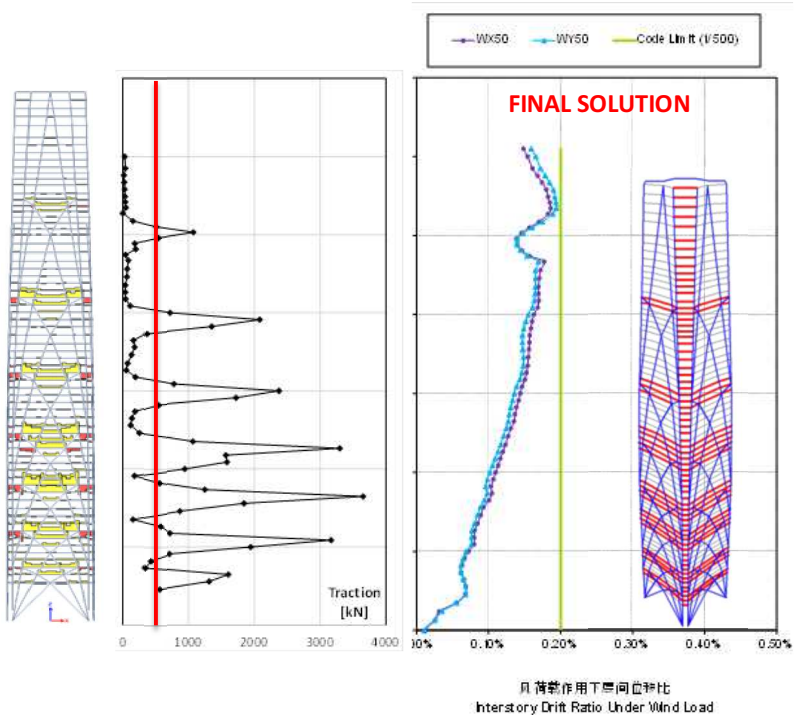

a) b) c)

Figure 6-17 OT1. Axial force in spandrel beams a) contour, b) values along the elevation, c) Interstory drift check under wind loads for the final solution

A share of the horizontal forces at the basis of the triangular module is carried out from the concrete slab connected to the spandrel beam. The tension stress in the concrete could be greater than the concrete tension strength (2 MPa) causing the cracking in the slab; the aim of the third special study is to evaluate the effect of this cracking on the global behavior of the building. The tension stresses in the concrete slab have been evaluated using the results of the FE models; considering slabs with 100% of the membrane stiffness, the tension stress in the slabs are diffusely greater than the concrete tension strength (Figure 6-18a). Considering a 50% of the slab membrane stiffness, the tensions in the slab decrease but still a wide part of the slab shows tensions greater than 2 MPa (Figure 6-18b); the concrete of the slab does not crack only if a 10% of slab stiffness is considered (Figure 6-18c). This reduction of membrane stiffness of the slab causes a double effect i) the tension forces in the spandrel beam increase (Figure 6-19a), ii) the "box" behavior of the building decreases and so its overall horizontal stiffness (Figure 6-19b). The final design of the structure considers the cracks in the slab, adopting in the FE model only the 10% of the membrane stiffness of the slabs.

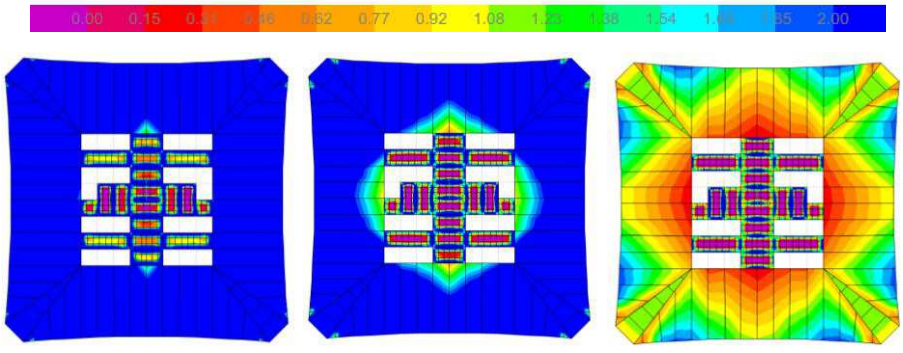

a) b) c)

Figure 6-18 OT1. Stress in the slab for a) 100%, b) 50% and c) 10% of the slab membrane stiffness

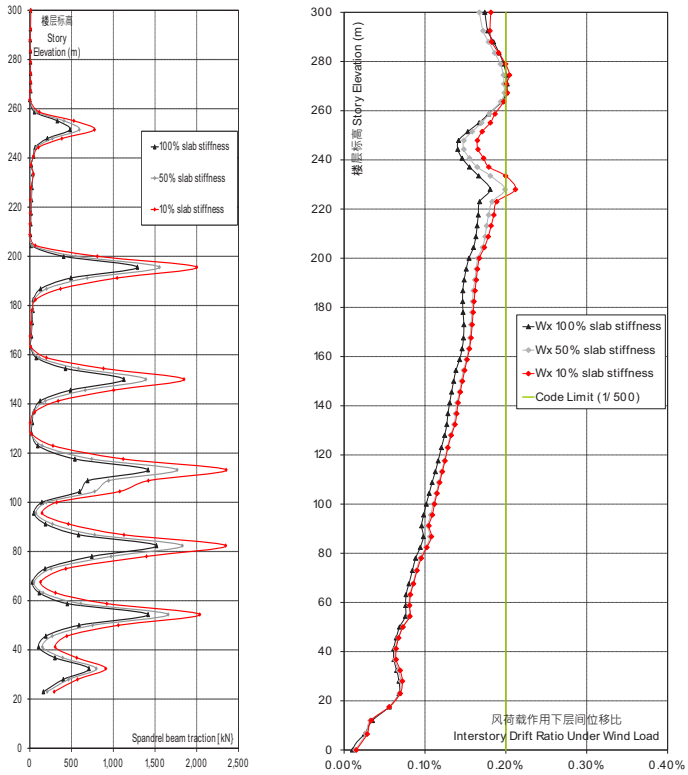

a) b)

Figure 6-19 OT1. Effect of the slab cracking, a) axial forces in the spandrel beams, b) Interstory drift check

The last special study concerns the seismic behavior and design of the Office Tower 1; as reported in par. 7.2.2. the tower is located in a moderately seismic region (seismic intensity VII), therefore the seismic behavior of the structure should be carefully analyzed. The optimized perimetral diagrid configuration has a high lateral stiffness and a great performance in the elastic field against wind load but it has a very low ductility. The proposed solution is to improve the ductility of the perimetral frame adding ductile elements which work as structural fuses during the non-linear behavior of the building. The idea is to use the

beams at the four corners of the buildings plan as ductile fuses (Figure 6-20), with an approach similar to the more traditional Eccentric Braced Frames. In fact "the most attractive feature of EBFs for seismic-resistant design is their high stiffness combined with excellent ductility and energy-dissipation capacity. The bracing members in EBFs (the diagrid in the Office Tower) provide the high elastic stiffness characteristics of CBFs. Yet, under very severe earthquake loading, properly designed and detailed EBFs provide the ductility and energy dissipation capacity characteristics of MRFs", [41].

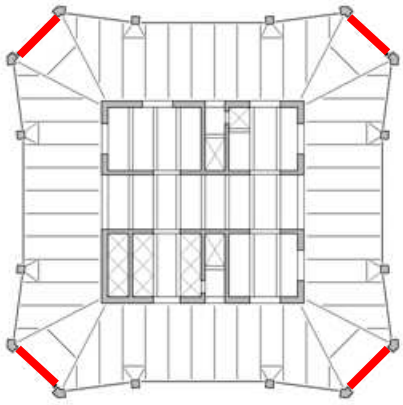

Figure 6-20 OT1. Typical plan with ductile link (in red)

The plastic behavior of the link is function of the link length; under horizontal action the link is subject to high shear force along its entire length and high bending moments at its ends. If the link is short, then under increasing lateral load on the frame, the link will yield in shear (forming plastic shear hinges) with relatively little moment yielding at its ends. On the other hand, if they are very long, the links will form conventional plastic moment hinges at the ends, with little or no shear yielding. As a results, short links are referred to as shear links, and long

links as moment links. The energy dissipation and ultimate failure mechanism for these two classes of links differ substantially. There is, of course, an intermediate length range of links where significant amounts of both shear and moment yielding occur [41].
The links are usually classified in function of their length as in the following

- short links $$e \leq 0.8\frac{M_{Rd}}{V_{Rd}}$$ (7.1)
- intermediate links $$0.8\frac{M_{Rd}}{V_{Rd}} \leq e \leq 1.5\frac{M_{Rd}}{V_{Rd}}$$ (7.2)
- long links $$e \geq 1.5\frac{M_{Rd}}{V_{Rd}}$$ (7.3)

where M_{Rd} and V_{Rd} are respectively the plastic moment and plastic shear of the links.
The seismic design approach requires that the links remain elastic under frequent earthquake and yields under rare earthquake. In a first model (Figure 6-21) an unique double T steel section (HN700x400x13x24) is used for the link along all the building elevation. The links have variable lengths along the building height (from 2.6 m at the base to 11.4 m at the building top); as a result links are intermediate in the lower part of the building while links are long in the upper part. The performances of this first simplified design have been evaluated through FE analysis; in particular Figure 6-21 shows the values of shear (blue bars) and moment (red bars) obtained in the links by means of a linear dynamic analysis considering the frequent (solid bars) and rare earthquakes (dashed bars). The structure behavior is not satisfactory; the plastic strength of the links (reported with green vertical bars in Figure 6-21) is not included between the values of moment and shear obtained in the link for frequent and rare earthquake (e.g. at the bottom and at the top of the building the links are oversized).

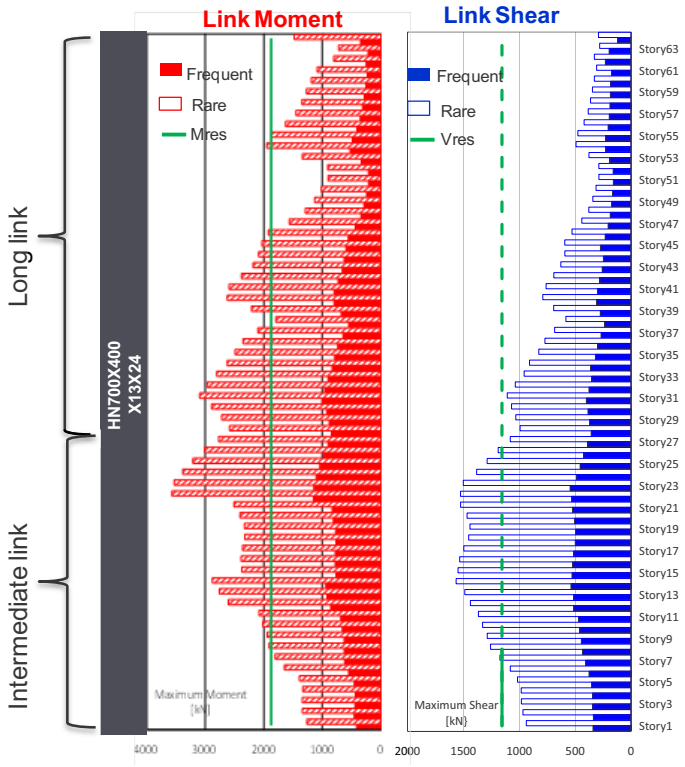

a) b)

Figure 6-21 OT1. Preliminary seismic design; loads in the links for frequent (solid bars) and rare (dashed bars) earthquake, a) Moment, b) Shear

Through an iterative approach, in the final solution four different cross section are used for the ductile links (HN500x500x7x16, HN650x300x10x15, HN700x300x13x20, HN500x10x16). The performance of the final solution are reported in Figure 6-22. In the lower part of the building (below level 10) the links are short (shear plastic hinges) while above level 10 the links are long with moment plastic hinges. The Figure 6-22 shows that the plastic strength of the

links is included between the values of the forces in the link for the frequent and rare earthquake.

The reduction of the cross section of the links affects also the elastic behavior of the building; in particular the horizontal stiffness of the building decreases, mainly because with smaller links the box behavior of the structure is reduced.

Non linear static and dynamic analyses are necessary to investigate the plastic behavior of the building, to asses that the diagonal elements of the diagrid do not yield before the links and also to evaluate the interaction between the central core and the external frame.

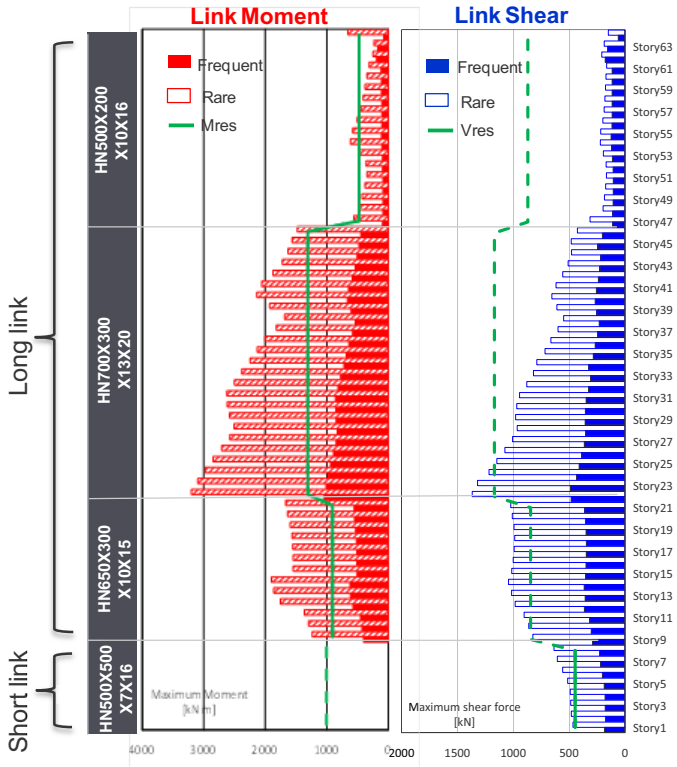

Figure 6-22 OT1. Final seismic design; loads in the links for frequent (solid bars) and rare (dashed bars) earthquake, a) Moment, b) Shear

6.4 Final design OT1 – Structural Results

Once the behavior of the building was investigated and understood through the results of the special studies described in the previous paragraph, the structure has been redesigned. The results of the final design are described in the following in terms of diagrid cross sections (Figure 6-23a), spandrel beams sections (Table 6-4), link sections (Figure 6-23b), core configuration and shear wall thickness (Figure 6-24).

The final solution shows good performance; the structure is well designed both under gravity and lateral loads, with good stiffness, ductility and high efficiency. The dynamic analysis shows a stiff structure (first period along x 5.11 sec Figure 6-25a, for a total height of 320m) and a symmetric behavior in plan (second mode along y with period equal to 4.96 sec , Figure 6-25b, close to the first period). Furthermore the structure has a great torsional stiffness as shown by the gap between the third rotational mode (2.7 sec, Figure 6-25c) and the first two translational mode (around 5 sec.), mainly thanks to the stiff perimetral frame.

Figure 6-26a and b shows the interstory drift along the building height under seismic and wind action respectively; it is clear that the wind action governs the design and that in particular the most demanding check is related to the interstory drift limitation (<0.2%). The values of the interstory drift are very close to the limit resulting in a well designed structure.

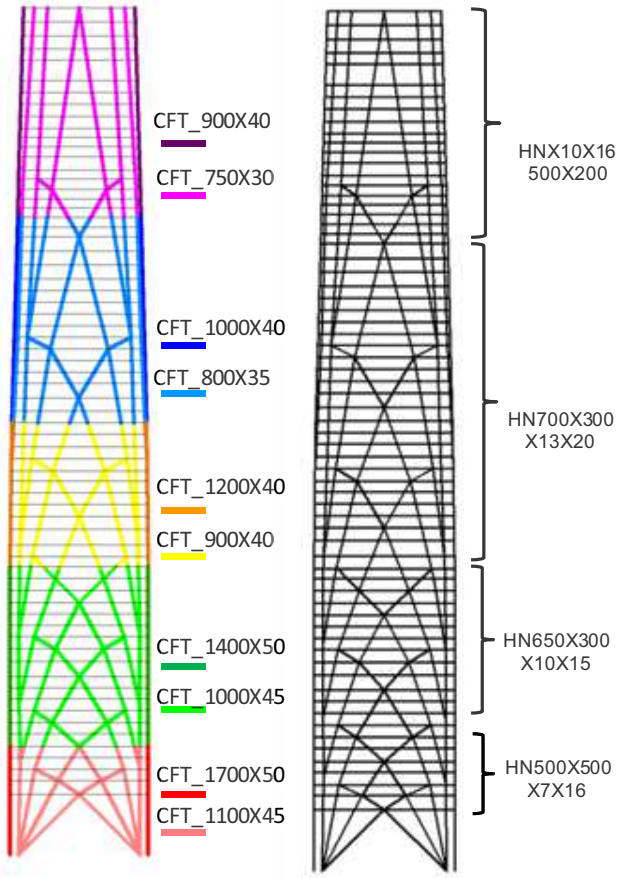

Figure 6-23 OT1 final design Structural cross section a) for diagrid members, b)for link beams

SPANDREL BEAM	
Length	Section
< 6 m	HN500X200X10X16
6 m < L < 15 m	HN700X400X13X24
L > 15 m	HN1000X300X21X40

Table 6-4 OT1 final design. Structural cross section for spandrel beams

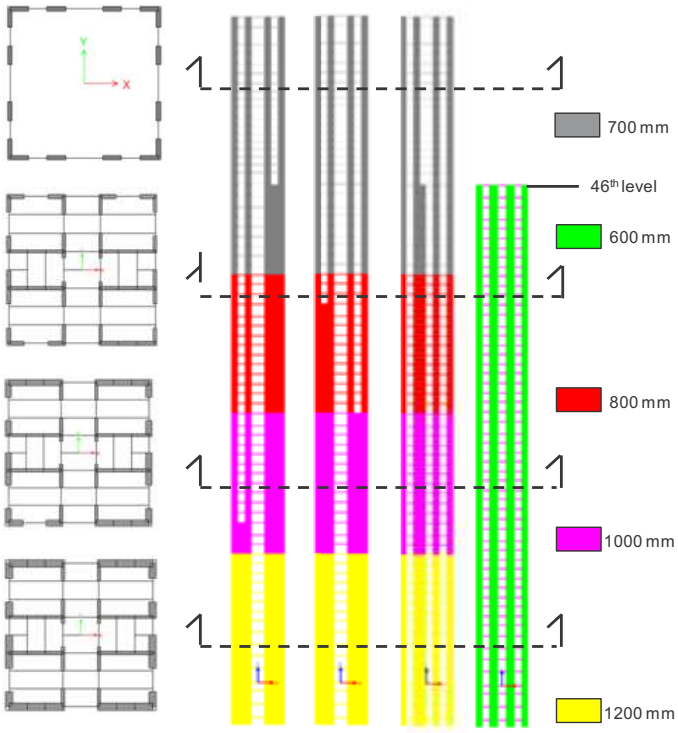

a) b) c)

Figure 6-24 OT1 final design. a) Variation of the central core structural plans along the elevation, b) thickness and geometry of the walls on the core perimeter, c) thickness and geometry of the internal walls

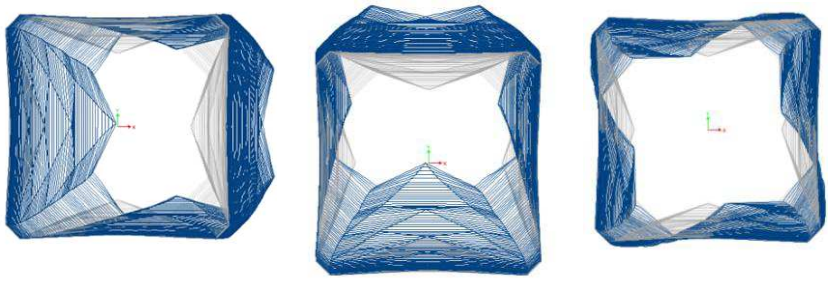

a) b) c)

Figure 6-25 OT1 final design result a) First mode, b) Second mode, c) Third mode

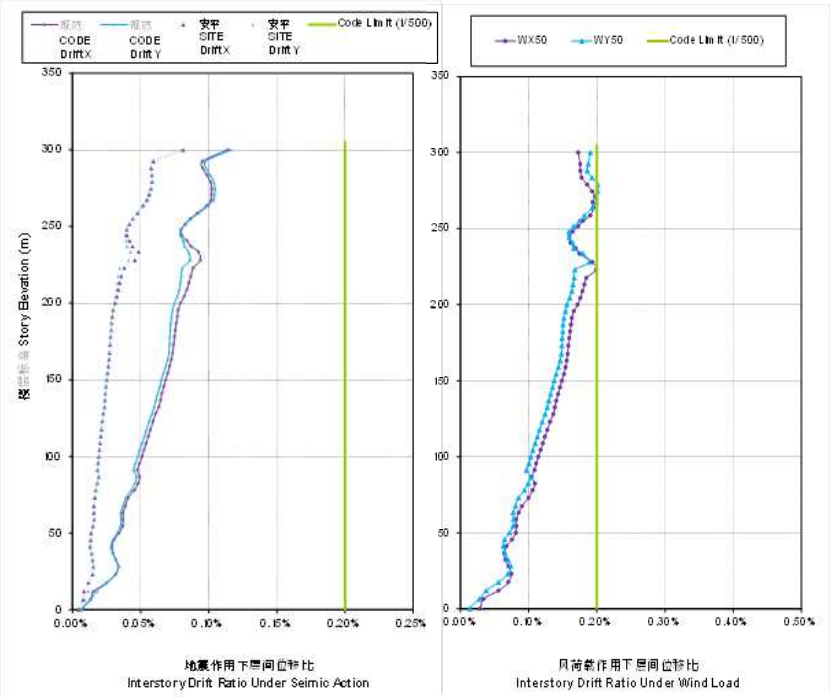

a) b)

Figure 6-26 OT1 final design result. Interstory drift check a) for seismic loads, b) for wind loads

The high efficiency of the external frame is evident in Figure 6-27, which report the percentage of global shear and overturning moment carried out from the internal core and from the perimetral diagrid. At the basis the diagrid carries 73% of the overturning moment, thanks to the higher flexural stiffness of the frame; this result is predictable and trivial considering that the structural members of the diagrid are more perimetral than the core walls. Surprisingly the perimetral frame carries also a great amount of the overall shear (81%); usually the shear is carried by the internal shear walls but the perimetral frame thanks to its optimized geometrical configuration has high shear stiffness.

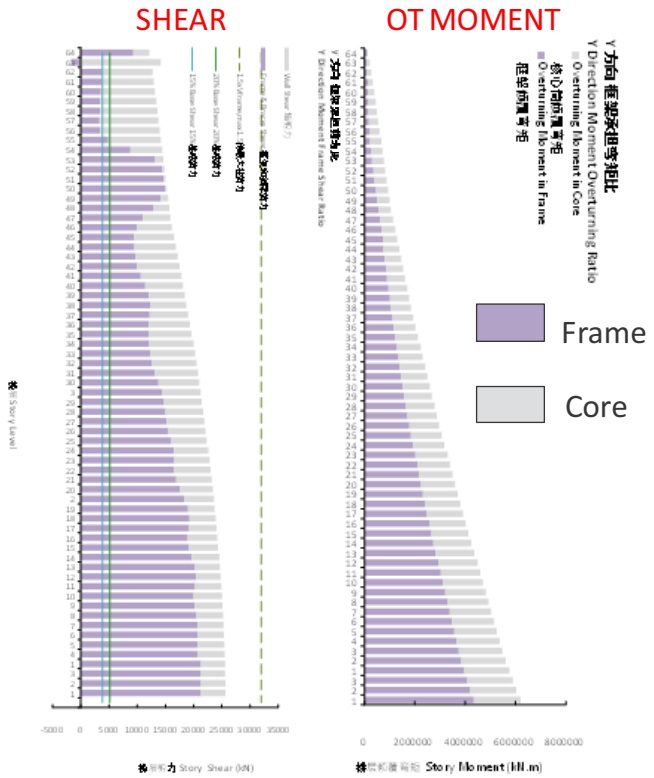

a) b)

Figure 6-27 OT1 final design results. Distribution of the wind loads between the central core (in grey) and the external frame (in violet) a) shear, b) overturning moment

6.5 Comparison with different structural solutions OT1

The optimized geometrical configuration of the perimetral diagrid (Figure 6-28a) shows great performance and efficiency under gravity and lateral load, with a low consumption of the structural materials (i.e. concrete: volume 58058 m^3, unit volume 0.41 m^3/m^2; steel : weight 20547 t, unit weight 143 kg/m^2).

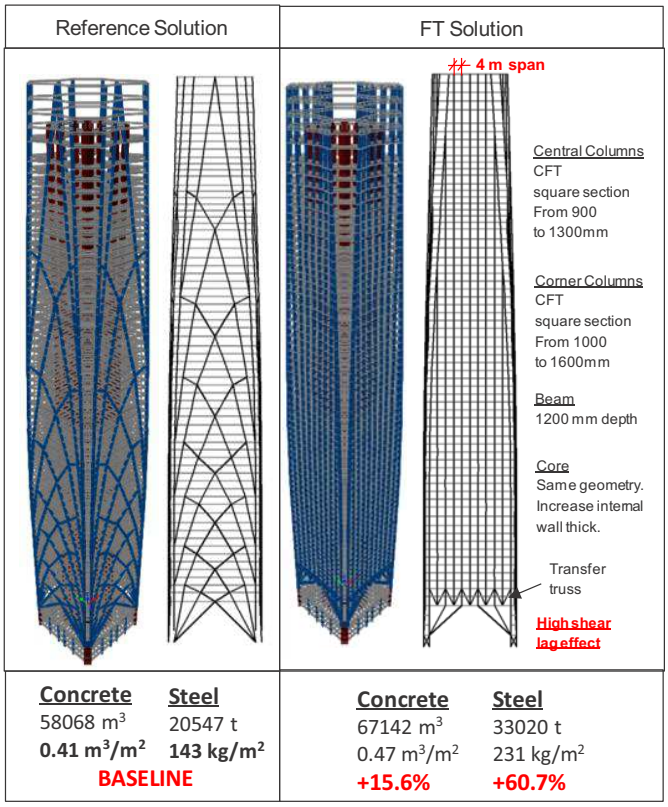

a) b)

Figure 6-28 OT1. Geometry and structural material consumption for a) reference solution, b) FT solution

Using the proposed solution as reference point, three (more traditional) structural solutions have been designed and analyzed for the perimetral frame. In order to have an actual comparison between the different solutions, no changes have been considered to i) the overall geometry of the building, ii) the geometry and the plan variation along the height of internal core, iii) the atriums at the basis and at the top of the building. The performances of the structures are assessed through finite element models.

The first solution is a framed tube (FT solution) with column span equal to 4 m (Figure 6-28b). At the building basis in order to create the high atrium of the reference solution, the spacing between the columns must be increased; for this aim a two story transfer truss has been designed as reported in Figure 6-28b, to collect the gravity loads in the corner columns. The FE analysis shows high shear lag effect and a consequent strong reduction of the lateral stiffness of the structure; with the aim of reducing the shear lag effect and increase the stiffness of the frame tube, the cross section of the columns (1600mm x 1600 mm at the basis and 1000mm x 1000mm at the top) and of the spandrel beams (1200 mm depth) have been increased. Although a reduction of the shear lag is observed, the lateral stiffness of the structure is still not enough to satisfy the interstory drift check under wind loads; a relevant increase of the shear walls thickness is necessary. The FT final solution has very low efficiency as shown by the structural material consumption (concrete: volume 67142 m^3, unit volume 0.47 m^3/m^2; steel: weight 33020 t, unit weight 231 kg/m^2), with a severe increase respect to the reference solution (+15.6% for the concrete, +60.7% for the steel).

In the second solution, the shear lag is reduced through megadiagonals on the façade preserving the 4 m spacing between the perimetral columns (i.e. Brace Tube, BT solution, Figure 6-29a); at the building base, the transfer truss is still necessary to have the high atrium. As expected, the shear lag strongly decreases because the megadiagonals tie together all the perimetral columns and reduce the shear deformation of the perimetral frame. To satisfy the interstory drift checks under wind loads, only the increase of the cross section of the spandrel beams is necessary (double t steel section 850 mm depth). The BT solution shows a good efficiency but still has an increase of structural material consumption respect to the initial solution (concrete: volume 61087 m^3,

unit volume 0.43 m^3/m^2 equal to +5.1%; steel: weight 33020 t, unit weight 231 kg/m^2 equal to +26%).

For the third solution, a diagrid structure has been designed (DG solution); the triangular module is two story height with an angle of diagonal elements equal to about 60° (Figure 6-29b). Using this diagrid geometry there is not a need for a transfer truss at the building basis. The structure shows a good performance, anyway there is still an increase in the structural material consumption respect to the initial solution (concrete: volume 61184 m^3, unit volume 0.43 m^3/m^2 with +5.3%; steel: weight 25841 t, unit weight 178 kg/m^2 with +24%).

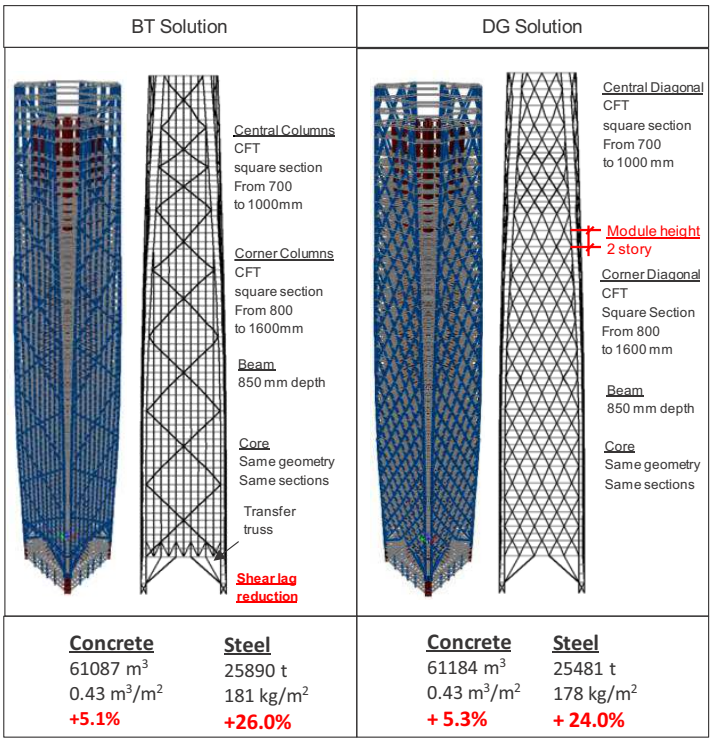

a) b)

Figure 6-29 OT1. Geometry and structural material consumption for a) BT solution, b) DG solution

6.6 Conclusion

Through the analysis and the special studies on the Office Tower 1, it has been possible to fully understand the structural behavior of the structure. The following main aspects have been pointed out:

- the structure has a high flexural and shear stiffness but it shows lacks of stiffness at floor between the "panel point" of the optimized diagrid;
- the shear walls within the central core avoid local deformability problems and increase the overall horizontal stiffness;
- under vertical loads, high tension have been observed in the slabs; the reduced membrane stiffness of the cracked slab affects the horizontal stiffness of the building and require an increase of the cross section for the diagrid members;
- the structure is the most efficient comparing to other structural systems;

It is worthy to underline however that the angle selected for the diagrid is not the most efficient, as described in par.1 and 2 so that a more efficient diagrid could be designed considering steeper angle.

7 Conclusions and extensions

The new challenges in the design of tall buildings give rise to the development of a new repertoire of structural solutions, aiming for efficiency, robustness, sustainability, ductility and aesthetic impact. The research community is giving growing attention to this topic, mainly focusing on the study of the structural behavior of innovative structural systems and on the research of new structural form. In this thesis the behavior of innovative systems is investigated to understand the fundamental structural issues and in order to give suggestions and simplified formulations for the design and the assessment of tall buildings.

The first part of the thesis is focused on the diagrid systems, "a hallmark of 21st century Modernism" [Volner 2011]. Diagrid structures for tall buildings have become very popular among engineers and architects, thanks to the inherent qualities of structural efficiency, decorative attributes and morphological versatility. The number of project and realizations involving diagrids steadily increases every year, with diagonals members arranged according to various geometrical patterns. However the academic research only recently focused to diagrid structures, providing contributions on design criteria and structural assessment.

Recognizing the lack of a thorough survey on diagrid patterns and of specific studies on the relevant design criteria, a wide research activity on this topic have been embraced, with the aim of exploring the different possibilities of the diagrid system. With this aim, simplified approaches for the structural design of Diagrid are proposed in Chapter 2 thanks to

the high simplicity and structural legibility of this system. Furthermore the triangular module allows to study different structural configurations with the aim of increase the system efficiency; in particular in chapter 3 the diagrid structures characterized by regular patterns are compared to alternative geometrical configurations, obtained by changing the angle of diagonals as well as by changing the number of diagonal along the building height.

The results obtained from the analysis of the regular and alternative diagrids, show peculiar "local" behavior of the diagrid system; in Chapter 4 these local issues are investigated and a methodology for establishing the need for a specific secondary bracing system (SBS) as a function of the diagrid geometry is proposed.

In the second part of this thesis alternative structural pattern are investigated; the proposed design procedure based on the RVE concept and homogenization methods allow to deal with regular and irregular geometrical patterns to be adopted in tube structural configurations and verify the efficiency of the considered geometry.

Finally an optimized configuration for a perimetral frame of a real tall building in China is analyzed, firstly evaluating the building performance and issues, and then comparing the optimized structure with more traditional structural solutions.

The main contributions of this thesis in the three described topics can be summarized as follows:

- in the design of diagrid system for tall buildings the stiffness and strength requirements are both necessary and unavoidable; they are not separately sufficient for an exhaustive sizing process of the diagonal members. It has been observed that in structures with lower values of the diagonal angle the strength design is more stringent and resulting diagonal members are larger than according to stiffness design, while the opposite occurs in the

case of steeper diagonal angles, where the stiffness mainly governs the design;

- the structural assessment of the alternative diagrid solutions (i.e. with varying angle or number of diagonals along the building height) has shown that several patterns can be considered equally efficient, i.e. exhibit similar values of structural weight and of building top drift, suggesting that different geometrical arrangements of diagonal members, designed for the same stiffness and strength requirements, give rise to similar values of global material consumption;
- all analyzed diagrid models exhibited problems concerning stability of interior columns (i.e. multi-storey buckling modes) and/or local flexibility (excessive interstory drift); the above local problems are completely solved after the introduction of a Secondary Bracing Systems (SBS) at the central core location, and, against a modest increase of structural weight (about 3%), any flexural engagements in the diagrid member is eliminated;
- the hexagrids, being bending-dominated structures, are inherently less stiff, and consequently, less weight efficient, than diagrids, that are stretch-dominated structures. Anyway the floor structure and the consequent rigid diaphragm effect provides a considerable increase of the stiffness of the hexagrid, making it comparable to the diagrid;
- the optimized diagrid described in chapter 7 shows efficiency higher than other more traditional structural solutions for tall buildings (Framed Tube, Braced Tube, Diagrid).

7.1 Suggestion for future work

Though several aspects in the structural design of innovative structures for tall buildings have been analyzed in this Thesis, the following topics seem interesting and require further in-depth analysis.

7.1.1 Design procedure optimization

The design procedure proposed in Chapters 2 and 3 uses as optimization parameter the "s" factor, defined as the bending to shear deformation at the top of the building. Through this factor it is possible to find the deformed configuration that allows to satisfy the stiffness requirements with the less amount of structural material, i.e. the most efficient solutions. The different deformed configurations are obtained with different distributions of structural material along the building height, e.g. structure more stiff at the basis and less at the top or vice versa. Following this approach, further considerations seem necessary to formalize the influence of the deformed configuration of the buildings on the structural efficiency.

Furthermore a similar parameter should be introduced in the design procedure proposed in Chapter 5. This procedure, still in an embryonic phase, could be improved considering a variation in the stiffness of the equivalent homogenized cantilever beam along the building elevation and introducing an optimization rule.

7.1.2 Seismic Evaluation of Diagrid

Concerning the Diagrid system, the main aim of this thesis is to investigate the structural behavior in the elastic field and give simplified design formulations; anyway the study of the post-elastic behavior of the Diagrid seems very interesting and has, in the practice design, a fundamental role.

In the scientific literature the non-linear behavior of the Diagrid system has been analyzed [7], [26], [23], [45] underlining "a limited capacity for energy dissipation and ductility" [26] and "quite brittle behavior compared with the performance of the tubular frame structures" [23] and proposing different solutions for improving the Diagrid plastic behavior, e.g. add shear-link fuse devices by modifying the triangular module [26] or use Buckling Restrained Brace (BRB) for the diagonals [23]. In this thesis, some initial considerations concerning the post-elastic behavior of an optimized diagrid under seismic loads are proposed in Chapter 7, introducing a sort of "capacity design".

Further studies seem necessary on these topics, in order to formalize a seismic design procedure for Diagrid and identify the critical points in the seismic design process of this system.

7.1.3 Non regular Patterns

The major quality of the design procedure proposed in Chapter 5 is that it can be applied to every structural patterns (not only triangular or hexagonal unit, as seen for Diagrid and Hexagrid respectively). An interesting application, now under investigation, is to apply the same procedure for the design and the structural evaluation of non periodic pattern, inspired by the nature.

Similar solutions have been already reported in the scientific literature, [10] using as starting point the Voronoi diaphragm. The Voronoi

tessellation is the partitioning of a plane with n points into convex polygons such that each polygon contains exactly one generating seed and every point in a given polygon is closer to its generating point than to any other.

Figure 7-1 Voronoi tessellation in nature

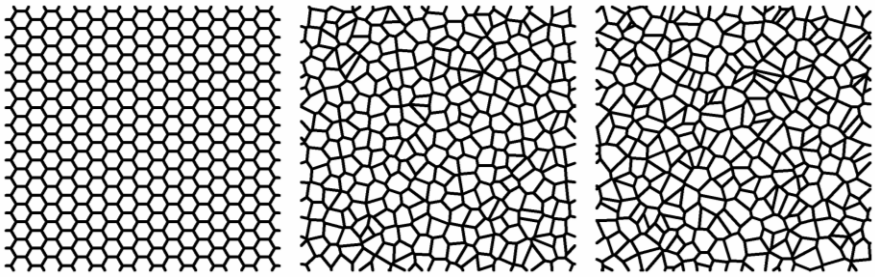

Figure 7-2 Examples of Voronoi tessellation with different level of irregularity

Several analyses have been carried out in order to formalize a design procedure for structures inspired by the Voronoi tessellation (Figure 7-2). Considering the irregular nature of these structural patterns, the homogenized mechanical proprieties of the Voronoi patterns could be

calculated only with a statistical approach. In particular the procedure under development is based on the definition of correction factors which allow to modify the mechanical proprieties of regular patterns from which the Voronoi is generated, taking into account the irregularity of the pattern.

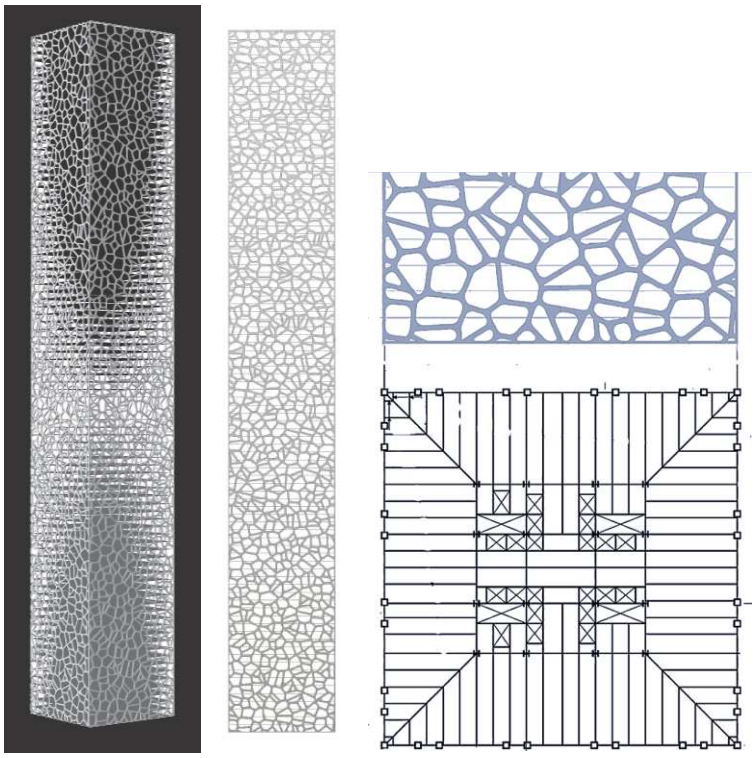

Figure 7-3 Building with Voronoi structures on the perimeter

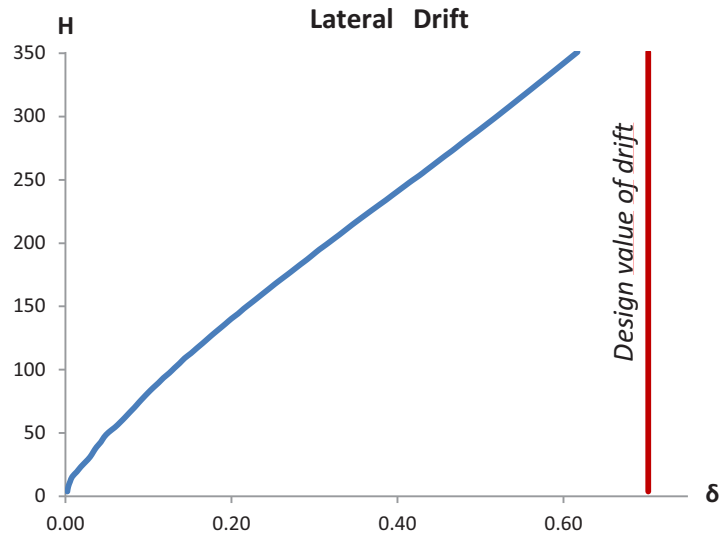

Figure 7-4 Structural performance of the Building with Voronoi structures

The reliability of the design procedure is under investigation; though the preliminary results have shown a good performance of the tall building with a Voronoi structures (Figure 7-3 and Figure 7-4), further analysis seem necessary.

8 Bibliography

[1] Abdelrazaq A, Baker W, Hajjar JF, and Sinn W, 1993. Column buckling considerations in high-rise buildings with Mega-Bracing, *Is Your Structure Suitably Braced?* Proceedings of the Structural Stability Research Council Annual Technical Session and Meeting, Milwaukee, Wisconsin, April 6-7, 1993, SSRC, Bethlehem, Pennsylvania, pp. 155-169

[2] AISC-LRFD 1999. Load and Resistance Factor Design Specification for Structural Steel Building, American Institute of Steel Construction.

[3] AISC, 2010. Specification for Structural Steel Buildings, ANSI/AISC, American Institute of Steel Construction, Chicago, IL

[4] ArcelorMittal. 2010. The ArcelorMittal Orbit - Full Planning Application. Design and Access Statement. June 2010. Ashby M.F. 2006. The properties of foams and lattices. Philosophical Transactions of the Royal Society, **364**, 15-30.

[5] Ashby M.F. 2006. The properties of foams and lattices. Philosophical Transactions of the Royal Society, **364**, 15-30.

[6] ASCE 7-05. 2006. Minimum design loads for buildings and others structures. American Society of Civil Engineers

[7] Baker W., Besjak C., Sarkisian M., Lee P., Doo C.S. 2010. Seismic Performance Factors for Steel Diagrid Framed Systems Using ATC-63 Methodology. Proceedings of SEAOC 2010 Convention. 21-25 Sept. 2010, Indian Wells, California.

[8] Baker W.F. 2013. Structural possibilities. In: The Tall Buildings Reference Book, Eds.: Parker D. and Wood A., Routledge.

[9] Besjak C., Kim B., Biswas P. 2009. 555m Tall Lotte Super Tower, Seoul, Korea. Proceedings of the 2009 Structures Congress. April 30–May 2, 2009. Austin, Texas. American Society of Civil Engineers.

[10] Beghini, L.L., Beghini A., Katz N., Baker W.F., Paulino G.H., 2014. Connecting architecture and engineering through structural topology optimization. Engineering Structures, Volume 59, February 2014, Pages 716-726, ISSN 0141-0296.

[11] Corvez D., Weill J.-M. (C&E Engineering), 2008. Self-stabilizing exterior lattice work: the Ductal Solution. Ductal Solutions No.7 "Mesh on show"– July 2008. http://www.ductal-lafarge.com/wps/portal/ductal/1_1_C-Ductal_NewsLetterCSI Analysis Reference Manual for SAP2000, ETABS and SAFE, 2009.

[12] deMeijer J.H.M. 2012. Lateral stiffness of hexagrid structures. Master's thesis.Eindhoven University of Technology Department of the Built Environment Structural Design

[13] Lowry P. 2005. Pittsburgh Then & Now: What were they thinking?. 1960s: IBM Building. Pittsburgh Post-Gazette, December 18, 2005. http://www.post-gazette.com

[14] Fraldi M., Cowin. 2004. Inhomogeneous elastostatic problem solutions constructed from stress-associated homogeneous solutions, J. Mech. Phys. Solids, 52.

[15] Fu, X.Y., Gao Y., Zhou Y., Yang X. 2012. Structural Design of Sino Steel International Plaza. CTBUH 2012 9thWorld Congress, Shanghai.

[16] Galambos T.V., 1998 Guide to Stability Design Criteria for Metal Structures, Fifth Edition. Editor John Wiley & Sons.

[17] Geschwindner, L. F., and Lepage A., 2013. Notes on the Nodal and Relative Lateral Stability Bracing Requirements of AISC 360, AISC Engineering Journal, American Institute of Steel Construction, Chicago, IL., 50(3), 169-179.

[18] Gibson J., Ashby M.F.1988. Cellular Solids: structure and properties, J. Mech. Phys. Solids, 46-1988.

[19] Goldberg P. 2005. Triangulation. The New Yorker, December 19, 2005. http://www.newyorker.com

[20] Goldsmith M. 1953. The tall building: the effects of scale. Master Thesis, 1953, Illinois Institute of Technology, Chicago.

[21] Hales, T. C. 2001. The honeycomb conjecture. Discrete & Computational Geometry, 25(1), 1-22.

[22] Hirschmann EW. 1965. The hull-core structure—an American design for office buildings. The Structural Engineer 43(11): 369–376.

[23] Kim, J. and Lee, Y.-H. (2012), Seismic performance evaluation of diagrid system buildings. Struct. Design Tall Spec. Build., 21: 736–749. doi: 10.1002/tal.643

[24] Kwan A.K. H. 1994. Simple method for approximate analysis of framed tube structures. J. of Structural Engineering, Vol. 120, No.4.

[25] Mele E, Toreno M, Brandonisio G, and De Luca A, 2012. Diagrid structures for tall buildings: case studies and design considerations. *The Structural Design of Tall and Special Buildings* doi:10.1002/tal1029

[26] Moghaddasi N.S., Zhang Y., 2013. Seismic analysis of diagrid structural frames with shear-link fuse devices. Earthquake Engineering and Engineering Vibration. Volume 12, Issue 3, pp 463-472

[27] Montuori, G. M., Mele, E., Brandonisio, G. and De Luca, A. 2013 **a**, Design criteria for diagrid tall buildings: Stiffness versus strength. Struct. Design Tall Spec. Build.. doi: 10.1002/tal.1144

[28] Montuori G.M., Mele E., Brandonisio G., De Luca A. 2013 **b**. Secondary Bracing Systems for diagrid structures in tall buildings. *Under review, submitted to:* Engineering Structures.

[29] Montuori G. M., Mele E., Brandonisio G., De Luca A. 2014, c. Secondary bracing systems for diagrid structures in tall buildings. Engineering Structures 75, 477–488.

[30] Moon K-S, Connor JJ, Fernandez JE, 2007. Diagrid structural system for tall buildings: characteristics and methodology for preliminary design. *The Structural Design of Tall and Special Buildings* 16(2): 205-230.

[31] Moon K-S, 2008a. Sustainable structural engineering strategies for tall buildings. *The Structural Design of Tall and Special Buildings* 17(5): 895-914.

[32] Moon K.S. 2008b. Optimal Grid Geometry of Diagrid Structures for Tall Buildings. Architectural Science Review, 51:3, 239-251.

[33] Moon K-S, 2008c. Material-saving design strategies for tall buildings structures. In *CTBUH 8th World Congress, Dubai. March 3-5, 2008*.

[34] Moon K-S, 2011. Diagrid structures for Complex-Shaped Tall Buildings. *Procedia Engineering, Volume 12, 2011, Pages 1343-1350.*

[35] Morgan F. and Bredt J.F. 2000. Geometric Measure Theory. 3rd Edition. A Beginner's Guide. Elsevier Inc.

[36] Moussavi F, 2009. The function of form. *Actar and the Harvard University Graduate School of Design, 2009*.

[37] Munro D, 2004. Swiss Re's Building, London. *Nyther om stàlbyggnad* 3: 36-43.

[38] Nair R S. Simple solutions to stability problems in the design office. In: 1988 National Steel Construction Conference. 1988. p. 38.

[39] Nemat-Nasser S., Hori M.1999. Micromechanics: Overall Properties of Heterogeneous Materials,2nd Edition, North-Holland.

[40] Peterson I. 1999. The Honeycomb Conjecture. Science News, 156, 60-61 July 24, 1999 Http://www.sciencenews.org/sn_arc99/7_24_99/bob2.htm

[41] Popov E.P. & Engelhardt M.D. (1988) Seismic Eccentrically Braced Frames. J Constr Steel Res

[42] Schulitz H.C, Sobek W., Habermann K.J. 2001. Steel construction manual. Birkhäuser. Munich, Germany, 2001.

[43] Szpiro G. 2003. Kepler's conjecture: how some of the greatest minds in history helped solve one of the oldest math problems in the world. John Wiley & Sons, Inc., Hoboken, New Jersey.

[44] Taranath B. 1998. Steel, Concrete, and Composite Design of Tall Buildings. 2nd edition, McGraw-Hill.

[45] Teng J., Guo W. L., Rong B. S., Li Z. H., Dong Z. J., 2010 Research on Seismic Performance Objectives of High-Rise Diagrid Tube Structures, Advanced Materials Research, Vols 163-167, pp. 1100-1106

[46] Timoshenko S., 1936. Theory of elastic stability. McGraw-Hill Book Co., New York, 1936.

[47] Thornton C.H., Scarangello T.Z., 1988. Localized Stability Problems in Large Structural Systems. Proceedings of the Structural Stability Research Council Annual Technical Session and Metting, Minneapolis, Minnesota, 1988.

[48] Toreno M., Fraldi M., Giordano A., Mele E., De Luca A. 2011. Bubble-frame: assessment of a new structural typology starting from the Water Cube. Proc. SEWC 2011 , paper No.143

[49] Torroja E. 1960. Razón y ser de los tipos estructurales. Italian Translation: La concezione strutturale—Logica ed intuito nella ideazione delle forme, Levi F (ed). UTET: Torino, 1966.

[50] Winter G., 1960. Lateral Bracing Of Columns And Beams. Transactions of the American Society of Civil Engineers, Vol. 125, No. 1, January 1960, pp. 807-826

[51] Yura J. A., 1996 Winter's bracing approach revisited, Engineering Structures, Volume 18, Issue 10, October 1996, Pages 821-825, ISSN 0141-0296.

[52] Volner I. 2011. Dissecting Diagrid. Architect - The Magazine of the American Institute of Architects. October, 2011. http://www.architectmagazine.com

[53] Zhang C., Zhao F. and Liu Y., 2012. Diagrid tube structures composed of straight diagonals with gradually varying angles. Struct. Design Tall Spec. Build., 21: 283–295. doi: 10.1002/tal.596

[54] Zhang H.-Y., Beliveau J.-G. and Huston D.R., 1993. Minimum Lateral Stiffness for Equally Spaced Braces in Columns, Journal of Engineering Mechanics, ASCE, Vol.119, NO.9., pp 1888-1897